Naval Research Laboratory

Stennis Space Center, MS 39529-5004

NRL/MR/7440--11-9349

Unmanned Aircraft Systems Meteorology and Oceanography Sensing Analysis of Alternatives: Year One Study Report

Paul Elmore

Geospatial Sciences and Technology Branch
Marine Geosciences Division

K. Todd Holland
Bill Sanders

Seafloor Sciences Branch
Marine Geosciences Division

William Stevens
Adrian Fontanilla
Anson Brune

Applied Operations Research Inc.
Solana Beach, California

Jay Veeramony
Gregg Jacobs

Ocean Dynamics and Prediction Branch
Oceanography Division

Pete Spence

QinetiQ North America
Stennis Space Center, Mississippi

Larry Phegley

Meteorological Applications Development Branch
Marine Meteorology Division

Chris Wackermann

GD-AIS
Ypsilanti, Michigan

November 22, 2011

Distribution authorized to the Department of Defense and U.S. DoD contractors only; administrative/operational use; November 2011. Other U.S. requests for this document shall be referred to Battlespace Awareness and Information Operations Program Office (PMW 120), Navy Program Executive Office for C4I.

REPORT DOCUMENTATION PAGE

Form Approved
OMB No. 0704-0188

Public reporting burden for this collection of information is estimated to average 1 hour per response, including the time for reviewing instructions, searching existing data sources, gathering and maintaining the data needed, and completing and reviewing this collection of information. Send comments regarding this burden estimate or any other aspect of this collection of information, including suggestions for reducing this burden to Department of Defense, Washington Headquarters Services, Directorate for Information Operations and Reports (0704-0188), 1215 Jefferson Davis Highway, Suite 1204, Arlington, VA 22202-4302. Respondents should be aware that notwithstanding any other provision of law, no person shall be subject to any penalty for failing to comply with a collection of information if it does not display a currently valid OMB control number. **PLEASE DO NOT RETURN YOUR FORM TO THE ABOVE ADDRESS.**

1. REPORT DATE *(DD-MM-YYYY)*
22-11-2011

2. REPORT TYPE
Memorandum Report

3. DATES COVERED *(From - To)*

4. TITLE AND SUBTITLE

Unmanned Aircraft Systems Meteorology and Oceanography Sensing Analysis of Alternatives: Year One Study Report

5a. CONTRACT NUMBER

5b. GRANT NUMBER

5c. PROGRAM ELEMENT NUMBER

6. AUTHOR(S)

Paul Elmore, K. Todd Holland, Bill Sanders, William Stevens,* Adrian Fontanilla,* Anson Brune,* Jay Veeramony, Gregg Jacobs, Pete Spence,† Larry Phegley, and Chris Wackermann‡

5d. PROJECT NUMBER

5e. TASK NUMBER

5f. WORK UNIT NUMBER
74-4126-A0

7. PERFORMING ORGANIZATION NAME(S) AND ADDRESS(ES)

Naval Research Laboratory
Marine Geosciences and Oceanography Divisions
Stennis Space Center, MS 39529-5004

Naval Research Laboratory
Meteorology Division
Monterey, CA 92075-2077

8. PERFORMING ORGANIZATION REPORT NUMBER

NRL/MR/7440--11-9349

9. SPONSORING / MONITORING AGENCY NAME(S) AND ADDRESS(ES)
PEO C4I, PMW120
Attn: Dr. Edward C. Mozley
APM Future MetOc Capabilities
4301 Pacific Highway, Building OT-1, Room 2851
San Diego, CA 92110-3127

10. SPONSOR / MONITOR'S ACRONYM(S)

SPAWAR/PMW-120

11. SPONSOR / MONITOR'S REPORT NUMBER(S)

12. DISTRIBUTION / AVAILABILITY STATEMENT

Distribution authorized to the Department of Defense and U.S. DoD contractors only; administrative/operational use; November 2011. Other U.S. requests for this document shall be referred to Battlespace Awareness and Information Operations Program Office (PMW 120), Navy Program Executive Office for C4I.

13. SUPPLEMENTARY NOTES

*Applied Operations Research Inc., 420 Stevens Ave., Suite 230, Solana Beach, CA 92075-2077
†QinetiQ North America, MSAAP Bldg 9121 Moses Cook Rd, Stennis Space Center, MS 39529
‡General Dynamics Advanced Information Systems, 1200 Joe Hall Dr., Ypsilanti, MI 48197

14. ABSTRACT

The purpose of this unmanned aircraft system (UAS) meteorology and oceanography (METOC) sensing analysis of alternatives (AoA) is to assess the potential U.S. Navy warfighting value-added of using UAS platforms and sensors to collect environmental data in the atmosphere and ocean surface and subsurface environments. In this study, we have considered the impact of UAS METOC sensing using persistent (e.g., BAMS), tactical (e.g., Fire Scout), as well as small tactical (e.g., ScanEagle) UAS platform classes. We have considered the use of dual-use organic sensors as well as potential future METOC specific sensors and expendables. The goal of the Fiscal Year 2009 study reported here is to capture and quantitatively assess the potential value-added of a broad range of UAS METOC sensing strategies and associated impacted Naval mission areas, e.g., mine warfare, expeditionary warfare, Naval special warfare, air warfare, and antisubmarine warfare. These analyses have been conducted in the context of illustrative tactical situations based on relevant portions of applicable DoD planning scenarios.

15. SUBJECT TERMS
Unmanned aircraft systems
Remote sensing
METOC

16. SECURITY CLASSIFICATION OF:			17. LIMITATION OF ABSTRACT	18. NUMBER OF PAGES	19a. NAME OF RESPONSIBLE PERSON
					Paul Elmore
a. REPORT	b. ABSTRACT	c. THIS PAGE	SAR	118	19b. TELEPHONE NUMBER *(include area code)*
Unclassified Limited	Unclassified Limited	Unclassified Limited			(228) 688-4613

Standard Form 298 (Rev. 8-98)
Prescribed by ANSI Std. Z39.18

This page intentionally left blank.

Revision History

Version 1.0 (Initial Draft): 1 August 2009, Initial AOR Inc. draft report.

Version 1.1 (Second Draft): 21 August 2009, incorporated initial EXW and ASCM TACSIT results.

Version 1.2 (Third Draft): 26 August 2009, incorporated UAS platform and sensor information and initial ASW TACSIT results. Incorporated review comments provided by Doug Backes (NAVAIR), Dr. Todd Holland (NRL 7400), and Larry Phegley (NRL 7500).

Version 1.3 (Fourth Draft): 30 August 2009, incorporated Section 5.3 inputs provided by Drs. Paul Elmore Holland and Bill Sanders (NRL 7400).

Version 1.4 (Fifth Draft): 6 September 2009, incorporated Section 5.2 updates provided by Dr. Jay Veeramony (NRL 7300), Section 5.3 updates provided by Drs. Paul Elmore Holland and Bill Sanders (NRL 7400), and Section 5.5 updates provided by Pete Spence (NRL 7300).

Version 1.5 (Sixth Draft): 20 October 2009, incorporated Section 5.5 updates provided by Pete Spence (NRL 7300) and Adrian Fontanilla and Anson Brune (AOR Inc.).

Version 1.6 (Seventh Draft): 2 November 2009, incorporated Section 4.0 updates provided by Todd Holland (NRL 7300) and Section 5.2 and 5.3 updates provided by Jay Veeramony and Paul Elmore.

Version 1.7 (Eighth Draft): 6 November 2009, incorporated Section 4.0 updates provided by Todd Holland (NRL 7300) and Chris Wackerman and Section 5.3 and Appendix H and I updates provided by Paul Elmore.

Version 1.8 (Ninth Draft): 9 November 2009, incorporated Section 4.0 updates provided by Chris Wackerman and Section 5.2 updates provided by Jay Veeramony.

Version 1.9 – 1.11 (Final Drafts): 30 June 2011, changes by Paul Elmore to references and formatting for publication of report as a Naval Research Laboratory Memorandum Report.

This page intentionally left blank.

Table of Contents

1.0 Executive Summary 1

2.0 Introduction 6

2.1 Study Goals 6
2.2 Study Approach 6
2.3 Unmanned Aircraft Systems (UAS) 7
2.3.1 Broad Area Maritime System (BAMS) 7
2.3.2 Vertical Takeoff and Landing Tactical Unmanned Aerial Vehicle (VTUAV) 7
2.3.3 ScanEagle Small Tactical UAV (STUAV) 8
2.4 UAS Sensing Technologies 9
2.4.1 Dual Use and METOC Specific Sensors and Mission Areas 9
2.4.2 Relevant MIW, NSW, ASW, and AW Environmental Parameters 10
2.4.3 BAMS Sensor Suite 12
2.4.4 Fire Scout VTUAV Sensor Suite 13
2.4.5 ScanEagle Sensor Suite 13
2.5 Potential for UAS METOC Data Collection and Exploitation 14
2.6 OPNAV UAS METOC Sensing Priorities 16

3.0 METOC Data Collection Requirements 17

3.1 Atmospheric METOC Sensing 17
3.2 Littoral Ocean METOC Sensing 18
3.3 Near-Shore, Beach Zone Sensing 19
3.4 Mission Area Specific METOC Sensing Requirements 20

4.0 Ocean Sensing Feasibility Analysis 22

4.1 Overview and Analysis Objectives 22
4.2 Ocean Sensing Applications 22
4.2.1 Bathymetry Estimation 22
4.2.2 Wave Spectra Estimation 24
4.3 Ocean Sensor Technologies 26
4.3.1 Optics 26
4.3.2 Radar 28
4.3.3 LIDAR 34
4.3.3 Multispectral and Hyperspectral 35
4.4 Summary Capabilities Matrix 36

5.0 Mission Area (TACSIT) Analysis 38

5.1 Mapping of OPNAV Priorities to TACSITs 38
5.2 Expeditionary Warfare, Navy Special Warfare Landing TACSIT 38
5.2.1 Identification of Study Team 39
5.2.2 Mission Area (TACSIT) Overview 39
5.2.3 Analysis Objectives and Methodology 40
5.2.4 Effectiveness Analysis Results 43
5.2.5 Summary Conclusions 47
5.3 Mine Hunting and Clearance TACSIT 50
5.3.1 Identification of Study Team 50
5.3.2 Background 50

5.3.3 Mission Area (TACSIT) Overview *53*
5.3.4 Analysis Objectives and Methodology *54*
5.3.5 Effectiveness Analysis Results *56*
5.3.6 Summary Conclusions *58*
5.4 Cruise Missile Defense, Straits Transit TACSIT 59
5.4.1 Identification of Study Team *59*
5.4.2 Mission Area (TACSIT) Overview *60*
5.4.3 UAS Experimentation Plan *62*
5.4.4 UAS Experiment Results *64*
5.4.5 UAS Data Denial Analysis Results *65*
5.4.6 Potential Impact of UAS Wind Collections on Fires *66*
5.4.7 Summary Conclusions *68*
5.5 ASW Search and Screen TACSIT 69
5.5.1 Identification of Study Team *69*
5.5.2 Mission Area (TACSIT) Overview *70*
5.5.3 Analysis Objectives and Methodology *71*
5.5.4 Effectiveness Analysis Results *76*
5.5.5 Summary Conclusions *80*
5.6 Other TACSITs 81

6.0 Year One Study Results 82
6.1 Summary Warfighting Impact Assessment 82
6.2 Ranking of Likely Mission Impacts 84
6.3 Key UAS Technologies and Readiness Levels 85
6.4 Initial C2 Data Flow and CONOPs Specifications 86

7.0 Year Two Study Plans and Objectives 87
7.1 Formulate Initial Navy UAS METOC Sensing Strategy 87
7.2 Conduct Key Technology Demonstrations 87
7.3 Conduct Inventory Analysis and Life Cycle Cost Estimation 87
7.4 Refine Initial C2 Data Flow and CONOPs Specifications 87

Appendix A – References A-1

Appendix B – Acronym List B-1

Appendix C – U.S. Army Corps of Engineers Field Research Facility C-1

Appendix D – Webster Field UAS Experiment (23 Feb - 12 Mar 2009) D-1
D.1 Experiment Results – Observed Conditions D-1
D.2 RAOB vs. UAS Data Collections D-1
D.3 AREPS Reflectivity Plots D-2

Appendix E – Webster Field UAS Experiment (18-29 May 2009) E-1
E.1 Experiment Results – Observed Conditions E-1
E.2 RAOB vs. UAS Data Collections E-2
E.3 AREPS Reflectivity Plots E-2

Appendix F – Webster Field UAS Experiment (13-19 August 2009) F-1
F.1 Experiment Results – Observed Conditions F-1
F.2 RAOB vs. UAS Data Collections F-1
F.3 AREPS Reflectivity Plots F-2

Appendix G – UAS Wind Estimation Errors G-1
Appendix H – MBES Key Bayesian Network Implementation H-1
Appendix I – Scour Model Review I-1

Points of Contact

Bob Winokur, CNO N84 TD, robert.s.winokur@navy.mil.

Steve Rutherford, Non-Acquisition R&D Management, OPNAV N84, Univ. of Washington - Applied Physics Lab, (207) 607-2456, steven.j.rutherford1.ctr@navy.mil.

CAPT Andrew Brown III, PMW-120 METOC Systems, PEO C4I/PMW-120, 619-524-7377, andrew.brownIII@navy.mil.

Thomas Piwowar, Assistant Program Manager (APM) for METOC Future Systems, PEO C4I/ PMW-120, (619) 524-7912, thomas.piwowar@navy.mil.

Edward Mozley, Deputy Assistant Program Manager (DAPM) for Future METOC Systems, PEO C4I/PMW-120, 858-537-0230, edward.mozley@navy.mil

Doug Backes, Air 4.5 S&T Integration, Fleet Liaison, NAVAIR, 301-342-2130, douglas.backes@navy.mil.

Eduardo Danganan, NAVAIR 4.10.2, Warfare Analysis and Integration, Maritime Dominance Analysis Branch, 301-342-8282, eduardo.danganan@navy.mil.

Paul Eiff, BAMS Future Capabilities, PMA 262 Support, 301-342-0039, paul.eiff@navy.mil.

Dr. Todd Holland, NRL 7440.3, 228-688-5320, todd.holland@nrlssc.navy.mil.

Dr. Chris Wackerman, General Dynamics Advanced Information Systems, 734-480-5413, chris.wackerman@gd-ais.com.

Dr. Gregg Jacobs, NRL Code 7320, Ocean Dynamics and Prediction, (228) 688-4720, gregg.jacobs@nrlssc.navy.mil.

Larry Phegley, NRL 7500, 831-656-4752, phegley@nrlmry.navy.mil.

Dr. Jay Veeramony, NRL Code 7320, Ocean Dynamics and Prediction, 228-688-4835, jay.veeramony@nrlssc.navy.mil.

Dr. Paul Elmore, NRL 7400, Marine Geosciences Division, 228-688-4613, paul.elmore@nrlssc.navy.mil.

Pete Spence, NRL Code 7320, Ocean Dynamics and Prediction, 228-688-5272, peter.spence.ctr@nrlssc.navy.mil.

Dr. Bill Sanders, NRL 7400, Marine Geosciences Division, wsanders@nrlssc.navy.mil.

Dr. William Stevens, Senior Operations Analyst, Applied Operations Research Inc., 858-437-8780 x103, bill.stevens@appliedor.com.

UAS METOC Sensing Analysis of Alternatives

1.0 Executive Summary

The purpose of this Unmanned Aircraft System (UAS) METOC Sensing Analysis of Alternatives (AoA) is to assess the potential US Navy warfighting value-added of using UAS platforms and sensors to collect environmental data in the atmosphere and ocean surface and subsurface environments. In this study we have considered the impact of UAS METOC sensing using persistent (e.g. BAMS), tactical (e.g. Fire Scout), as well as small tactical (e.g. ScanEagle) UAS platform classes. We have considered the use of dual use organic sensors (e.g. EO/IR cameras, SAR/ISAR, etc.) as well as potential future METOC specific sensors and expendables (e.g. humidity sensor, dropsondes, etc.). The goal of the FY-09 study reported here is to capture and quantitatively assess the potential value-added of a broad range of UAS METOC sensing strategies and associated impacted Naval mission areas, e.g. Mine Warfare (MIW), Expeditionary Warfare (EXW), Naval Special Warfare (NSW), Air Warfare (AW), and Anti-Submarine Warfare (ASW). Other potential mission support areas, e.g. high altitude helo operations and weather imagery collection, were considered but not quantitatively assessed. These analyses have been conducted in the context of illustrative tactical situations (TACSITs) based on relevant portions of applicable OPLANs or other DoD planning scenarios. The goal of future efforts will be to continue the analyses started in FY-09 with an increased focus on concept verification demonstrations and experimentation with real world operational and/or prototype UAS platforms and sensors, in order to provide needed inputs in support of a Navy vision for UAS-based METOC sensing.

The UAS METOC Sensing AoA Study Team included the following organizations, researchers and technical roles:

- **NAVAIR** (Doug Backes, Paul Eiff, Andrew Pontzer and Eduardo Danganan): UAS platform and sensor programmatic representation. UAS experimentation. Mapping of TACSITs to DoD scenarios and operational plans (OPLANs).

- **NRL Code 7400** (Dr. Todd Holland and Dr. Paul Elmore): UAS sensor feasibility analysis and MIW TACSIT analysis.

- **NRL Code 7300** (Dr. Gregg Jacobs, Dr. Jay Veeramony, Dr. Charlie Barron, Pete Spence): EXW/NSW and ASW TACSIT analyses.

- **NRL Code 7500** (Larry Phegley): AW UAS experimentation and AW TACSIT analysis.

- **Applied Operations Research, Inc.** (Dr. Bill Stevens, Alex Mackenzie and Adrian Fontanilla): Study team coordination and reporting, AW UAS experimentation and TACSIT analysis support, ASW TACSIT search effectiveness analysis.

The major conclusions of the FY-09 Unmanned Aircraft System (UAS) METOC Sensing Analysis of Alternatives (AoA) can be summarized as follows:

Manuscript approved September 13, 2011.

Air Sensing Feasibility Analysis:

- Three UAS experiments conducted at Naval Air Station (NAS) Patuxent River, Webster Field Annex confirm the viability of small tactical UAS (STUAS) temperature, pressure, humidity, and wind speed and direction soundings consistent with radiosonde observations (RAOBs). Note that while issues were encountered with wind speed and direction estimation accuracies, these issues are understood and can be corrected for (see Appendix G).
- Prior analysis, e.g. Ref. [13], has confirmed the viability of UAS temperature, pressure, humidity and wind speed and direction observations (via onboard sensors or future dropsonde capabilities) on Navy Operational Global Atmospheric Prediction System (NOGAPS) and Coupled Ocean/Atmosphere Mesoscale Prediction System (COAMPS) forecast errors in data-denied areas. A COAMPS data denial experiment, leveraging the experiment data collected at Webster Field, is planned.
- Most Joint and Navy UAS platforms have requirements for, at a minimum, temperature, pressure, humidity and wind speed and direction observations and METOC production center NWP data assimilation capabilities are available to leverage this data. Work is required to establish the C2 connectivity needed to deliver this data to Joint and Navy METOC production centers and to insure the timely delivery of NWP products to in-theater Naval assets.

Ocean Sensing Feasibility Analysis:

- The technical feasibility of optical sensing of wave period/direction and radar sensing of wave spectra and subsequent inversion for bathymetry is well established.
- UAS employment CONOPs optimization is likely required to extract maximum benefit from UAS environmental sensing in support of Modified Surf Index (MSI) and percent mine burial estimation.
- Coupled full wave spectra estimation (wave direction, period, and height) plus bathymetry estimation is required to substantially impact MSI and percent mine burial estimation. Wave direction and period can be estimated passively (e.g. via video), while wave height requires active sensing (e.g. using radar, possibly LIDAR, or an in situ wave buoy).

Expeditionary Warfare, Naval Special Warfare TACSIT Analysis:

- For MSI estimation for the environment at Duck, NC, using sensors that improve only bathymetry yield marginal warfighting impact. ScanEagle EO bathymetry sensing results in 25% agreement with ground truth MSI vs. 16% in the No UAS sensing case. All other sensing alternatives result in somewhat less operational impact.
- For MSI estimation in the Duck, NC environment, bathymetry + wave spectra sensing is expected to yield a more substantial warfighting impact however. Initial model runs with radar wave spectra estimation supports this hypothesis. BAMS EO plus radar sensing yields a 43% agreement with ground truth MSI for favorable radar look angles and wind speeds and clearly suboptimal radar dwell times. It is probable that increasing radar dwell will result in substantially increased MSI estimation performance.

- UAS surveys and the supporting data assimilation and modeling CONOPs and required C2 connectivity is likely to be complex and coordination with OCEANOPSCOM Directorates is required to establish an operationally feasible CONOPs and data connectivity plan. We estimate that a minimum MSI improvement from the estimated 16% accurate in the No UAS Sensing case to 75% or greater accurate in the UAS Sensing case will be required to make the investment in UAS sensing, data assimilation, and modeling a cost effective option.

Mine Warfare TACSIT Analysis:

- For mine burial estimation in the Duck, NC FRF, bathymetry estimation yields marginal warfighting impact result.
- For mine burial estimation in the Duck, NC FRF, bathymetry plus wave spectra estimation is expected to yield a more substantial warfighting impact. Initial mine burial model runs with radar wave spectra estimation supports this hypothesis. Additional model runs are needed to quantify this impact.
- UAS surveys and the supporting data assimilation and modeling CONOPs and required C2 connectivity is likely to be complex and coordination with OCEANOPSCOM Directorates is required to establish an operationally feasible CONOPs and data connectivity plan. Additional connectivity with the MIW Environmental Post-Mission Analysis system will also be required. Since mine burial from wave action is largely correlated with orbital velocity at the bottom, we estimate that a minimum orbital velocity improvement from the estimated 16% accurate in the No UAS Sensing case to 75% or greater accurate in the UAS Sensing case will be required to make the investment in UAS sensing, data assimilation, and modeling a cost effective option.

Air Warfare (AW) TACSIT Analysis:

- Prior analyses, (c.f. pp. 71-72 below and Ref. [14]) have confirmed the viability of Doppler radar data assimilation as well as the potential impact of 3D wind estimation in METOC data denied areas on Joint Surface Strike and Joint Surface Fires Support scenarios.

Anti-Submarine Warfare TACSIT Analysis:

- Prior analysis, see Ref. [11], showed the value of persistent, regional ocean glider sensing in support of mid-frequency (MF) active ASW search effectiveness. Persistent, wide area sensing results in tactically exploitable model-driven forecast improvements.
- This analysis shows the impact of spatially/temporally localized UAS sensing in the search area. Spatially and temporally localized sensing in the search area results in data-driven forecast improvements complementary to wide area, persistent glider (or other UUV/USV/manned) in situ sensing improvements. Note that while the average UAS cumulative probability of detection (CPD) improvement exceeds the mean glider CPD improvement, there is considerably more variation in the UAS result. Persistent and spatially/temporally dense glider observations tend to provide a reliable CPD improvement. Short term, local UAS observations are more “hit or miss”; UAS CPD improvements tend to be near optimal (when observations happen to capture key local oceanographic features) or minimal (when they do not).

- A BAMS or VTUAV mini-AXBT (or X-glider) capability will require a BAMS wing pod or similar VTUAV delivery mechanism. While there is no BAMS Increment 1 requirement for a wing pod, BAMS Program Office discussions are underway concerning BAMS Increment 2 wing pod solutions for communications relays, SIGINT collections, etc.
- BAMS pod solutions have drawbacks, including the likelihood of icing at high altitudes, substantially reduced BAMS flight endurance and resulting impacts on BAMS CONOPs, BAMS power budget constraints and limits, pod space constraints, and competition with other BAMS missions (e.g. communication relay operations, SIGINT collections, etc.) for pod space.
- The combined impact of persistent, regional glider observations and spatially and temporally focused UAS observations in the search area was not considered in this study.
- Impact on low frequency (LF) passive search operations is TBD.

Table 1-1 provides a summary of likely UAS METOC sensing operational impacts. These are broken into "Easy" and "Possible" UAS METOC sensing win categories. As one might expect, "easy" METOC wins are possible by solving the data distribution issues needed to leverage pervasive UAS atmospheric sounding data collections in data denied areas. Prior studies have shown that solving these data distribution issues would result in improved NWP forecast skill improvements and associated improvements in EM and wind speed and direction estimation.

Technically possible, but less straightforward, METOC wins are associated with wave spectra estimation (leveraging video, radar, LIDAR, MSI/HSI, or expendable wave buoys), inversion of the wave spectra to estimate bathymetry, and the use of expendables (mini-dropsondes, mini-AXBTs, X-gliders, and wave buoys). Wave spectra and bathymetry estimation, while founded on well-established science, implies the need for complex collection and data distribution strategies and supporting data assimilation and modeling ashore. The use of expendables implies the need for sensor miniaturization, wing pod or other dispensing mechanisms, and impacts on host tactical UAS platforms and associated employment CONOPs. Hence while the UAS METOC sensing benefits in these categories have the potential to yield a significant warfighting impact, significant technical, programmatic, and operational hurdles must be addressed.

Missing from the analysis conducted to date is work to be conducted in partnership with cognizant OCEANOPSCOM Directorates to develop initial CONOPS for exploitation of Dual Use organic sensor data streams as well as high payoff METOC specific and expendable sensor data streams. There is also a requirement to develop the cost factors needed to determine the inventory requirements to support the proposed UAS sensing CONOPs; e.g. as needed to support a Program Life Cycle Cost Estimate (PLCCE).

Hence the goal of the FY-10 UAS METOC Sensing AoA will be to develop an initial UAS METOC sensing CONOPs, to develop the cost factors needed to establish inventory requirements and to conduct a Program Life Cycle Cost estimate (PLCCE), and to continue the analyses started in FY-09 with an increased focus on concept verification demonstrations and experimentation with real world operational and/or prototype UAS platforms and sensors, in order to provide needed inputs in support of a Navy vision for UAS-based METOC sensing.

This work was conducted under the technical management leadership of Dr. Ed Mozley, Deputy Assistant Program Manager, Future METOC Systems, PEO C4I and Space, PMW-120. Dr. Mozley's METOC domain knowledge and his technical guidance and direction in support of this study is hereby gratefully acknowledged by the UAS METOC Sensing AoA Study Team.

Mission Domain	METOC "Easy" Wins	METOC "Possible" Wins
AW	• Leverage UAS organic TPH/ wind measurements. • Assimilate UAS Doppler radar for 3D wind estimation.	• Exploit possible future UAS mini-dropsonde capability. • Exploit possible future UAS MW sounder or MSI/HSI capabilities.
EXW/NSW Landing		• Exploit well-established video, radar, wave buoy wave spectra measurements and bathy inversions for MSI estimation.
MIW		• Exploit well-established video, radar, wave buoy wave spectra measurements and bathy inversions for mine burial estimation.
ASW Search		• Exploit possible future UAS mini-AXBT or X-glider capability iso ASW search ops.

Table 1-1. Bottomline Warfighting Impact Assessment.

2.0 Introduction

From the DoD Unmanned Aircraft Systems Roadmap 2005 – 2030, see Ref. [1], *"As the Department of Defense (DoD) develops and employs an increasingly sophisticated force of unmanned systems over the next 25 years (2007 to 2032), technologists, acquisition officials, and operational planners require a clear, coordinated plan for the evolution and transition of unmanned systems technology. With the publication of this document, individual roadmaps and master plans for Unmanned Air, Ground, and Maritime Systems UASs, UGVs, and UMSs (defined as Unmanned Undersea Vehicles (UUVs) and Unmanned Surface Vehicles (USVs)) have been incorporated into a comprehensive DoD Unmanned Systems Roadmap. This integrated Unmanned Systems Roadmap is the plan for future prioritization and funding of these systems development and technology, thus ensuring an effective return on the Department's investment. Its overarching goal, in accordance with the Strategic Planning Guidance (SPG), is to guide military departments and defense agencies toward logically and systematically migrating applicable mission capabilities to this new class of military tools. This Roadmap highlights the most urgent mission needs that are supported both technologically and operationally by various unmanned systems. These should be considered when prioritizing future research, development, and procurement of unmanned systems technology to ensure an effective return on the Department's investment."*

2.1 Study Goals

The goal of the FY-09 study reported here is to capture and quantitatively assess the potential value-added of a broad range of UAS METOC sensing strategies and associated impacted Naval mission areas, e.g. Expeditionary Warfare (EXW) and Naval Special Warfare (NSW) landing operations, Mine Warfare (MIW), Air Warfare (AW) including straits transits and cruise missile ship defense (ASCM), and Anti-Submarine Warfare (ASW) search operations. These analyses are being conducted in the context of illustrative tactical situations (TACSITs) based on relevant portions of applicable OPLANs or other DoD planning scenarios. The goal of the FY-10 effort will be to continue the analyses started in FY-09 with an increased focus on concept verification demonstrations and experimentation with real world operational and/or prototype UAS platforms and sensors, in order to provide needed inputs in support of a Navy vision for UAS-based METOC sensing.

2.2 Study Approach

This Navy UAS METOC sensing analysis of alternatives (AoA) is employing the following five-step analysis process:

1. Define the full range of UAS atmospheric sensing possibilities and likely impacts. Consider the impact of UAS METOC sensing using persistent (e.g. BAMS), tactical (e.g. Fire Scout), as well as small tactical (e.g. ScanEagle) UAS platform classes. Consider "Dual Use" organic sensors (e.g. EO/IR cameras, SAR/ISAR, etc.) as well as potential future "METOC specific" and "expendable" sensors (e.g. humidity sensor, dropsondes, etc.).
2. Identify what platforms, sensors, and data assimilation techniques are needed to meet Navy/USMC sensing requirements in relevant mission areas and TACSITs.
3. Demonstrate via analysis and experimentation the warfare return on investment (ROI) and

what-it-takes-to-win (WITTW) metrics associated with UAS sensing and data assimilation. Conduct verification demonstrations, observing system experiments (OSEs) and/or observing system simulation experiments (OSSEs), or TBD other experiments in which a relevant TACSIT is selected, a UAS sensing strategy is articulated, and a combination of real world datasets and/or simulated representations of UAS sensing performance is used to compare "current" numerical weather prediction (NWP) or ocean data assimilation and modeling with "current + UAS". Compile as much evidence as possible to support the suitability of each sensor type to identified METOC sensing applications.

4. Determine the inventory requirements to support UAS sensing requirements; e.g. as needed to support a Program Life Cycle Cost Estimate (PLCCE).
5. In partnership with cognizant OCEANOPSCOM Directorates develop initial CONOPS for exploitation of Dual Use organic sensor data streams as well as high payoff METOC specific and expendable sensor data streams.

2.3 Unmanned Aircraft Systems (UAS)

Three classes of Navy unmanned aircraft systems (UASs) are considered in this study (see Figure 2.3-1 below); *persistent* (as represented by the Navy Broad Area Maritime System – BAMS), *tactical* (as represented by the Navy Fire Scout Vertical Takeoff and Landing Tactical Unmanned Aerial Vehicle – VTUAV), and *small tactical* (as represented by ScanEagle).

2.3.1 Broad Area Maritime System (BAMS)

From Ref. [1], *"The Navy is developing the BAMS unmanned aircraft (UA) to provide a persistent, maritime, worldwide access, ISR capability. Operating as an adjunct to the Multi-mission Maritime Aircraft (MMA), the BAMS UA will conduct continuous open-ocean and littoral surveillance of targets as small as 30-foot vessels. The BAMS UA will be unarmed, possess high endurance, and will operate from land-based sites worldwide. BAMS UAS of up to 5-6 air vehicles at each operating location will provide persistence by being airborne 24 hours a day, 7 days a week out to on-station ranges of 2,000 nautical miles. Worldwide access will be achieved by providing coverage over nearly all the world's high-density sea-lanes, littorals, and areas of national interest from its operating locations. BAMS UA will also contribute to providing the Fleet Commander a common operational picture of the battlespace day and night. Additionally, a communication relay capability will provide the Fleet Commander a 'low hanging satellite' capability, linking him to widely dispersed forces in the theater of operation and serving as a communication node in the Navy's FORCEnet strategy.*

2.3.2 Vertical Takeoff and Landing Tactical Unmanned Aerial Vehicle (VTUAV)

From Ref. [1], *"The Fire Scout Vertical Take-Off and Landing (VTOL) Tactical UAV (VTUAV) program is currently in engineering and manufacturing development (EMD). Five RQ-8A air vehicles and four ground control stations are now in developmental testing. Over 100 successful test flights have been accomplished demonstrating autonomous flight, tactical common data link (TCDL) operations, Multi-Mission Payload performance, and ground control station operations. The Army selected the four-bladed RQ-8B model as its category IV UA for its future combat system (FCS) in 2003. Planned delivery for the first two prototypes is in 2006. The Navy has selected the RQ-8B to support the Littoral Combat Ship (LCS) class of surface vessels.*

From Navy Tactics, techniques, and Procedures (NTTP) 3-15.24 (Ref. [19]), *"Fire Scout VTUAV's primary mission will be to provide situation awareness (SA) and intelligence, surveillance, reconnaissance, and targeting (ISR-T) to tactical users, including amphibious task force (ATF) and mine countermeasures (MCM) forces at sea and landing force (LF) units ashore. Its long endurance, sophisticated payloads, ability to take off and land vertically, and autonomous operating capability make it uniquely capable of providing long range surveillance and targeting under the most demanding tactical conditions. Fire Scout will be employed from the Littoral Combat Ship (LCS) where* Coastal Battlefield Reconnaissance and Analysis (*COBRA) will be its payload as part of the MIW mission package (MP)."*

Also from Ref. [19], *"The COBRA system is a clandestine UAV capability, and it will be employed as the payload for the Fire Scout VTUAV from the LCS as part of the MIW MP where it will support amphibious operations by detecting minefield patterns and obstacles in the surf zone (SZ) and beach zone (BZ) to the beach exit. COBRA will be flown during preassault or preaction operations between 500 and 1,100 feet above proposed landing sites and beaches. Near real-time information and easily visible characteristics are provided by COBRA's forward-looking surveillance camera. If data links allow, transmission of mine detection data is downlinked to the ground processing station for immediate processing. If no downlink is available, video data can be extracted from an onboard cassette after the VTUAV lands."*

Also from Ref. [19], *"The COBRA system includes two down-looking, multi-spectral video cameras with overlapping fields of view for a wide swath; a forward-looking surveillance video camera; and the COBRA Tactical Information Display System (TIDS). Position and time are encoded on all video channels. Any one video channel down-linked during the mission and decoded in real time provides the position track of the aircraft plotted in real time on any digital satellite, airborne image, or digital map. The real time track, coupled with real-time, downlinked, forward-looking, surveillance video serves as a navigational aid to the aircraft pilot and the COBRA system operators during the mission. The multispectral imagery is postprocessed in the COBRA TIDS ground station that automatically coregisters the multispectral imagery from both cameras and stitches together a 1-second data set that covers an area of approximately 50 meters by 50 meters; detects mine-sized spectral anomalies; and statistically determines whether the decision area is a minefield."*

2.3.3 ScanEagle Small Tactical UAV (STUAV)

From Ref. [1], *"ScanEagle is a long endurance, low cost UA. It recently supported JFCOM's Forward Look exercises, and two systems of eight aircraft each deployed to Iraq to provide force protection for the 1st Marine Expeditionary Force (I MEF). ScanEagle carries an inertially stabilized camera turret for EO/IR imagery. Its sensor data links have integrated Cursor on Target (CoT) capability, allowing it to be interoperable with other legacy systems and enabling the operator to integrate operations with larger, high-value UA such as Predator through the ground control station. Its Skyhook (near-vertical recovery system) and pneumatic catapult launcher allow operations from ships or from remote, unimproved areas. ScanEagle's longest endurance flight aloft is 20.1 hours. A planned version will feature improved endurance of over 30 hours."*

Figure 2.3-1. UAS Classes and Timeframes.

2.4 UAS Sensing Technologies

From Ref. [1], *"Requirements for sensing payloads on UA extend not just to intelligence collection and reconnaissance surveillance and target acquisition to provide operations support, but also to weapons delivery, due to their reliance on detecting and identifying the target to meet rules of engagement (ROE) constraints and to improve aim point accuracy. The dominant requirement for sensing is for imaging (visible, infrared, and radar), followed by signals (for the SIGINT and SEAD missions), chemical (WMD), biological (WMD), radiological (WMD), meteorological (METOC), and magnetic (anti-submarine warfare (ASW) and MCM)."*

2.4.1 Dual Use and METOC Specific Sensors and Mission Areas

There are three categories of UAS METOC sensors as follows: "Dual Use" sensors are organic to the UAS platform but applicable to METOC sensing; "METOC Specific" sensors are special purpose METOC sensors that could possibly be added to the UAS platform; and "Expendable" sensors are METOC specific sensors that also require a wing pod or similar mechanism for dispensing an expendable sensor. Table 2.4.1-1 lists the UAS sensors considered in this report including sensor category, associated UAS platform, and warfare mission areas potentially impacted by METOC sensing with each sensor type.

Sensor	Category	Actual or Potential Platform	USW			AW
	Dual Use METOC Specific Expendable	BAMS VTUAV ScanEagle	MIW	SPECOPS	ASW	Various
EO/IR	D	All	X	X		
SAR/ISAR	D	All	X	X		X
Multispectral (MSI)	D	All	X	X	X	X
Hyperspectral (HSI)	M	All	X	X	X	X
LIDAR	M	No Current	X	X	X	X

Calibrated IR	M	No Current			X	
Onboard Temp	D	All				X
Onboard Humidity	M,D	All				X
Onboard Winds	D	All				X
Mini-Dropsonde	M,E	B,V			X	X
Mini-AXBT	M,E	B,V			X	
Wave Buoy	M,E	B,V	X	X		
Penetrometer	M,E	B,V	X	X		

NOTES:
1. D=Dual Use, M=METOC Specific, E=Expendable.
2. Dual Use sensors are organic to the platform but applicable to METOC sensing.
3. METOC Specific sensors are special purpose METOC sensors that could possibly be added to the UAS platform.
4. Expendable sensors are METOC specific sensors that also require a wing pod or similar mechanism for dispensing an expendable sensor.

Table 2.4.1-1. Mapping of Dual Use, METOC Specific, and Expendable UAS Sensors to UAS Platforms and Mission Areas.

2.4.2 Relevant MIW, NSW, ASW, and AW Environmental Parameters

Tables 2.4.2-1 through 2.4.2-4 list environmental parameters potentially applicable to UAS sensing for Mine Warfare (MIW), Expeditionary Warfare (EXW), Anti-Submarine Warfare (ASW), and Air Warfare (AW). Each environmental parameter listed is ranked in terms of tactical significance (H=high, M=medium, L=low) for relevant sets of ocean depths and atmospheric altitudes. The environmental parameters addressed in this study focus on the parameters with high tactical relevance, which are highlighted below in bold, red letters.

Environmental Datasets and Parameters	Domain (Surf, VSW, SW, Deep) and Importance (H, M, L)			
	Surf	VSW	SW	Deep
Seafloor				
Bathymetry	**H**	**H**	**H**	M
Sediment Grain Size	M	H	H	M
Clutter Density	M	H	H	L
Bottom Roughness	M	H	H	L
Expected Mine Burial	**H**	**H**	**H**	L
Water Column				
Currents	**H**	**H**	**H**	H/M
Water Clarity	L	H	H	H/M
Temperature and Salinity	L	M	H	H
Waves	**H**	**H**	**M**	M/L
Acoustic Properties	N/A	H	H	H

NOTES:
1. Highlighted rows are addressed in this study.
2. Surf=Surf zone of wave energy dissipation, 0-10 feet, VSW=Very shallow water, 10-40 feet, SW=Shallow water, 40-200 feet, Deep=>200 feet.
3. Bathymetry sensing leverages EO/IR, SAR/ISAR, and Hyperspectral dual use sensors plus LIDAR METOC specific sensor.
4. Wave sensing also leverages EO/IR, SAR/ISAR, and Hyperspectral dual use sensors plus LIDAR METOC specific sensor.
5. Current estimation leverages bathymetry and wave sensing plus numerical ocean modeling.
6. Mine burial estimation leverages bathymetry and wave sensing plus numerical ocean modeling plus Mine Burial Expert System burial probability estimation.

Table 2.4.2-1. Environmental Parameters Relevant to MIW (See Ref. [17]).

Environmental Datasets and Parameters	Domain (Surf, Shelf, Inlet, Harbor) and Importance (H, M, L)			
	Surf Zone	Inner Shelf	Inlets	Harbors
Seafloor				
Bathymetry	**H**	**H**	M	M
Water Column				
Currents	**H**	**H**	H	H
Tides	**H**	**H**	H	H
Water Temperature	M	M	M	M
Waves and Surf	**H**	**H**	M	L
Underwater Acoustics	N/A	H	H	H
Underwater Optics	N/A	H	H	H
Atmosphere				
EM Ducting	L	L	H	H
Visibility	M	M	H	H
Wind Speed and Direction	M	M	M	M

NOTES:
1. Highlighted rows are addressed in this study.
2. Surf zone defined to be area from beach out to extent of area with continuous wave breaks.
3. The inner shelf is the area outside of breaker zone where waves strongly impacted by bathymetry; bounded approximately by 15-meter depth contour.
4. Bathymetry sensing leverages EO/IR, SAR/ISAR, and Hyperspectral dual use sensors plus LIDAR METOC specific sensor.
5. Wave sensing also leverages EO/IR, SAR/ISAR, and Hyperspectral dual use sensors plus LIDAR METOC specific sensor.
6. Current estimation leverages bathymetry and wave sensing plus numerical ocean modeling.

Table 2.4.2-2. Environmental Parameters Relevant to NSW (See Ref. [18]).

Environmental Datasets and Parameters	Domain (Littoral, Shelf, Abyssal) and Importance (H, M, L)		
	Littoral/Straits	Shelf/Slope	Abyssal Plains
Water Column			
Ambient Noise	H	H	H
Sea Surface Temperature	M	M	M
Water Temperature vs. Depth	**H**	**H**	**H**
Water Salinity vs. Depth	**H**	**H**	**H**
Atmosphere (Periscope)			
EM Ducting	L	L	H
Visibility	M	M	H
Wind speed and direction	M	M	M

NOTES:
1. Highlighted rows are addressed in this study.
2. BAMS ISR sensing could potentially support ambient noise modeling and estimation.
3. Calibrated IR sensing could support SST measurements.
4. BAMS AXBT or x-glider deployments could potentially support temperature and salinity vs. depth measurements.

Table 2.4.2-3. Environmental Parameters Relevant to ASW (See Ref. [3]).

Environmental Datasets and Parameters	Altitude Range and Importance (H, M, L)			
	Surface to 20m	Surface to 2km	2-10km	> 10km
Temperature vs. height	**H**	**H**	M	L
Humidity vs. height	**H**	**H**	M	L
Wind speed vs. height	**H**	**H**	M	M
Visibility	H	H	H	M

NOTES:
1. Highlighted rows are addressed in this study.

2. BAMS MW sounder and/or dropsondes could support temperature, humidity, and wind soundings. 3. BAMS MFAS radar could potentially support 3D wind estimation.

Table 2.4.2-4. Environmental Parameters Relevant Air Warfare (AW).

2.4.3 BAMS Sensor Suite

Table 2.4.3-1 defines the current BAMS persistent class UAS organic sensor suite plus potential next increment METOC specific and expendable sensors that could be added to the BAMS organic sensor suite. Warfighting applications associated with each BAMS current or potential future METOC sensing capability are also listed.

UAS Platform	Sensor Suite	Category Organic Sensor METOC Sensor Expendable	METOC-Warfighting Applications
BAMS	Multi-Function Active Sensor (MFAS) Active Electronically Steered Array (AESA)	Organic	1. SAR/ISAR imaging for bathy and wave spectra sensing. 2. Doppler radar collection and assimilation of 3D winds and precipitation 3. Surface ocean currents
	Multi-Spectral Targeting System (MTS-B) EO/IR Turret	Organic	1. VSW, SW bathymetry estimation 2. Wave direction, period
	Tropospheric Airborne Met Data Reporting (TAMDAR) like system	Organic	1. Air temperature 2. Humidity 3. Horizontal winds
	Light Detection and Ranging (LIDAR)	METOC Specific	1. VSW, SW bathymetry estimation 2. VSW, SW sediment type estimation 3. Spot ocean visibility
	Hyperspectral Sensor	METOC Specific	1. Bathymetry and wave sensing
	MW Sounder	METOC Specific	1. Atmospheric sounding
	Calibrated IR Sensor	METOC Specific	1. SST
	Mini-Dropsonde	METOC Specific, Expendable	1. Air temperature 2. Humidity 3. Horizontal winds 4. Visibility
	Mini-AXBT	METOC Specific, Expendable	1. Ocean temperature vs. depth 2. Ocean salinity vs. depth
	X-glider	METOC Specific, Expendable	1. Ocean temperature vs. depth 2. Ocean salinity vs. depth
	Wave Buoy	METOC Specific, Expendable	1. Full wave spectra

NOTES:
1. Organic sensors are organic to the platform but applicable to METOC sensing.
2. METOC Specific sensors are special purpose METOC sensors that could possibly be added to the UAS platform.
3. Expendable sensors are METOC Specific sensors that also require a wing pod or similar mechanism for dispensing an expendable sensor.

Table 2.4.3-1. ID of BAMS Organic, METOC Specific, and Expendable Sensor Possibilities and Warfighting Applications.

2.4.4 Fire Scout VTUAV Sensor Suite

Table 2.4.4-1 defines the current Fire Scout VTUAV tactical class UAS organic sensor suite plus potential next increment METOC specific and expendable sensors that could be added to the Fire Scout organic sensor suite. Warfighting applications associated with each Fire Scout current or potential future METOC sensing capability are also listed.

UAS Platform	Sensor Suite	Category Organic Sensor METOC Sensor Expendable	METOC-Warfighting Applications
Fire Scout VTUAV	Maritime Multi-Mode Radar	Organic	1. Ocean imaging for bathy and wave spectra sensing. 2. Doppler radar collection and assimilation of 3D winds and precipitation
	Brite Star II EO/IR	Organic	1. VSW, SW bathymetry estimation 2. Wave direction, period
	Coastal Battlefield Reconnaissance and Analysis (COBRA)	Organic	1. VSW, SW bathymetry estimation 2. Wave direction, period
	Joint Multi-Mission Electro-Optical System (JMMES)	Organic	1. VSW, SW bathymetry estimation 2. Wave direction, period
	Air Temperature Sensor	Organic	1. Atmospheric sounding via ascent/descent collections
	Wind Speed Sensor	Organic or METOC Specific?	1. Atmospheric sounding via ascent/descent collections
	Humidity Sensor	METOC Specific	1. Atmospheric sounding via ascent/descent collections
	Calibrated IR Sensor	METOC Specific	1. SST
	Mini-Dropsonde	METOC Specific, Expendable	1. Air temperature 2. Humidity 3. Horizontal winds 4. Visibility
	Mini-AXBT	METOC Specific, Expendable	1. Ocean temperature vs. depth 2. Ocean salinity vs. depth
	X-glider	METOC Specific, Expendable	1. Ocean temperature vs. depth 2. Ocean salinity vs. depth
	Wave Buoy	METOC Specific, Expendable	1. Directional wave spectra

NOTES:
1. Organic sensors are organic to the platform but applicable to METOC sensing.
2. METOC Specific sensors are special purpose METOC sensors that could possibly be added to the UAS platform.
3. Expendable sensors are METOC Specific sensors that also require a wing pod or similar mechanism for dispensing an expendable sensor.

Table 2.4.4-1. ID of Fire Scout Organic, METOC Specific, and Expendable Sensor Possibilities and Warfighting Applications.

2.4.5 ScanEagle Sensor Suite

Table 2.4.4-1 defines the current ScanEagle small tactical class UAS organic sensor suite plus potential next increment METOC specific and expendable sensors that could be added to the

Scaneagle organic sensor suite. Warfighting applications associated with each ScanEagle current or potential future METOC sensing capability are also listed.

UAS Platform	Sensor Suite	Category Organic Sensor METOC Sensor Expendable	METOC-Warfighting Applications
ScanEagle STUAS	EO/IR Turret	Organic	1. VSW, SW bathymetry estimation 2. Directional wave spectra
	Nano-SAR (Optional sensor)	Organic	1. SAR imaging for bathy and wave sensing.
	Air Temperature Sensor	Organic?	1. Atmospheric sounding via ascent/descent collections
	Wind Speed Sensor	Organic?	1. Atmospheric sounding via ascent/descent collections
	Humidity Sensor	METOC Specific	1. Atmospheric sounding via ascent/descent collections
	Multispectral Imager	METOC Specific	1. Bathymetry and wave sensing
	Hyperspectral Imager	METOC Specific	1. Bathymetry and wave sensing
	Calibrated IR Sensor	METOC Specific	1. SST
	Mini-AXBT?	METOC Specific, Expendable	1. Ocean temperature vs. depth 2. Ocean salinity vs. depth

NOTES:
1. Organic sensors are organic to the platform but applicable to METOC sensing.
2. METOC Specific sensors are special purpose METOC sensors that could possibly be added to the UAS platform.
3. Expendable sensors are METOC Specific sensors that also require a wing pod or similar mechanism for dispensing an expendable sensor.

Table 2.4.5-1. ID of ScanEagle Organic, METOC Specific, and Expendable Sensor Possibilities and Warfighting Applications.

2.5 Potential for UAS METOC Data Collection and Exploitation

From the Committee on Environmental Information for Naval Use, of the National Research Council, see Ref. [3], *"The availability of unmanned airborne vehicles (UAVs) and unmanned underwater vehicles (UUVs), and their expanded capability to covertly collect intelligence, surveillance, and reconnaissance information in denied areas using a variety of electro-optical (EO) and acoustic sensors, creates a largely untapped potential for the unintended use of such information to support the development or validation of METOC products or forecasts.* ***The Oceanographer of the Navy and the Commander of Naval Meteorology and Oceanography Command (CNMOC) should work with the broader community within the U.S. Department of Defense (DOD) and elsewhere to expand efforts to make intelligence, surveillance, and reconnaissance information and data with environmental content more accessible to the METOC community.****"*

Also from Ref. [3], *"The U.S. Marine Corps' traditional role in expeditionary warfare and renewed focus on littoral operations involving the U.S. Navy continue to drive the need for environmental information in coastal areas where access is frequently denied. Efforts to improve secure, low-profile communications, reduce the risk to personnel in coastal areas from chemical and biological agents (either from the tactical deployment of weapons of mass destruction by enemy forces or the destruction of such weapons by friendly forces), and provide accurate assessments of atmospheric conditions during the planning and implementation of*

strike missions have placed a greater emphasis on coastal meteorology. This includes development of predictive meteorological capability at fine scales and intensive data gathering in coastal environments. Military operations in these areas require data in forward operations areas. UAVs are ideally suited for this and provide additional opportunity for data gathering on behalf of METOC. ***The Office of the Oceanographer of the Navy should work with the Space and Naval Warfare Systems Command (SPAWAR) and the operational commands to further develop and deploy atmospheric sensors on UAVs that will permit the collection of essential environmental information without impairing the intelligence, reconnaissance, or surveillance efforts they are largely designed to carry out.****"*

Also from Ref. [3], *"Strike warfare involves the use of combat aircraft, cruise missiles, and (as recently demonstrated in Afghanistan) armed unmanned aerial vehicles (UAVs) to (1) penetrate an adversary's defenses from the air, (2) deliver precision ordnance on either fixed or mobile targets, and (3) assess battle damage while ensuring a safe return to the base of operations. In the context of naval strike warfare, this means air operations from aircraft carriers or ship-launched cruise missiles. Increasingly, there is recognition that many strike missions (especially those targeting mobile or opportunistic targets) have a time-critical dimension such that weapons systems must be selected and delivered precisely on target with a very short decision cycle. Such time-critical assaults require near real-time environmental information from battlefield sensors, and these data must be processed and disseminated from the sensors to the weapons system within minutes. Such rapid target identification, location, and destruction place extraordinary demands on METOC capabilities. Factors affecting tactical and time-critical strike missions include precise target identification and location, EM-EO ducting, winds aloft, winds-at-target, vertical wind shear, atmospheric turbulence, aerosols, humidity, precipitation, slant-range visibility, cloud cover, cloud ceiling, precipitation, weather fronts, severe weather, icing conditions aloft (for UAVs), space weather (if relying on direct GPS communication), atmospheric refraction effects, atmospheric scintillation, forecast along flight path and for duration of strike operations, precipitation rate, characteristics of surface and near surface clutter."*

Also from Ref. [3], *"Environmental information for undersea warfare primarily concerns understanding how the ocean impacts acoustic propagation and the design and performance of Navy sonar systems. Sonars are usually divided into passive, which exploits radiated sound from a source, or active, which uses echoes to resolve the range and Doppler shift of a source. Support for both passive and active antisubmarine warfare (ASW) missions dominated funding for environmental characterization during the Cold War. It still does, but with the emphasis now on littoral waters instead of the historic focus on deep water. Moreover, the shift of Navy missions toward the littoral has placed increased emphasis on mine countermeasure (MCM) systems as well as torpedoes."* Ref. [3] continues, *"The platforms specifically relevant to undersea warfare can be divided as follows: submarines, surface ships, aircraft, and surveillance systems. Furthermore, the missions of each can be listed: for submarines, self-defense, ASW, antisurface warfare, ISR (intelligence, surveillance, and reconnaissance), CVBG (carrier battle group escort), Naval Special Warfare and deployments, clearing contested areas and commercial shipping routes, and forward strike (cruise missile launching). The undersea warfare for surface ships, typically cruisers and destroyers, concerns self-defense, ASW, and CVBG escort. Aircraft, both maritime patrol aircraft and helicopters, are almost solely concerned with ASW operations. Similarly, the Integrated Undersea Surveillance System, including fixed assets such as the remnants of the SOSUS system, the ADS advanced deployable*

system, the fixed deployable system, and SURTASS (Surveillance Towed Array System) are concerned with both ASW and commercial ship surveillance." Accordingly, the opportunity for UAS METOC sensing in support of ASW includes the use of expendable bathythermographs (BTs) for temperature and salinity profiling and possibly the use of calibrated infrared (IR) sensors for sea surface temperature (SST) measurements.

2.6 OPNAV UAS METOC Sensing Priorities

CNO N84 (Oceanographer of the Navy) and CNO N81 (Warfare Assessments and Analysis) were consulted to determine Navy UAS METOC sensing priorities. The feedback received in response is summarized below in Figure 2.6-1, which shows these priorities and how they map into a set of proposed mission areas or tactical situations (TACSITs). Four TACSIT areas are considered in this report as follows: (1) expeditionary warfare, rapid insertion, and amphibious warfare; (2) mine hunting and clearance; (3) anti-ship cruise missile defense and straits transit; and (4) ASW search and screen. The results of these analyses are presented below in Sections 5.2 through 5.5.

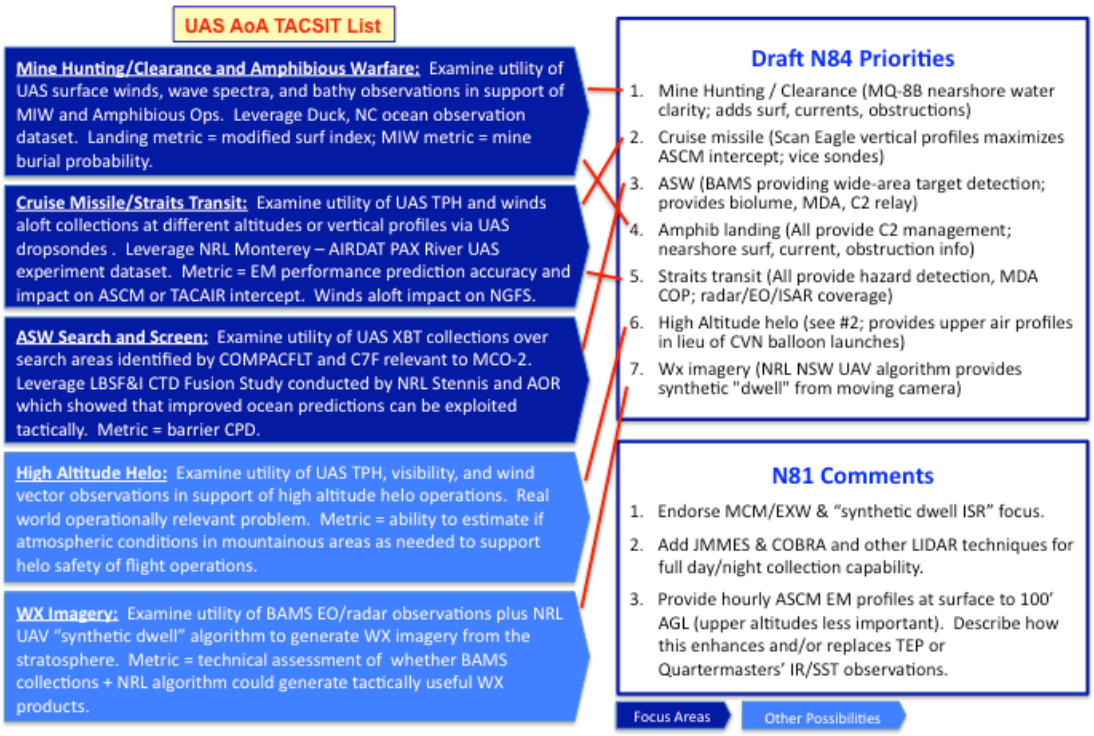

Figure 2.6-1. Mapping of N84/N81 Priorities to Selected TACSITs.

3.0 METOC Data Collection Requirements

This section captures relevant atmospheric, littoral ocean, and beach zone METOC data collection requirements in terms of the parameters to be collected and associated required accuracies and spatial/temporal resolutions. Given a specific tactical situation or mission, it is often possible to be more precise about METOC sensing requirements. Methodologies for capturing mission specific requirements are also discussed in this section.

3.1 Atmospheric METOC Sensing

Environmental satellites and aircraft carry various types of remote- and aircraft-based sensing instruments for gathering data from the Earth's surface and atmosphere, but the primary sensors fall into one of two categories: imagers and sounders.

Optical imagers provide images of the Earth's surface and cloud cover. These images are derived from radiation samples collected from the Earth and its atmosphere. The satellite or aircraft imager collects radiation samples as it scans the earth, and then directs the radiation to a radiometer that measures its intensity. These radiation measurements are digitized and communicated to METOC production centers. Each scan of the imager produces a line of samples and successive lines are collected to produce a line-by-sample swath of data.

Imagers measure radiation at several specific bandwidths of the spectrum, filtering out other wavelengths. Each bandwidth is referred to as a channel. Different types of satellite and aircraft imagers have different channels, but all have at least one channel that measures visible radiation (reflected sunlight) and at least one channel that measures IR radiation (radiated heat emitted by all objects on Earth). Visible light is usually measured in percent albedo (a measure of brightness or reflectance) and IR radiation is converted to a temperature measurement. Since visible images require sunlight, they are usually available only during the daylight portion of a satellite's orbit. Satellites and aircraft can produce IR images during both daylight and nighttime hours.

Microwave imagers, such as radar, transmit microwave signals to the Earth's surface and measure the reflected signal. Once the radar has emitted a microwave signal, the power reflected by the objects hit by the signal is measured. This is called the backscatter. The rougher the object is the higher amount of backscatter it creates, which produces a brighter image. For example, cities are very rough surfaces and appear generally very bright. Smoother objects appear darker, so a calm sea would appear dark. The microwave signal penetrates clouds, so the satellites can acquire images regardless of current weather conditions and during both day and night.

Sounders. In addition to imagers, many weather satellites and aircraft carry one or more instruments known as sounders. The sounder collects data samples from different levels of the atmosphere to provide a three-dimensional array of atmospheric measurements of conditions such as pressure, temperature, and humidity. These data are communicated back to METOC production centers where they can be processed into meteorological overlays that can be superimposed on, for instance, other received optical or microwave images.

Table 3.1-1 shows generic atmospheric collection requirements in terms of relevant environmental parameters, required parameter accuracy and required spatial/temporal resolution.

Parameter – Region Accuracy Space Resolution Time Resolution	Applicable Altitudes			
	Surface to 20 m	**Surface to 2 km**	**2 to 10 km**	**Greater than 10 km**
Temperature	±0.2°C Surface & Elev Pt 1 Minute	±0.5°C 50 Meters 15 Minutes	±1.0°C 200 Meters 60 Minutes	±2.0°C 500 Meters Infrequent
Water Vapor	±0.05g/kg (~0.5%) Elevated Point 1 Minute	±0.1 g/kg (1-2%) 50 Meters 15 Minutes	±0.2g/kg(1-10%) 200 Meters 60 Minutes	No Requirement No Requirement No Requirement
Aerosol Extinction	+/- 0.01 km^{-1} Elevated Point 1 Minute	+/- 0.02 km 50 Meters 15 Minutes	+/- 0.05 km 200 Meters 60 Minutes	No Requirement No Requirement No Requirement
Wind Velocity	+/- 0.2 m/s Elevated Point 1 Minute	+/- 0.5 m/s 50 Meters 15 Minutes	+/- 1.0 m/s 200 Meters 60 Minutes	No Requirement No Requirement No Requirement

Table 3.1-1. Upper Air Data Collection Requirements.

3.2 Littoral Ocean METOC Sensing

COMINEWARCOM[1], the Commandant of the Marine Corps, and the Naval Research Laboratory (NRL) (see Refs. [12]), have defined data type and accuracy requirements for oceanographic data collections in support of Naval littoral warfare. The general requirements are as follows:

- Horizontal spatial resolution: The area of coverage is from the shoreline to 60 nautical miles seaward and/or area of activity (AOA). The horizontal spatial resolution is 100 meters (~ 3.24 arc seconds).
- Temporal refresh rate: Updates of dynamic data occur every 12 hours.
- Bioluminescence sources: Specify at depth, by type and strength of illumination (the documents do not quantify what "strength of illumination" means).

Table 3.2-1 specifies the remaining requirements and identifies data with minimum requirements that exceed those listed above.

Data Type	Accuracy	Additional Coverage Requirements
Bathymetry	± 2% of depth or ± 2 meters, whichever is smaller	
Water Column Temperature	± 1°C	Vertical: Specified at surface and bottom.
Water Column Salinity	± 3 parts per thousand	Vertical: Specified at surface and bottom. Temporal: 6 hours
Electrical Conductivity	± 0.1 millimho/cm	Temporal: 6 hours
Sound Speed Profile	± 3 m/s	Vertical: Specified at surface

[1] Now merged into Naval Mine and Anti-Submarine Warfare Command (NMAWC) as of 1 October 2006.

		and bottom.
Sea Swell / Wave Height	± 0.5 m, given in 5° increments	
Prevailing Currents and Drift	± 0.1 knots, given in 5° increments	Vertical: Specified at surface and bottom.
Tides	± 0.5 m	Temporal: 15 minutes
Ice Edge	± 0.5 km	Temporal: 15 minutes
Surf	± 0.1 knots, given in 5° increments	
Turbidity	± 0.3 m, omni-directional	
Bottom Reverberation, Back Scatter, and Bottom Loss	± 0.2 dB	
Bottom Pressure Fluctuation	± 0.1 cm	
Ambient Noise Level	± 3 dB from 5 to 40 kHz in 1/3 octave bands	
Measured Transmission Loss (i.e. Acoustic Scattering and Reverberation)	± 2 dB	

Table 3.2-1. Littoral Ocean METOC Sensing Requirements.

3.3 Near-Shore, Beach Zone Sensing

Near-shore, beach or surf zone sensing requirements are defined by Navy surf observation (SUROB) and Modified Surf Index (MSI) calculation procedures. The Modified Surf Index or MSI is a single dimensionless number that provides a relative measure of the conditions likely to be encountered in the surf zone. For the reported or forecast conditions, the MSI provides a guide for judging the feasibility of landing operations for each type of landing craft. When applied to a known or forecast surf condition, the MSI calculation provides the commander with an objective method of arriving at a safe and reasonable decision with respect to committing landing craft and amphibious vehicles. Table 3.3-1 shows generic near-shore, beach or landing zone collection requirements in terms of relevant environmental parameters, required parameter accuracy and required spatial/temporal resolution.

Data Type	Accuracy
Wave Height	Average wave height of 100 consecutive waves to nearest 0.5 feet.
Significant Wave Height	Average wave height of the highest 33 of 100 consecutive waves to nearest 0.5 feet.
Maximum Wave Height	Maximum wave height of 100 consecutive waves to nearest 0.5 feet.
Wave Period	Total time elapsed while observing 100 consecutive

	waves, divided by 100, to the nearest 0.5 seconds.
Wave Type	Percentage of spilling[2], plunging[3], and surging[4] waves.
Wave Angle	Wave angle is the angle the wave makes with the beach, as seen from the landing craft's perspective. Recorded as moving toward either the right or left flank.
Littoral Current	Speed of the current that moves parallel or adjacent to the shoreline in knots to the nearest 0.1 knot.
Size of Surf Zone	Width of the surf zone, which extends from the outermost breaker to the limit of the uprush on the beach, in feet.
Bathymetry	Measured to within + 2% of depth or + 2 meters, whichever is smaller.

Table 3.3-1. Near-Shore, Beach Zone METOC Sensing Requirements.

3.4 Mission Area Specific METOC Sensing Requirements

Given a specific tactical situation or mission, the atmospheric, littoral ocean, and beach zone METOC data collection requirements discussed above can often be made more precise as discussed further below. Scientific, engineering, and performance metrics can be defined in a manner that leads to a process for translating BonD Tier 1 environmental uncertainties to corresponding BonD Tier 2 system performance uncertainties, to corresponding BonD Tier 3 performance or operational effectiveness related uncertainties. In this way it is possible to trace back Tier 3 operational requirements to Tier 2 system performance prediction resolution and accuracy requirements to Tier 1 environmental characterization resolution and accuracy requirements.

Scientific Metrics capture the degree to which a physical property can be measured, predicted, and/or forecast. E.g. how well can the ocean temperature and salinity field be nowcast or forecast over a grid of ocean locations and depths? Environmental spatial and temporal variability, and the degree to which the underlying physics can be modeled or represented in data are drivers of these scientific metrics. These metrics hence are designed to answer the question, *How well is the underlying atmosphere/ocean physics understood?*

Engineering Metrics capture the resulting ability to estimate or predict system performance. E.g. given one's ability to nowcast or forecast ocean surface, water column, and bottom/sub-bottom conditions, how well can one estimate detection range for a specific sonar, sonar operating mode, threat, and threat operating mode? These metrics are hence designed to answer

---

[2] **Spilling** waves break gradually over a distance. White water forms as they crest and expands down the face of the breaker. Only the top portion of the wave curls over however. Light foam may wash gently up the shore. This type of wave is normally found with a flat bottom beach. It is usually the most observed type of wave.

[3] **Plunging** waves peak up and form an advancing vertical wall of water. The crest advances faster than the base of the breaker, curls, and then descends violently into the trough. This type of breaker sometimes causes an explosive sound as trapped air escapes behind the wave. It is usually found on a medium to steep sloping beach, with little wind or an offshore wind.

[4] **Surging** waves advance at the same rate as the base of the breaker, they surge up the beach as a wall of water. They may or may not be accompanied by white water, and are usually found on very steep beaches.

the question, *How does understanding of the underlying atmosphere/ocean physics translate to system performance prediction capability?*

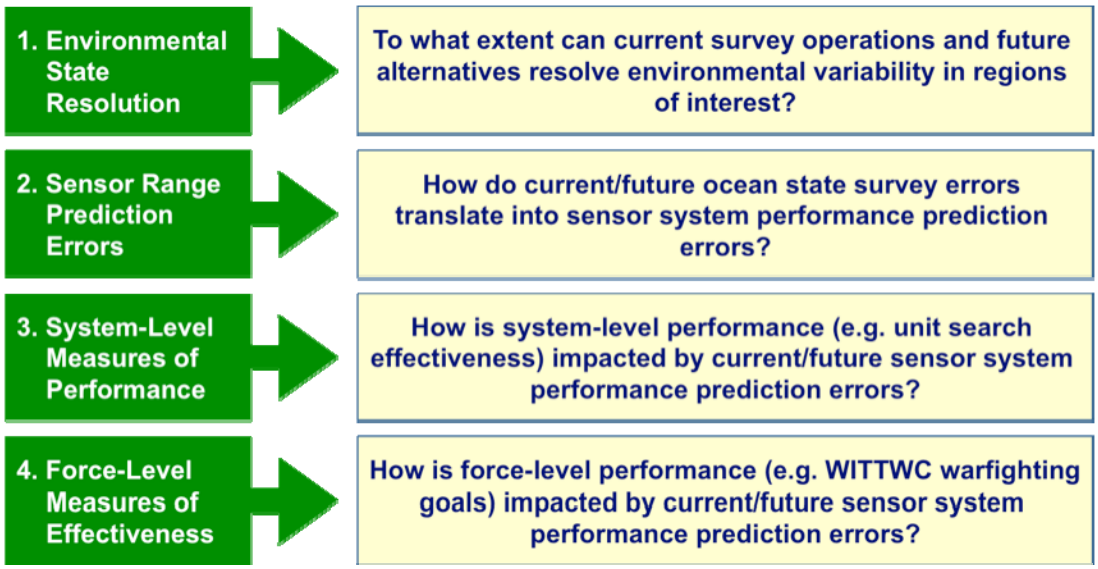

Figure 3.4-1. Effectiveness Analysis Approach.

Performance Metrics capture the resulting degree to which warfighting effectiveness is impacted. E.g. given one's ability to estimate sonar detection range as a function of searcher, target, and environmental state, what levels of operational effectiveness can be expected for relevant friendly and threat assets and missions? These metrics are hence designed to answer the question, *How does system performance prediction capability translate to operational effectiveness?*

To map scientific metrics to engineering to operational metrics, the four-step process pictured in Figure 3.4-1 is employed. First, comparisons are made between the assumed ground truth environment and the nowcast of forecast environment, providing scientific metrics. Second, system performance parameters (e.g. sonar detection ranges) computed using the ground truth environment are compared to those computed using a predicted environment over relevant sets of system configurations, tactical geometries, and environments, providing engineering metrics. Thirdly and fourthly, ground truth system performance and estimates of system level performance given the expected levels of environmental uncertainty are used as inputs to operations research optimal planning algorithms to compare system-level and force-level warfighting effectiveness respectively in the absence of environmental uncertainty vs. effectiveness when expected uncertainties are accounted for, providing performance metrics.

4.0 Ocean Sensing Feasibility Analysis

4.1 Overview and Analysis Objectives

The objective of the ocean sensing feasibility analysis reported here is to establish via simulation and physical modeling the feasibility of using UAS platforms and associated tactical dual use optical, radar, LIDAR, and multi/hyperspectral sensors to sense littoral bathymetry, ocean wave spectra, and other relevant ocean properties. The results of this simulation and modeling has been used to determine likely bathymetry and wave spectra estimation errors as a function of UAS platform and sensor characteristics, specific ocean littoral areas of interest, and UAS employment concepts of operation (CONOPs). The results of this analysis are directly supportive of the objectives of the Expeditionary Warfare, Rapid Insertion, and Amphibious Landing and Mine Hunting and Clearance TACSIT analyses described below in Sections 5.2 and 5.3.

The high number of possible UAS platform and sensor configurations and employment CONOPs that could be used for UAS METOC sensing complicates this analysis. For example, there are a range of flight altitudes and slant distance to target settings that could be chosen for a variety of sensors supporting any particular mission. To the extent feasible, we have reduced the number of possibilities by limiting consideration to planned flight scenarios for sensors defined for use with BAMS, VTUAV, and ScanEagle (to the extent that these are known). Confirmation of the simulation and modeled results presented here via real world experimentation will eventually be required.

Dr. Todd Holland of NRL Stennis, Code 7400 and Dr. Chris Wackerman of General Dynamics Advanced Information Systems are the lead analysts for the ocean sensing feasibility analysis reported here. Doug Backus and Eduardo Danganan of NAVAIR provided relevant UAS platform and sensor system characteristics and performance (C&P) data required by this sensor feasibility analysis.

4.2 Ocean Sensing Applications

Two main ocean sensing applications are considered in this UAS METOC Sensing AoA; estimation of frequency-directional ocean wave spectra from wave-resolving remotely sensed image sequences and shallow water bathymetry estimation via inversion based on the linear, finite-depth, dispersion equation for surface gravity waves. The two estimation techniques are summarized briefly below.

4.2.1 Bathymetry Estimation

From Holland (Ref. [4]), *"Remote sensing methods have been developed to estimate bathymetry through the use of a theoretical relationship between wave speed and water depth known as the linear, finite depth, dispersion equation for surface gravity waves. The authors describe a validation effort encompassing several hundred observations of wavenumber magnitude for sea-swell frequencies obtained over a wide variety of conditions to investigate possible error sources resulting from the practical application of this relationship. These wavenumber estimates were computed from pressure gauge signals using signal processing algorithms that can be equivalently applied to measurements of wave phase as imaged through remote sensors. The major goal was to determine the accuracy of the dispersion relation while*

attempting to minimize errors associated with sensor positioning, tidal variations, and Doppler shifts due to mean currents. For water depths outside the surf zone, the linear dispersion relation is highly accurate, with average depth estimation errors on the order of 3-9% of the observed depth. In shallower regions, nominally less than 4 m for this field site, where wave breaking is evident and nonlinear shoaling effects are more pronounced, normalized depth errors of over 50% were commonly observed with most predictions being deeper than observations. Strong correlation between these bias errors and measured wave heights emphasizes the importance of accounting for wave amplitude in the calculation of shallow water phase speeds for depth estimation. A simple depth correction is provided to allow for bathymetry estimation within the surf zone." These statements are critical to the feasibility of determining bathymetry via remote sensing.

Again from Holland (Ref. [4]), "*remotely sensed measurements of surface wave processes have been used since WorldWar II to indirectly infer bottom depths based on changes in observable wave characteristics, such as the shortening of waves as they shoal. Most of these applications rely on a simple, theoretical relationship between wavelength, period, and water depth, that is most commonly expressed as the linearized version of the finite depth, dispersion equation for surface gravity waves:*

$$\sigma - uk = \sqrt{gk \tanh(kh)}$$

where

σ = *radial frequency = 2π/T,*
k = *wavenumber magnitude = 2π/L,*
h = *water depth,*
T = *wave period,*
L = *wavelength,*
u = *mean current magnitude, and*
g = *acceleration due to gravity."*

Note that this equation can be solved directly for h, given values of u, σ, and k, using the inverse relation:

$$h = \frac{1}{k}\tanh^{-1}\left(\frac{(\sigma - uk)^2}{gk}\right).$$

Having a theoretical relationship for depth dependence upon wavenumber allowed a simulation tool to be developed to estimate the quality of bathymetric surfaces produced for each of a set of UAS remote sensing scenarios. Empirical relations between wavenumber estimation and motion imagery collection parameters (see Refs. [4]-[6]) have been employed to simulate bathymetry survey accuracy (% bathymetry or water depth error), resolution (horizontal spacing between consecutive bathymetry estimates), coverage (horizontal extent of survey area or patch), and dwell (time required to orbit the survey area once) for the following remote sensing variables:

- Survey platform altitude and speed,
- Grazing angle and horizontal field of view,
- Number of horizontal and vertical pixels,

- Number of desired bathymetry estimates,
- Typical local water depth, and
- Typical local wavelength.

The results of this simulation are used to assess the likely bathymetry sensing capabilities (expressed in terms of accuracy and resolution) of various logical UAS platform and sensor combinations in near-shore areas of interest.

4.2.2 Wave Spectra Estimation

From Hwang and Sletten (Ref. [20]), *"The close correlation of ocean surface waves and radar backscatter has been recognized since the early days of radar development [e.g., Crombie, 1955]. The main scattering mechanisms of radar sea returns were clarified by a series of theoretical and experimental research [e.g., Wright, 1966, 1968]. By the mid-1980s, extraction of wave spectral information reaches essentially a mature stage as reflected in the sophisticated 3-D spectral analysis of Young et al. [1985]. The results show convincingly that aside a scaling factor of the modulation transfer function (MTF), the wave-number-frequency spectrum derived from the spatiotemporal images of radar backscattering intensity is essentially the ocean surface wave spectrum. Excellent agreement in wave period and wave propagation direction is illustrated. The 3-D spectral processing technique continues to generate exciting results of spatial and temporal evolution of ocean surface waves [e.g., Dankert and Rosenthal, 2004]. The extensive information contained in the 3-D spectrum can even be used to derive the current velocity vector and bathymetry through the dispersion relation [Young et al., 1985; Trizna, 2001]. The issue of MTF relating the radar backscattering intensity to surface wave height is a much more difficult problem because the magnitude and phase of MTF are influenced by many factors, including the radar wavelength, look angle, look direction, slope of surface roughness spectrum, long wave period and direction, surface currents, wind speed, and wind direction [e.g., Alpers and Hasselmann, 1978; Plant et al., 1978, 1983, 1987; Plant, 1986; Thompson and Gasparovic, 1986; Hwang and Shemdin, 1990], although some simplified parameterizations have been suggested for operational application [e.g., Dankert and Rosenthal, 2004; Nieto Borge et al., 2004]."*

A synthetic aperture radar (SAR) adds an additional layer of complexity versus a real-aperture radar. A SAR generates its fine azimuth resolution by using the change in range between the scatterer and the radar to uniquely locate the scatterer in azimuth. Although this generates high-resolution imagery, it has the disadvantage that unknown scatterer motion cause smearing and shifting in the resulting SAR image. For the case of ocean surface waves, these effects manifest themselves in two ways. First, the constant, random surface motion of the small-scale waves (which are the actual radar scatterers on the ocean surface) coupled with their short coherency times result in smearing in the ocean image. In general this smearing can be modeled as multiplying the Fourier transform of the SAR image with a bandpass function of the form:

$$F(k_x) = \exp\left[-\frac{1}{2}\left(k_x \frac{R}{V}\sigma_v\right)^2\right]$$

where k_x is the azimuth wavenumber, R is the range from the SAR to the ocean surface, V is the velocity of the SAR, and σ_v is the standard deviation of radial velocities of random surface motions of the small-scale waves. Note that this is only a function of azimuth wavenumber and

thus results in smears in the azimuth direction only. The parameter σ_v varies based on local environmental conditions and is usually in the range of 0.2 (low winds) to 0.4 (high winds). In terms of imaging surface wave spectra, this smearing has the effect of bandpassing the wave spectra and removing energy from the waves whose wavelengths are shorter than approximately (R/V) σ_v in the azimuth direction. This implies that the reduction of wave spectrum energy can significantly depend on the look direction of the SAR with respect to the dominant waves. If the dominant waves are mainly range traveling (so that $k_x = 0$) then this will have little effect. If the dominant waves are mainly azimuth traveling (so k_x is at its maximum), then this can remove significant energy from the wave spectrum as imaged by the SAR.

The second effect is often referred to as velocity bunching. This effect is caused by the motions of the ocean surface induced by the passage of the long-scale waves – which essentially cause the ocean surface to bob up and down. Motion of the ocean surface toward the radar causes the scatterer to be shifted in one direction in the SAR image, while motion away from the radar causes shifts in the opposite direction, both by and amount $(R/V)V_r$ where V_r is the radial velocity of the ocean surface motion. The overall result of this is to cause the SAR image of ocean waves to have "peaked" waves versus more normal sinusoidal waves, and to cause a slight rotation of the dominant wave direction toward the radar range direction. This effect mostly re-arranges energy within the wave spectra versus removing energy.

Thus to first order we can simulate the effect of a SAR system on wave spectral energy by apply the bandpass above based on the SAR imaging geometry (i.e. the look direction of the SAR versus the dominant wave direction) and the local wind conditions (to determine the value of σ_v). This will capture most of the energy loss due to the SAR imaging effects; what it leaves out is the velocity bunching effect that can re-arrange energy within the spectrum. Note that a SAR is also a radar, and thus there is also a bandpass in the range direction due to the range resolution of the radar. That is, the radar will remove wave spectra energy for all waves whose range wavelength is less than twice the range resolution.

Thus the simulation we performed for the SAR images of wave spectra was to apply a bandpass to the original wave spectra that removed energy for all waves whose azimuth wave lengths was smaller than (R/V) σ_v and whose range wavelength was smaller than 2*(range resolution). Since the effect of this bandpass on the wave spectral energy depends on the look direction of the SAR and the local wind, we generate four simulation sets. We used two SAR look directions; (1) looking in the same direction as the dominant wave was propagating (this was called the "best" radar look direction since it minimizes the spectral energy loss due to the random motion of the ocean surface); and (2) looking orthogonal to this direction (this was called the "worst" radar look direction since it maximizes the loss of spectral energy). We also used two wind regimes: (1) a low wind regime where $\sigma_v = 0.2$; and (2) a high wind regime where $\sigma_v = 0.4$.

In this study we have employed a General Dynamics, Advanced Information Systems synthetic aperture radar (SAR) model to represent the likely ability of the BAMS Multi-Function Active Sensor (MFAS) to estimate wave spectra. The results are discussed below in Section 4.3.2. These results are also reflected in the EXW/NSW and MIW TACSIT analyses presented below in Sections 5.2 and 5.3.

4.3 Ocean Sensor Technologies

The sections below identify the UAS platform and sensor options considered here along with relevant sensor wave spectra and bathymetry estimation capabilities based on the estimation methodologies discussed above.

4.3.1 Optics

The UAS platforms and optics/radar sensors considered in this study are listed below in Table 4.3.1-1. Also listed are UAS platform maximum altitude, endurance, range, and maximum payload for each. Also listed is an assessment of likely sensing capability denoted by "B" for bathymetry sensing and a "W" for wave spectra sensing.

A bathymetry sensing simulation was developed based on methodologies described in Ref. [4], and an illustrative model output is shown in Figure 4.3.1-1 for a ScanEagle UAS flying at an altitude of 1500 meters. This simulation result shows ScanEagle bathymetric errors for wide field-of-view lens (20°) on gimbaled turret pointing at a constant in-water target location. The spatial coverage of the assumed imaged area (based on the slant range offset and lens field-of-view) is approximately 128 x 128 meters. Larger fields-of-view (or higher altitudes) will increase coverage, but will also eventually decrease the imaging resolution below what is required to observe wave crests (in our case, nominally 4 m). For this particular example, considerable improvement in accuracy results for orbits with dwells over the target on the order of at least 200 seconds.

UAS Platform	UAS Sensors	Max Altitude [ft]	Endurance [hr]	Range [nm]	Max Payload [lbs]	Likely Sensing Capability*
SilverFox	EO/IR Gimbal	10,000	10	20	6	B
ScanEagle (~STUAS)	EO/IR Turret nanoSAR	16,400	15+	60	13.2	B/W
Manta	EO/IR PTZ	16,000	5	20	15	B
FireScout	EO/IR/ Radar	20,000	8	150	600	B/W
BAMS / Global Hawk	EO/IR/ SAR/ISAR	60,000	30	5400	3000	B/W
Reaper	EO/IR/ SAR	50,000	24	1655	3750	B/W

Table 4.3.1-1. Relevant UAS Platforms and Optics/Radar Sensors.

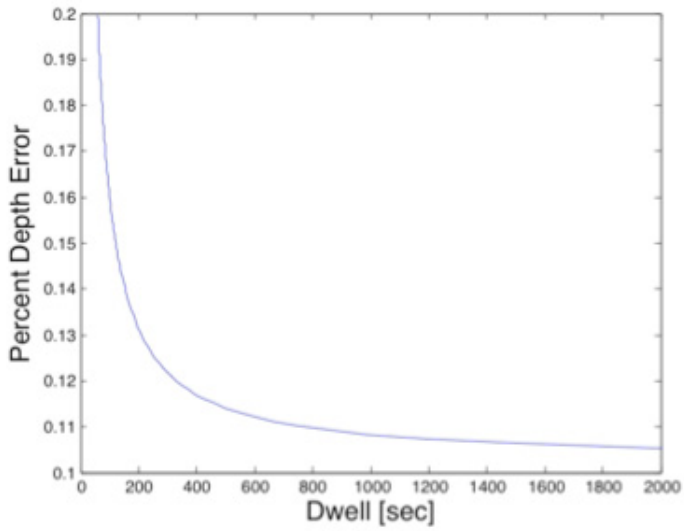

Figure 4.3.1-1. Bathymetry Error vs. Dwell Time (for ScanEagle flying at 1500 meters).

Table 4.3.1-2 shows the results of bathymetry sensing simulation model runs for ScanEagle, Fire Scout (VTUAV), and BAMS. This table shows the assumed flight altitude and speed for each UAS option plus simulated bathymetric error (in units of percent depth error), sounding spacing in feet, and time required to survey 1 square kilometer in minutes. In these runs it is assumed that a wide field-of-view lens (20°) is available on gimbaled turret to stare at a specific offshore target during a circular orbit flight path with 45° graze. NAVAIR info indicates that the BrightStar II EO payload planned for VTUAV has a WFOV of 30 degrees and the MTS-B turret planned for BAMS has a WFOV camera also of 30 degrees. Note however that EO lenses typically used as spotters for detection may have much narrower field-of-view (~2°). In the ScanEagle and Fire Scout cases, the camera used is assumed to be an analog imager with a pixel resolution of approximately 720x480, whereas the BAMS sensor has approximately twice that resolution, equivalent to "high-definition" (HD) video.

UAS Platform	EO Sensor	Flight Altitude [ft]	Flight Speed [knots]	Bathymetric Error [%]	Sounding Spacing [ft]	Time to survey 1 km² [min]
ScanEagle (~STUAS)	Turret w/ SD Video	4921	50	8.5	53	102
FireScout	Turret w/ SD Video	9842	100	5.5	105	25
BAMS / Global Hawk	Turret w/ HD Video	14,764	150	4.5	159	11

Table 4.3.1-2. ScanEagle, Fire Scout, and BAMS Bathymetry Simulation Results.

Several notes apply to the results presented in Table 4.3.1-2 as follows:

1. Dwell times are a function of UAS flight speed. It is the amount of time that the UAS takes to orbit the aimpoint at the particular altitude and graze angle.
2. The accuracy and sounding spacing are (inversely) tied together. Higher altitude UAS platforms (for a given camera/lense combination) can image a larger domain with reduced bathymetric error (but increased sounding spacing). We can also change the dwell (via the altitude and flight speed), which will similarly impact the accuracy (longer dwell times result in higher accuracy).
3. We also assumed a 20-degree horizontal field of view for all the cameras (and a 45 degree slant angle). NAVAIR info suggests that is not typical for many systems, which have spotter scopes to maintain high pixel resolution (or NIRS) at long standoff. However NAVAIR info indicates that the BrightStar II EO payload planned for VTUAV has a WFOV of 30 degrees and the MTS-B turret planned for BAMS has a WFOV camera also of 30 degrees. Hence the 20-degree assumption should be conservative.

4.3.2 Radar

As discussed above, coupled video estimation of wave direction and period, along with radar estimation of the full wave spectra including wave height, is expected to produce enhanced bathymetry inversions and enhanced subsequent estimation of MSI and mine burial probabilities. General Dynamics (GD) has put together a simulation system for generating synthetic aperture radar (SAR) images of the ocean surface. The paragraphs that follow provide an overview description of this SAR simulation system and the validation that has been performed with the resulting imagery.

As mentioned in the SAR simulation model, the dominant impacts of a SAR imaging sensor on wave height estimation are the bandpass of the wave spectra data caused by the motion of the small-scale waves on the ocean surface, and the re-arranging of spectral energy to different wavelength caused by the motion of the large-scale waves. Measures of wave height spectral energy (such as significant wave height) are dominantly effect by the bandpass since it can eliminate large amounts of the wave spectral energy from the SAR image of the waves, whereas the re-arranging of spectral energy does not significantly affect integrated spectral measures.

Essentially this bandpass is oriented to be orthogonal to the SAR look direction (i.e. in the azimuth direction) with a wavenumber cutoff of approximately $[2\pi]\backslash[(R/V)\sigma_v]$ where R is the range from the sensor to the ocean surface, V is the velocity of the sensor, and σ_v is the standard deviation of radial velocities induces by the small-scale wave motion. Because the orientation depends on the SAR look direction, its impact on wave spectral measures can vary significantly depending on the relationship between the SAR look direction and the wave propagation direction. Figure 4.3.2-1 shows the "best radar look" which is when the SAR is looking is the same direction as the waves are propagating. This is defined as the "best" since it puts the most wave spectral energy within the SAR bandpass. In figure 4.3.2-1, the wave spectral energy is represented by the colored circles and the SAR bandpass is represented by the transparent blue rectangle. The SAR look direction is indicated in the figure, and it can be seen that in this configuration most of the wave energy is within the bandpass. In contrast, Figure 4.3.2-2 shows the "worst" radar look direction, where the look direction is orthogonal to the wave propagation direction. This puts the least amount of wave spectral energy in the bandpass.

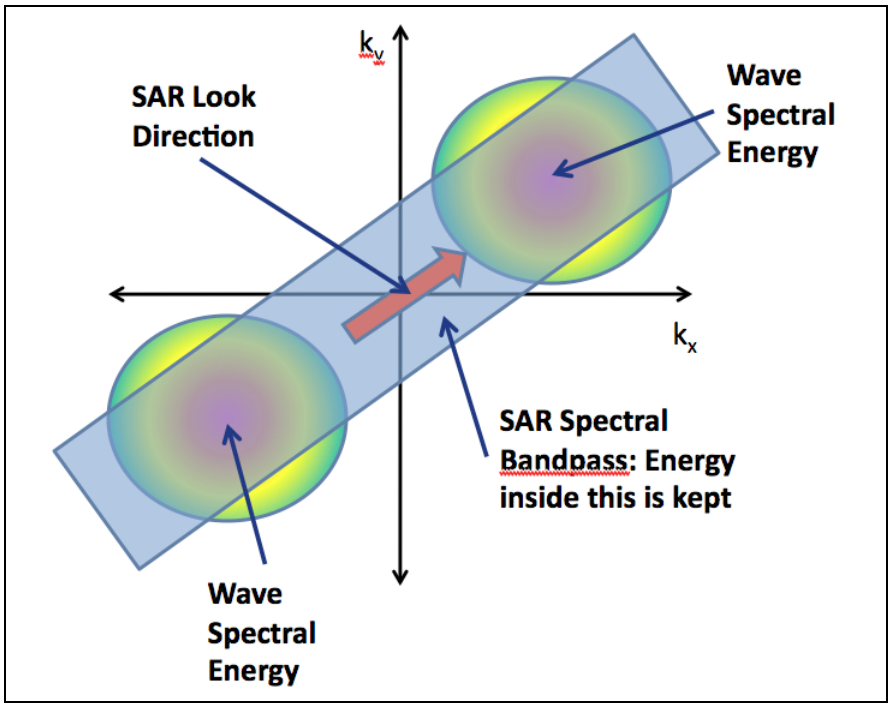

Figure 4.3.2-1. Best Radar Look Direction: SAR Looking in Wave Propagation Direction.

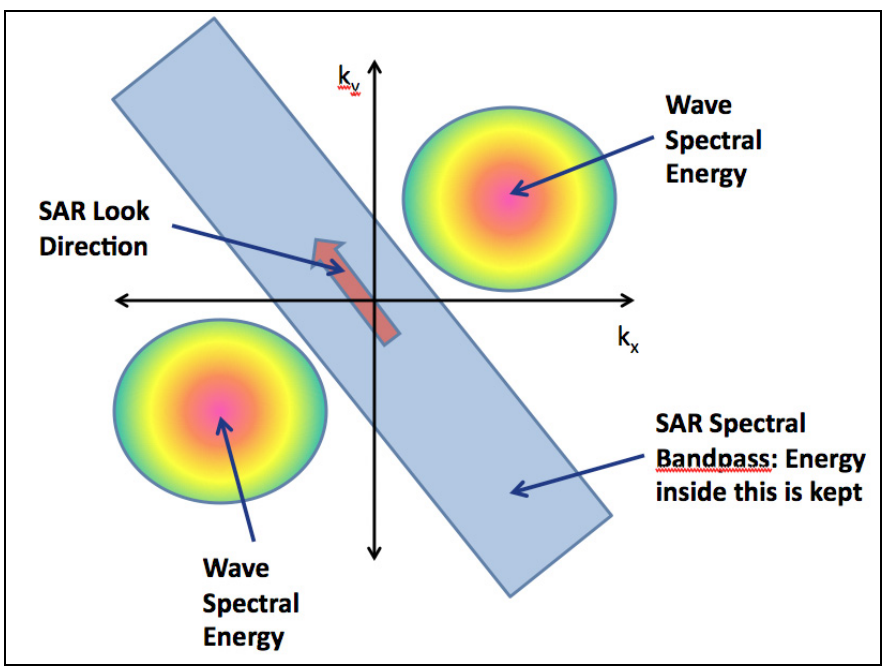

Figure 4.3.2-2. Worst Radar Look Direction: SAR Looking Orthogonal To Wave Propagation Direction.

In addition, the local wind speed will determine what the value of σ_v is, which will usually range from 0.2 (low wind) to 0.4 (high wind). The larger the value of σ_v the smaller the bandpass as illustrated in Figure 4.3.2-3, which shows the same conditions as Figure X1 except

for a higher wind and thus smaller bandpass. Note that less of the wave spectral energy is within the bandpass in Figure 4.3.2-3 as compared to Figure 4.3.2-3.

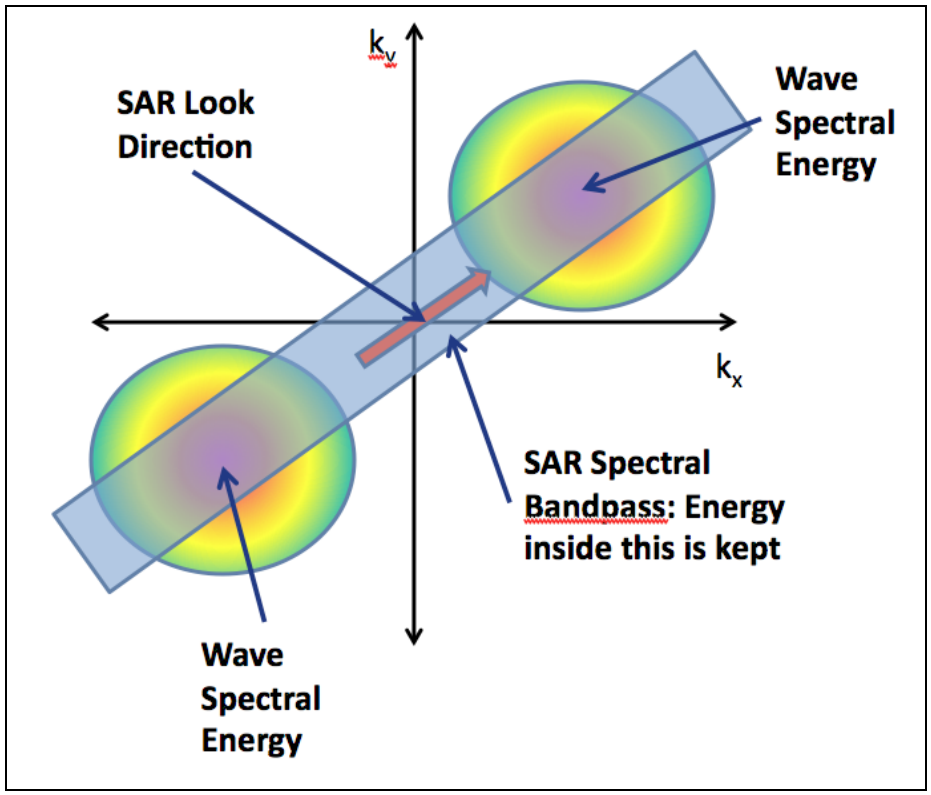

Figure 4.3.2-3. Effect of Local Wind: Higher Wind Speed Generates Smaller Bandpass.

We can see these effects in the SAR simulation that were run for the EXW cases. Figure 4.3.2-4 plots the ratio of total SAR-derived wave spectral energy to total energy in the waves. Perfect reconstruction of the wave energy from the SAR would give this metric a value of one. Four cases are plotted in Figure 4.3.2-4; Best radar look with low wind, best radar look with high wind, worst radar look with low wind, and worst radar look with high wind. Not surprisingly, the best look, low wind case gives the best results (highest values for the ratio), although even this case can lose up to 50% of the energy depending on the width of the wave spectral energy, but most cases are higher than 70%. Note that going from low wind to high wind in the best look direction cases we lose approximately another 10% of the spectral energy. When we move to the worst radar look conditions, we are effectively losing almost all the wave spectral energy. At best we are capturing 40% of the energy, and usually we have less than 10% of the energy. Clearly, to get robust estimates of the wave spectral energy depends significantly on the radar look direction with respect to the wave propagation direction. We can clearly improve our estimates of wave spectral energy of we allow the radar to dwell on a piece of the ocean such that the look direction can rotate over the largest angular extent possible. This will give us the best chance of capturing the most amounts of wave spectral energy within the radar bandpass.

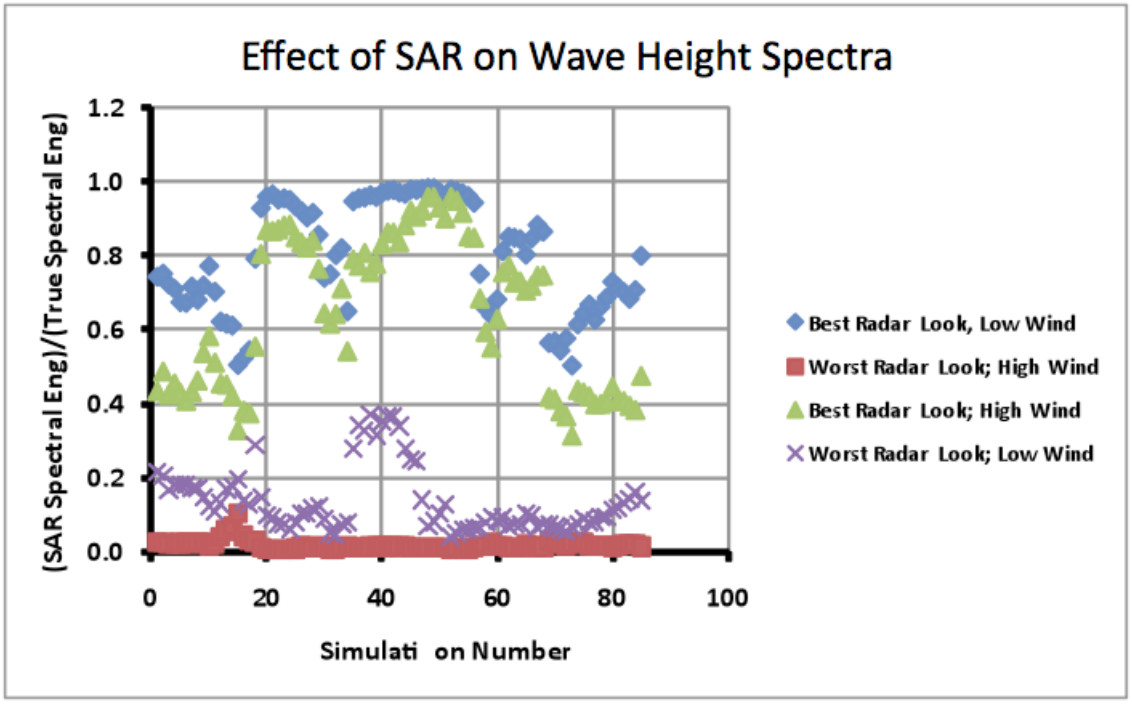

Figure 4.3.2-4. Effect of SAR on Wave Height Spectra.

There is also great interest in estimation peak parameters of the wave spectrum, such as dominant frequency or dominant wave direction. Clearly, as long as the dominant peak of the wave spectrum is within the radar bandpass we will estimate these well. If the dominant peak has rotated out of the bandpass, then we will get a false estimate based on whatever peak energy is within the bandpass. Note that this will usually be the value at the edge of the bandpass if the peak is outside. Figure 4.3.2-5 shows this effect by plotting the peak frequency of the wave spectral energy (along the x-axis) against the peak frequency in the SAR-derived estimate of the wave spectrum (y-axis). If we have the best radar look scenario, then even for the high wind case all but one of the points lie near or along the one-to-one line (the black line in Figure 4.3.2-5), indicating that we are getting good estimates of the peak location. In comparison, Figure 4.3.2-5 also shows results for the worst look direction, high wind, cases, where we are not getting any good estimates of the peak locations at all. Rather, once can see that the SAR-derived spectra have their peaks around one of two values, representative of where the edge of the radar bandpass intersect the wave spectra energy, and not related at all to the actual peak location.

Thus in general, the ability of a SAR sensor to estimate wave spectra depends significantly on the look direction of the radar with respect to the wave propagation direction, and somewhat less on the local wind speed. If we can collect data at the "best" look direction then we can reproduce 50%-90% of the integrated wave spectral energy, and usually faithfully reproduce the peak location. If the collect data at the "worst' look direction, the in essence we lose all information about the wave spectrum.

All of the results showed so far were for a radar system that notionally represented the Broad Area Maritime Surveillance (BAMS) sensor, where the parameter (R/V) was set to 91. It is also of interest to look at the same set of results but for radar sensors with different (R/V) parameters.

We considered the NanoSAR operating on ScanEagle. This system operates at a range of approximately 1 km with sensor velocities from 20 to 30 m/s. This implies that the value of (R/V) ranges from 30 to 50. If we use a nominal value for (R/V) of 40, note that this is a factor of 2.3 smaller than for BAMS, and therefore the SAR bandpass for the wave spectrum will be 2.3 times wider per the discussion above. This implies that NanoSAR data will be much more forgiving of look angle and wind speed effects. This is illustrated in Figures 4.3.2-6 and 4.3.2-7 where we have plotted the ratio of SAR-derived wave energy versus actual wave energy (Figure 4.3.2-6 to be compared to Figure 4.3.2-4) and the location of the SAR-derived spectral peak versus the actual spectral peak (Figure 4.3.2-7 to be compared to Figure 4.3.2-5). The NanoSAR results are better across the board than the BAMS results. For the best look direction the local wind does not significantly affect the results since the radar bandpass is large enough to encompass most of the spectral energy and the peak location even for the high wind simulations (Note that in Figure 4.3.2-7 the Best Look; High Wind results are plotted right on top of the Best Look; Low Wind results, which is why one can only see one of these two). In fact, even the Worst Look; Low Wind results are close in performance to the Best Look results. Thus one can see that the lower (R/V) value, and the subsequent larger radar bandpass, allows good reconstruction of the wave spectral energy and peak location for all look directions and low winds. It is only under high winds and the worst look direction that we start to seriously impact the ability of the SAR to estimate the wave spectrum.

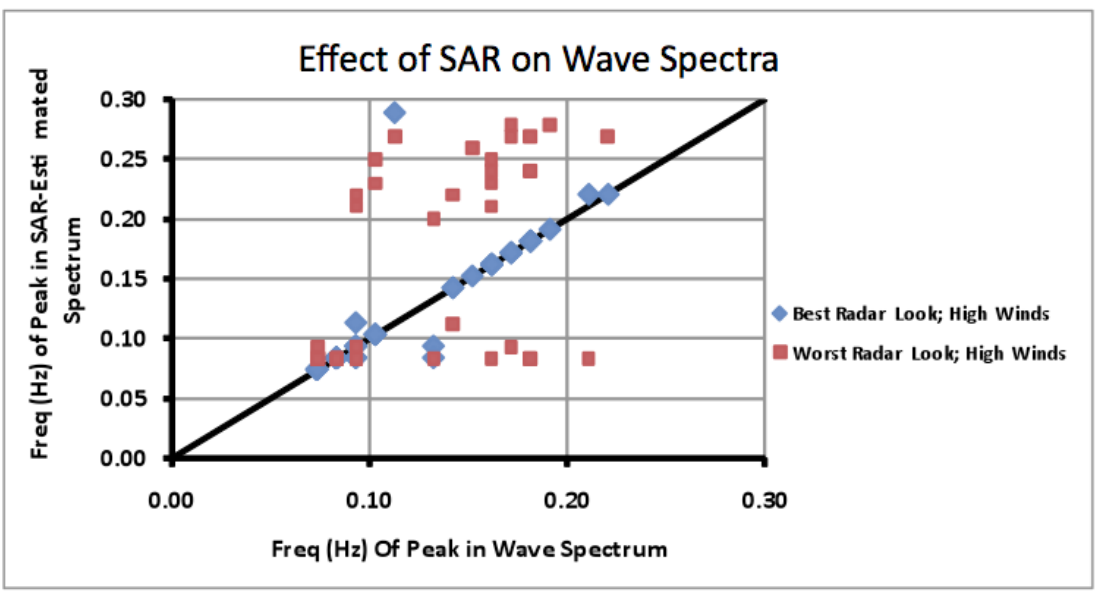

Figure 4.3.2-5. Effect of SAR on Wave Spectra.

Figure 4.3.2-8 shows the overall flow of the simulation system. It is designed to generate a realization of a SAR image from an assumed ground truth wave height field. The overall approach is to divide the ocean surface into two scales: (1) long-scale waves whose wavelengths are at least twice the size of the image sample spacing; and (2) short-scale waves whose wavelengths are smaller than the image sample spacing. The long-scale waves will determine the slope of each image cell (defined as the size of the image sample spacing) and the deterministic motions of each image cell over the time it takes to form the SAR image (which we will refer to as the integration time for the image). The short-scale waves determine the roughness of the ocean surface within each image cell (and therefore the brightness of the radar

cross section return) as well as the random motions of scatterers within each cell. Putting these together generates the information required to calculate the radar cross section in each image cell (middle dashed box in Figure 4.3.2-8) and the SAR smearing effects due to the motion of each cell (left dashed box in Figure 4.3.2-8).

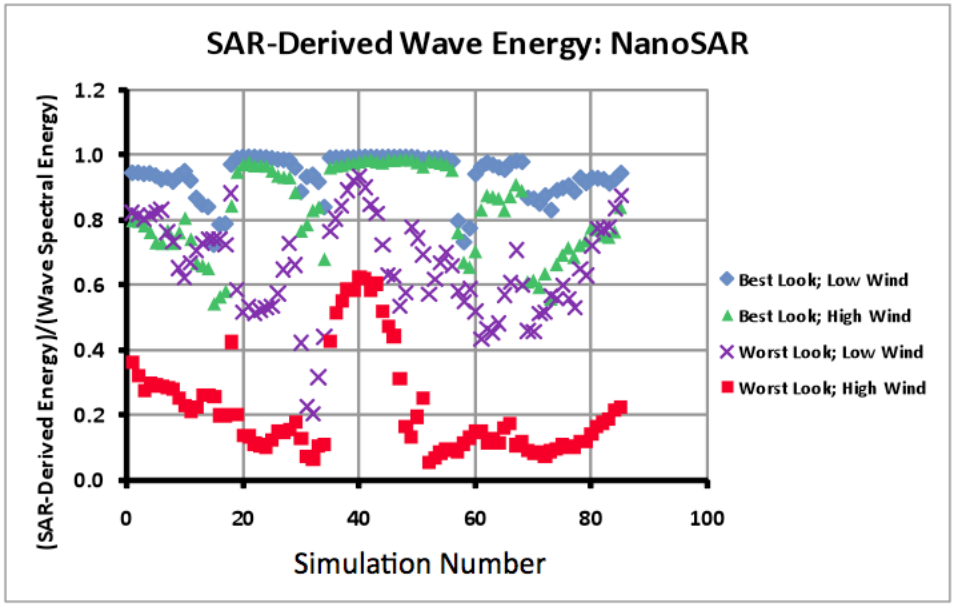

Figure 4.3.2-6. SAR-Derived Wave Energy: NanoSAR.

In addition, the simulation program has incorporated breaking wave effects (series of boxes on the right of Figure 4.3.2-8). This is done by calculating the vertical acceleration for each image cell, and using that to determine what fraction of the image cell contains breaking waves. This is then used to determine the radar cross section from the breaking waves.

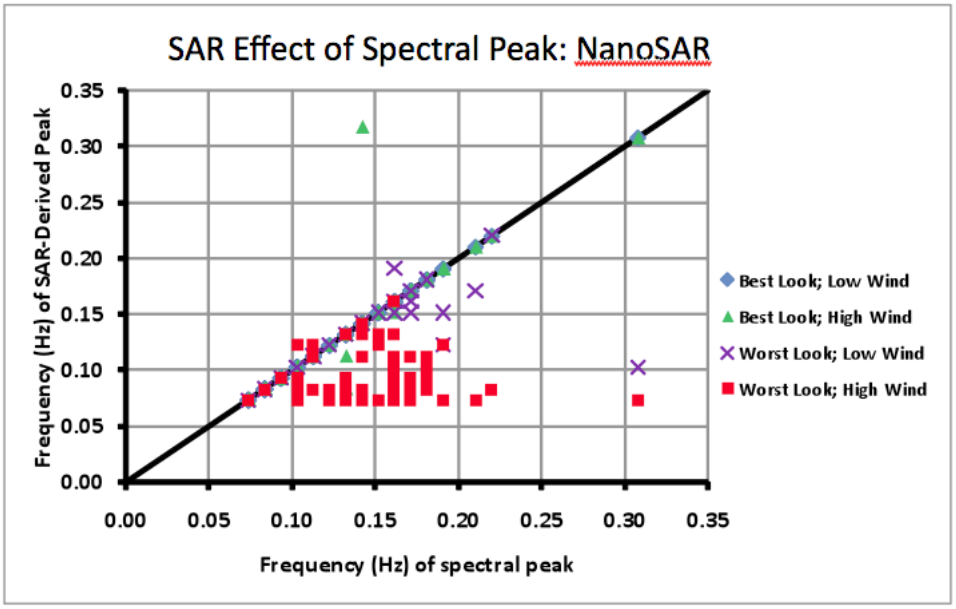

Figure 4.3.2-7. SAR Effect on Spectral Peak: NanoSAR.

This GD SAR model was employed to represent the likely performance of the BAMS multi-

function active sensor (MFAS) active electronically steered array (AESA). BAMS was assumed to be flying at 40,000 feet with a speed of 310 knots. The radar incidence angle was assumed to be 30 degrees with a resolution of 1 meter. For the Duck, NC datasets discussed below in Sections 5.2 and 5.3, four cases were run as follows:

These all assume that a single SAR image is used to estimate the wave spectrum. Increasing radar dwell will lead to improved wave spectrum estimation at the expense of increased survey times and data storage and processing requirements. The tactical impact of these radar results is reflected in the EXW/NSW and MIW TACSIT analyses presented below in Sections 5.2 and 5.3.

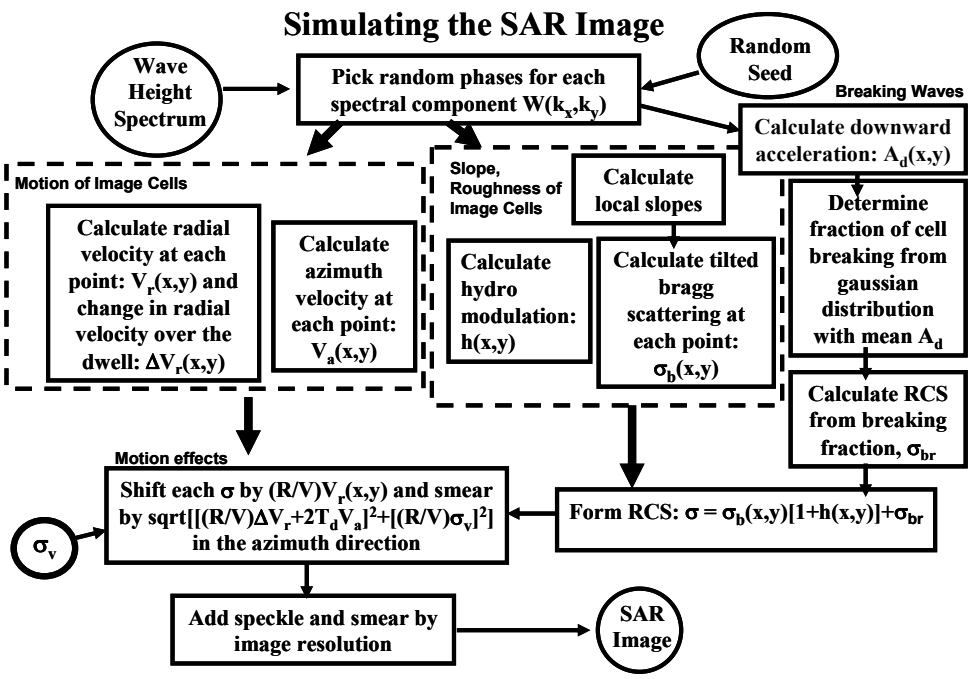

Figure 4.3.2-8. General Dynamics SAR simulation flow chart. Model for the motion of the ocean surface is shown in the left dashed box, for radar cross section is shown in the middle dashed box, and for breaking regions is shown in the right-most column of boxes.

Radar Look Angle	Winds
Best[5]	Low
Best	High
Worst[6]	Low
Worst	High

Table 4.3.2-1. GD SAR model run cases.

4.3.3 LIDAR

Several remote sensing methods have been suggested for directly surveying nearshore

[5] The best radar look angle is in the mean along wave direction.

[6] The worst radar look angle is in the mean across wave direction.

bathymetry. Two such examples are the use of light detection and ranging (LIDAR) technology and hyperspectral technology to make water depth measurements by estimating the depth of light penetration at various wavelengths to the bottom (Refs. [7], [8] and [10]). Data collection rates are approximately 5 km/hour with vertical bathymetry measurement accuracies on the order of 15 cm. However, such methodologies depend upon moderately high water clarity and are therefore not applicable in certain situations or locations and are generally limited to depths greater than 2 meters and less than about 18 meters. In addition, UAS power constraints have to date made LIDAR employment on a UAS platform infeasible.

LIDAR is an optical remote sensing technology that measures properties of scattered light to find range and/or other information of a distant target. The prevalent method to determine distance to an object or surface is to use laser pulses. Like the similar radar technology, which uses radio waves, which is light that is not in the visible spectrum, the range to an object is determined by measuring the time delay between transmission of a pulse and detection of the reflected signal.

Practical aircraft-based LIDAR systems do currently exist, e.g. from Ref. [21], *"The US Army Corps of Engineers (USACE) SHOALS (Scanning Hydrographic Operational Airborne Lidar Survey) program has evolved from an inlets R&D effort to a fully operational and constantly developing airborne coastal mapping initiative. The data collected in eight years of SHOALS survey operations have improved understanding of the coastal processes that drive shoreline change at USACE navigation and shore protection projects. The knowledge and experience gained from eight years of SHOALS operations have paved the way for a generational advancement in airborne coastal mapping by identifying complementary data sets to SHOALS bathymetry and by pinpointing aspects of survey planning, data collection, and data processing that could be automated for a more easily operated system. The result is the Compact Hydrographic Airborne Rapid Total Survey (CHARTS) system. CHARTS is an integrated bathymetric/ topographic/digital imagery system currently under development for the US Naval Oceanographic Office. A bathymetric lidar component operates at a rate of 1,000 Hz, while a topographic lidar component operates at 10,000 Hz. Digital imagery will be collected using a georeferenced camera that can provide a visual backdrop for the soundings and elevations collected by the other components. CHARTS will easily deploy from most photogrammetric aircraft of opportunity and will incorporate highly automated algorithms based on current SHOALS processing methodology. CHARTS will be commercially available as SHOALS-1000 following field-testing in August 2003. System flight parameters and sensor suite are ideal for further integration with additional sensors such as a hyperspectral imager. SHOALS-1000 will initiate a new era of complete coastal mapping from an airborne platform."*

4.3.3 Multispectral and Hyperspectral

As discussed above, in addition to LIDAR, multispectral imaging (MSI) and hyperspectral imaging (HSI) remote sensing is also available to make water depth measurements by estimating the depth of light penetration at various wavelengths to the bottom (Refs. [8], [9], and [11]). Data collection rates are again approximately 5 km/hour with vertical accuracies on the order of 15 cm. However, such methodologies depend upon moderately high water clarity and are therefore not applicable in certain situations or locations and are generally limited to depths greater than 2 meters and less than about 18 meters.

The following near-term UAS MSI and HSI capabilities are relevant to this UAS METOC

Sensing AoA:

- BAMS Multi-Spectral Targeting System (MTS-B) EO/IR Turret,
- Fire Scout VTUAV Brite Star EO/IR (12 channel) MSI sensor,
- USMC Fire Scout VTUAV Coastal Battlefield Reconnaissance and Analysis (COBRA) 3-band MSI sensor, and
- USMC future Fire Scout VTUAV Joint Multi-Mission Electro-Optical System (JMMES) 12-band MSI sensor.

Recently a small number of manufacturers (Galilio Avionica, BAE Systems, Bodkin Design and Engineering, Headwall Photonics, NovaSol and Resonon) have started fabricating and testing hyperspectral sensors for UAVs (Refs. [22]). Resonon (Bozeman, USA) produce the Manta Airborne Imaging System (MAIS) that was developed for the Manta UAV and has successfully completed many data collection acquisitions over both land and water. The system weighs 5.5 lbs and has 120 or 240 spectral channels and operates between 120 to 200Hz. The system is a push broom imager with nearly a 10-degree field of view and at 1000 feet above ground level gives a pixel size of approximately 16cm (6”).

4.4 Summary Capabilities Matrix

Table 4.4-1 provides a summary overview of the UAS METOC sensor technologies considered here for near-shore ocean sensing, including applicable environmental parameter estimation capabilities, depth domain, and other capability strengths and weaknesses. Note that a full wave spectra measurement (wave period, direction, height) is required to initialize wave models used in EXW/NSW and to achieve the levels of EXW/NSW and MIW warfighting payoff needed to make these UAS sensing applications cost effective. Two options exist for wave height sensing: (1) radar measurements; or (2) expendable wave height buoy deployments. LIDAR measurements are a third option but the technology is immature and power requirements are high.

Sensor	Estimated Parameters				Depth Domain	Notes
	Bathy	Wave Spectra				
		Period	Direction	Height		
Video Imagery	Yes	Yes	Yes	No	30 m, incl. surf zone	1. Mature wave period/direction estimation and bathy inversion 2. Onboard processing possible 3. Works with dispersive as well as dissipative wave regimes
Radar	Yes	Yes	Yes	Yes	30 m, no surf zone	1. Mature wave spectra estimation and bathy inversion 2. All weather capability 3. Onboard processing possible 4. Works with dispersive wave regimes only, no surf zone 5. Wide area coverage
LIDAR	Yes	Yes	Yes	Yes	2-18 m, no surf zone	1. Requires high water clarity 2. High power requirement 3. Wide area coverage 4. Wave height estimation is immature

						5. Some manual processing is typically required
MSI	Yes	Yes	Yes	No	2-15 m, no surf zone	1. Requires high water clarity 2. Large file sizes, JMMES output for 1km x 1 km image of 12 bands at 2 Hz is 346 GB/hour
HSI	Yes	Yes	Yes	No	2-18 m, no surf zone	1. Requires high water clarity 2. Very large files sizes; 80MB per compressed 100 band single image 3. Increased measurement robustness relative to MSI
Wave Buoy	Yes	Yes	Yes	Yes	All depths outside surf zone	1. Deployment mechanism TBD 2. Point vs. area measurement 3. Comms of data via SAT phone

Table 4.4-1. Summary UAS METOC Sensing Capabilities Matrix.

5.0 Mission Area (TACSIT) Analysis

As discussed above, the goal of the UAS AoA reported here is to capture and quantitatively assess the potential value-added of a broad range of UAS METOC sensing strategies and associated impacted Naval mission areas, e.g. Expeditionary Warfare, MIW, ASCM defense and Straits transit operations, and ASW search operations. This section presents the results of four analyses that have been conducted in the context of illustrative tactical situations (TACSITs) based on relevant portions of applicable OPLANs or other DoD planning scenarios.

5.1 Mapping of OPNAV Priorities to TACSITs

CNO N84 (Oceanographer of the Navy) and CNO N81 (Warfare Assessments and Analysis) were consulted to determine Navy UAS METOC sensing priorities. The feedback received in response is summarized below in Figure 5.1-1, which shows these priorities and how they map into a set of proposed mission areas or tactical situations (TACSITs). Four TACSIT areas are considered in this report as follows: (1) expeditionary warfare, rapid insertion, and amphibious warfare; (2) mine hunting and clearance; (3) anti-ship cruise missile defense and straits transit; and (4) ASW search and screen. The results of these analyses are presented below in Sections 5.2 through 5.5.

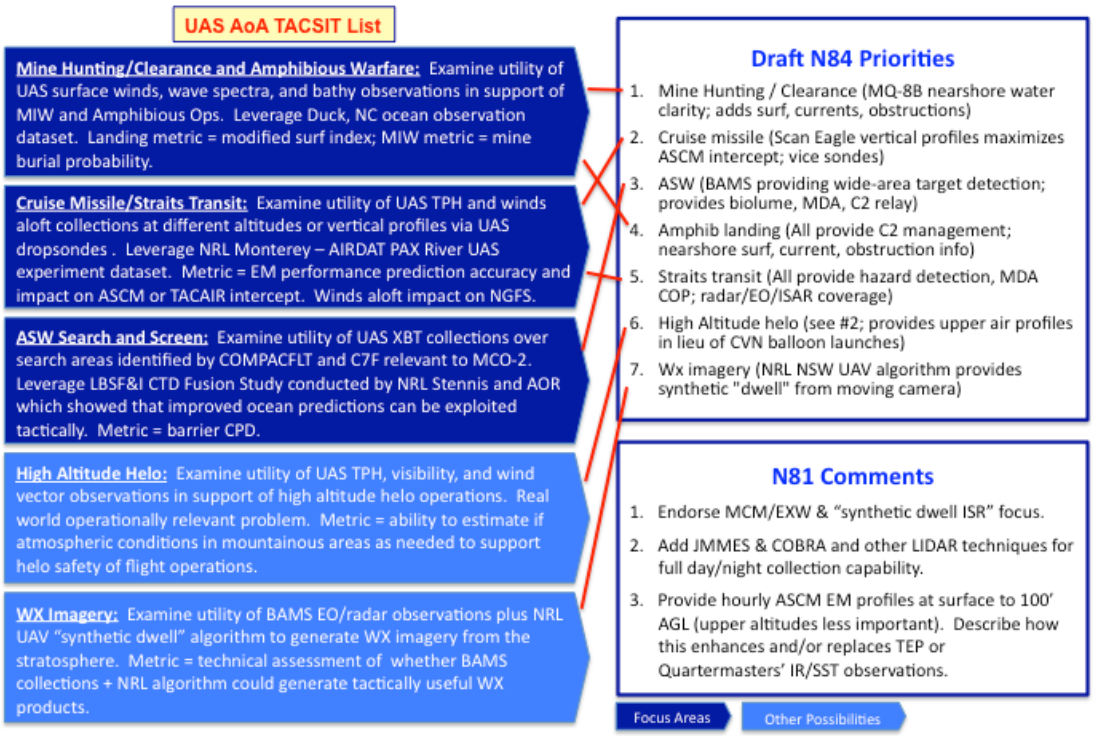

Figure 5.1-1. Mapping of N84/N81 Priorities to Selected TACSITs.

5.2 Expeditionary Warfare, Navy Special Warfare Landing TACSIT

From http://www.globalsecurity.org, *"Expeditionary Warfare is the foundation for 21st-century peacetime forward deployments, responses to crises world wide, and warfighting to protect America's citizens and friends and vital U.S. interests wherever and whenever they might be at risk. It is the essence of naval operations from the sea--anytime…anywhere. Marine Corps*

forces have long provided a scalable, tailorable and expeditionary combined-arms option, enabling joint commanders to deal with a wide range of contingencies. For decades, however, Marine power projection has included a deliberate buildup of combat power ashore. This buildup required the establishment of a force beachhead, with relatively fixed fire support, logistics, and command and control positions located ashore. Only after naval forces fought ashore and established a beachhead would the MAGTF begin to focus its combat power on the Joint Force's operational objective. A combination of naval initiatives in advanced mobility, fires, and sustainment capabilities, leveraging substantially enhanced information connectivity, will enable future Marine forces to be employed in a dramatically different manner, making them an even more effective tool of national power."

"Amphibious forces must be capable of performing missions ranging from humanitarian assistance and disaster relief to major theater war (MTW). Additionally, they can be configured and deployed to operate at various levels of conflict and in multiple theaters simultaneously. They can provide a presence that may preclude adventurous actions by a potential belligerent. Because they are seabased and because the decision to position and engage amphibious forces will always be easily reversible, amphibious forces greatly expand the repertoire of available response options. Among other national resources, they are particularly well placed to provide a demonstration of U.S. commitment and resolve to friends and allies as well as adversaries. Normally two to three ARGs are forward deployed: one in the Mediterranean / Arabian Gulf-Indian Ocean area, and one or two in the Western Pacific area. The other ships of the ARG are either working up to deploy, in transit, or in overhaul. One ARG/MEU is forward based in Sasebo and Okinawa Japan."

"To influence events overseas, America requires a credible, forwardly deployable, power projection capability. In the absence of an adjacent land base, a sustainable forcible entry capability that is independent of forward staging bases, friendly borders, overflight rights, and other politically dependent support can come only from the sea. The chaos of the future requires that the United States maintain the capability to project power ashore against all forces of resistance, ranging from overcoming devastated infrastructure to assisting a friendly people in need of disaster relief to countering the entire spectrum of armed threats."

In this TACSIT, we investigate the potential role of littoral area bathymetry and wave spectra sensing and estimation in support of Naval expeditionary warfare, rapid insertion operations, and amphibious landings.

5.2.1 Identification of Study Team

Dr. Jay Veeramony and Dr. Greg Jacobs of NRL Stennis, Code 7320 are the lead analysts for the Expeditionary Warfare, Rapid Insertion, Amphibious Landing TACSIT analysis presented below. Eduardo Danganan of NAVAIR generated a mapping of this TACSIT area to relevant DoD planning scenarios and OPLANs.

5.2.2 Mission Area (TACSIT) Overview

The purpose of the Expeditionary Warfare, Rapid Insertion, Amphibious Landing TACSIT analysis reported here is to explore the potential warfare value-added of conducting UAS electro-optical (EO) and radar survey operations in support of "*maintaining the capability to project power ashore against all forces of resistance, ranging from overcoming devastated*

infrastructure to assisting a friendly people in need of disaster relief to countering the entire spectrum of armed threats".

5.2.3 Analysis Objectives and Methodology

The specific UAS METOC sensing analysis objectives addressed in this TACSIT analysis are as follows:

- Assess the degree to which UAS sensing of bathymetry in the landing zone could result in improved estimates of Modified Surf Index (MSI). Note that MSI is a complex function of breaker height, period, type, and angle; littoral currents, surf zone width; wind speed and direction, etc.; hence complex physical modeling is required to assess MSI accuracy as a function of UAS wave and bathymetry sensing.
- Assess the degree to which these MSI estimation improvements could impact amphibious landing operational effectiveness. Note that MSI limits have been established for each applicable class of landing craft. If the estimated MSI exceeds the MSI limit for a particular craft, then landing is not feasible with that type of craft without increasing expected casualty rates beyond acceptable limits. Hence accurate estimate of MSI has a direct impact on operational effectiveness.
- Identify the UAS platforms, sensors, and survey CONOPs best suited to this Expeditionary Warfare, Rapid Insertion, Amphibious Landing operations application of UAS METOC sensing.

An Observing System Simulation Experiment (OSSE) analysis methodology was employed, which included the five major analysis steps described in the paragraphs that follow:

Simulate the Nature Environment. Each Nature run is the highest fidelity representation of the real ocean that we are capable of producing with all available observation, assimilation, and modeling techniques. Data collected at the U.S. Army Corps of Engineers (USACE) Field Research Facility (FRF) in Duck NC (see Appendix C) was used to construct each Nature Run; each of which represents a 48-hour period along 2000 meters of beach out to the 8-meter depth contour, see Figure 5.2.3-1. The specific Duck USACE FRF data employed includes wave data from the 8m array, the most recent surveyed bathymetry, and harmonic tides. The Delft3D modeling suite[7] has been employed to execute each 48-hour Nature Run simulation. Two model components of Delft3D are employed in a coupled mode; FLOW for current predictions and WAVE for wave field estimation. Model coupling is executed every three hours of simulated time; in these coupled calculations the currents determined by FLOW influence the wave field estimated determined by WAVE and visa versa. Twelve 48-hour Nature runs have been executed, the results of which are presented below in Section 5.2.4, which were selected so that significant waveheight (Hs) values ranged from 1.0 to 1.5 meters for 24-36 hrs of the total 48-hour forecast. This selection criterion corresponds to commonly occurring Duck NC wave field conditions for which accurate MSI estimation can be shown to have a significant warfighting impact.

[7] Delft3D (http://delftsoftware.wldelft.nl) is an integrated suite of predictive models for coastal predictions of waves, longshore currents, surf and sediment transport. It uses SWAN, Version 40.51 for wave predictions, and proprietary software for the other three components.

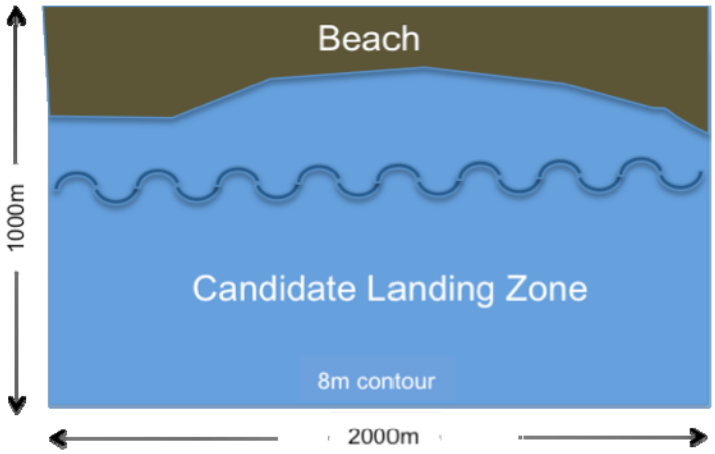

Figure 5.2.3-1. Nature Run Calculation Area.

Simulate the Environment Assuming No UAS Sensing. A "No UAS Sensing" run has been executed for each of the Nature runs described above. These simulations are used to represent how well the corresponding ocean area could be forecast without the aid of UAS in situ sensing. These "No UAS Sensing" simulations assume that in the absence of in situ sensing bathymetry would be derived from the Digital Bathymetry Database Variable Resolution (DBDB-V) and wave spectra would be derived from global NOGAPS simulations using archived winds and SWAN.

Conduct UAS Sensing Feasibility Analysis. The objective of the ocean sensing feasibility analysis reported above in Section 4.0 is to establish via simulation and physical modeling the feasibility of using UAS platforms and associated tactical dual use optical, radar, LIDAR, and hyperspectral sensors to sense relevant littoral bathymetry, ocean wave spectra, and other relevant ocean properties. The results of this analysis are employed in the "UAS Sensing" runs described below.

Simulate the Environment Assuming UAS Sensing Alternatives are Available. A "UAS Sensing" run has been executed for a subset of the Nature runs (5 of 12) described above. These simulations are used to represent how well the corresponding ocean area could be forecast assuming a set of possible UAS in situ sensing capabilities are available. Four UAS sensing capabilities are considered as described below in Table 5.2.3-1: ScanEagle and Fire Scout/VTUAV EO sensor with standard definition (SD) video, BAMS (or Global Hawk) EO sensing with high definition (HD) video, and Fire Scout/VTUAV hyperspectral sensing with the Joint Multi-Mission Electro-optical System (JMMES) sensor.

UAS Platform	EO Sensor	Bathymetry Error (%)	Sounding Spacing ft (m)
ScanEagle	Turret w/SD Video	8.5	53 (17.67)
Fire Scout	Turret w/SD Video	5.5	105 (35)
BAMS/ Global Hawk	Turret w/HD Video	4.5	159 (53)
VTUAV/JMMES	Hyperspectral	18 (limited <15 m)	1 (0.3)

Table 5.2.3-1. UAS Sensing Alternatives Considered.

In addition, for BAMS, the impact of EO video plus MFAS/AESA radar sensing of bathymetry plus the wave spectrum was also assessed.

These "UAS Sensing" simulations assume the bathymetry sensing capabilities listed above in Table 5.2.3-1 and that wave spectra would be derived from global NOGAPS simulations using archived winds and SWAN.

Note that the bathymetry errors and sounding spacings listed in table 5.2.3-1 will generally vary with local ocean depths, wave conditions, and UAS survey CONOPs. For each of the five Nature runs selected, we have sub-sampled the nature bathymetry from Duck, NC Coastal Research Amphibious Buggy (CRAB) survey data according to the sounding spacing. The Delft3D model grid resolution is 15 meters. In addition, we have introduced a random error in bathymetry according to the specifications in the table for each sensor. Hence there are a total of four separate "sensing" simulations for each of the five Nature runs, for a total of 20 "UAS Sensing" simulations. MSI values have been calculated from these runs to show which of the sensors provide the best MSI estimate relative to the associated ground truth Nature run estimate of MSI.

Estimates of LIDAR performance can be directly derived from the VTUAV/JMMES hyperspectral results; LIDAR MSI accuracy will be the same as hyperspectral accuracy, but the corresponding UAS survey times will generally differ.

Assess Tactical Impacts. The Modified Surf Index (MSI) is a function of breaker type, wave height, wave angle to shore, wave period, size of surf zone, littoral current, and water temperature. MSI limits have been determined for each class of landing craft and these limits impose "go / no go" constraints on landing operations. Hence MSI estimation accuracy has a direct impact on operational effectiveness and this provides the means to assess the likely operational impact of improved MSI estimation for specific landing zones as described in the section that follows.

The U.S. Special Operations Command (SOCOM) publishes critical Meteorological and Oceanographic thresholds for Special Operations Forces (SOF) operations. The current version is on the USSOCOM SIPRNET homepage (http://soop.socom.smil.mil/html/metocadm.html). METOC elements, critical thresholds, and impacts on operations are provided for the landing assets listed below:

- Parachute Operations
- SEAL Delivery Vehicle (SDV) Operations
- Combat Rubber Raiding Craft (CRRC):
- MK IV Patrol Boat (PB)
- Mini-Armored Troop Carrier (MATC)
- Patrol Boat, Light (PBL)
- Patrol Boat, Riverine (PBR)
- Rigid Inflatable Boat (RIBS)
- High Speed Boat (HSB)
- Patrol Craft (PC)
- MK V Special Operations Craft (MK V SOC)
- Swimmer Operations

Included in this document is a "safe" MSI threshold, a range of "care required" MSI values, and an "unsafe" MSI threshold for each landing craft listed above.

5.2.4 Effectiveness Analysis Results

Figure 5.2.4-1 shows an example bathymetry survey (on the left) and DBDB-V bathymetry (on the right) where the beach is oriented along the y-axis and the offshore direction is along the x-axis. This example shows sizeable (approximately 5-6 meter) bathymetry differences along the furthest offshore portion of these plots. Hence this is an example where it would be reasonable to assume that bathymetry survey data might yield significant warfighting effectiveness improvements.

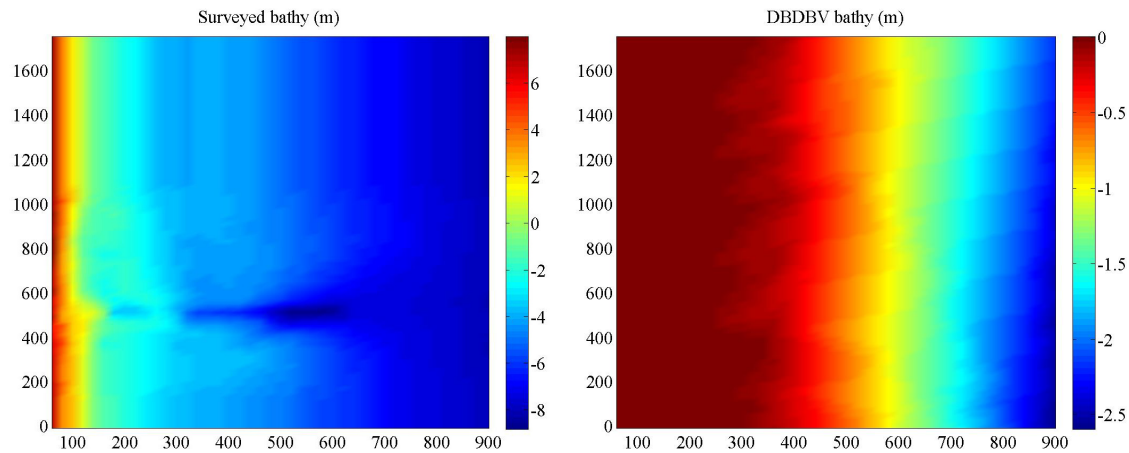

Figure 5.2.4-1. Example Surveyed (Left) and DBDB-V (Right) Bathymetry.

Figures 5.2.4-2 through 5.2.4-6 show the results of a comparison of "Nature" vs. "No Sensing" model runs for five 48-hour periods selected to be representative of typical Duck USACE FRF conditions while also providing the potential for MSI estimation improvement in the "UAS Sensing Runs" corresponding to the rows of Table 5.2.4-1. Shown along the top row of each of these figures is Nature (in blue) vs. No Sensing (in green) significant wave height (H_S) vs. time (0-48 hours) in meters, Nature vs. No Sensing wave period (T_P) vs. time in seconds, and Nature vs. No Sensing wave length (L_P) vs. time in meters. Shown in the middle row is Nature (in blue) vs. No Sensing (in green) modified surf index (MSI) values vs. time for the beach centerline (center plot), 500 meters north of centerline (left plot), and 500 meters south of centerline (right plot). The bottom row shows mean MSI differences (Nature - No Sensing MSI) vs. time, again for the beach centerline and + or – 500 meters from centerline.

The bottom rows of Figures 5.2.4-2 through 5.2.4-6 show the warfighting potential of UAS METOC data collections in these areas and times. These bottom row plots show the signed difference between "No Sensing" MSI estimates and the assumed ground truth "Nature" MSI vs. time. Recall that MSI limits (MSLs) have been established for each applicable class of landing craft and that these MSLs generally lie between MSI values of 6-12. If the estimated MSI exceeds the MSI limit for a particular craft, then landing is not feasible with that type of craft without increasing expected casualty rates beyond acceptable limits. Hence (No Sensing MSI - Nature MSI) negative values indicate under-estimated (i.e. too low) MSI values (which could lead to an overly optimistic "go" decision when environmental conditions could lead to

unacceptable risk), while positive values indicate over-estimated (i.e. too high) MSI values (which could lead to overly conservative landing "no go" decisions).

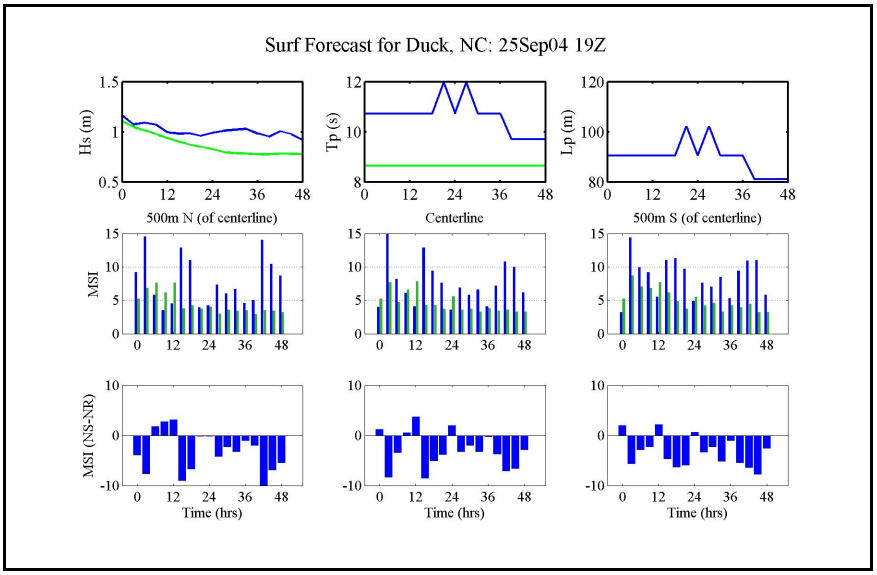

Figure 5.2.4-2. Nature Run vs. No Sensing Run, 25Sep04 19Z.

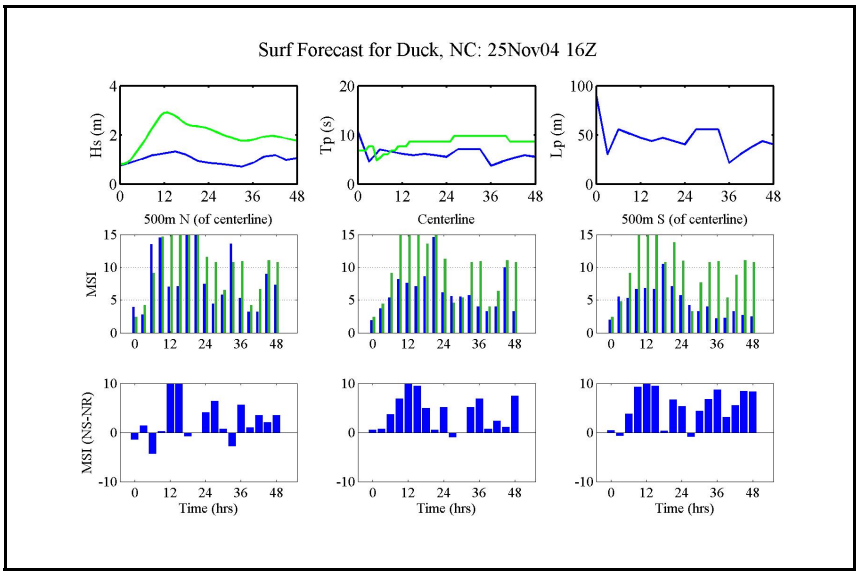

Figure 5.2.4-3. Nature Run vs. No Sensing Run, 25Nov04 16Z.

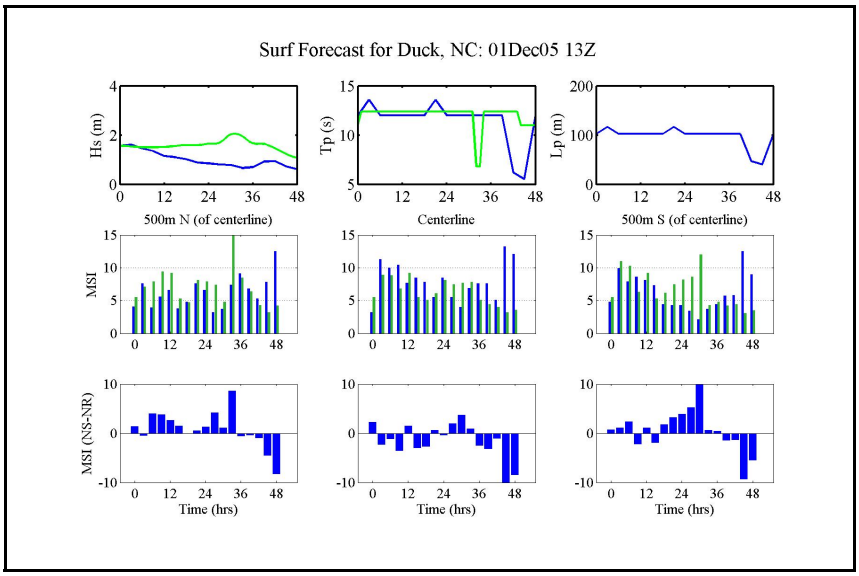

Figure 5.2.4-4. Nature Run vs. No Sensing Run, 01Dec05 13Z.

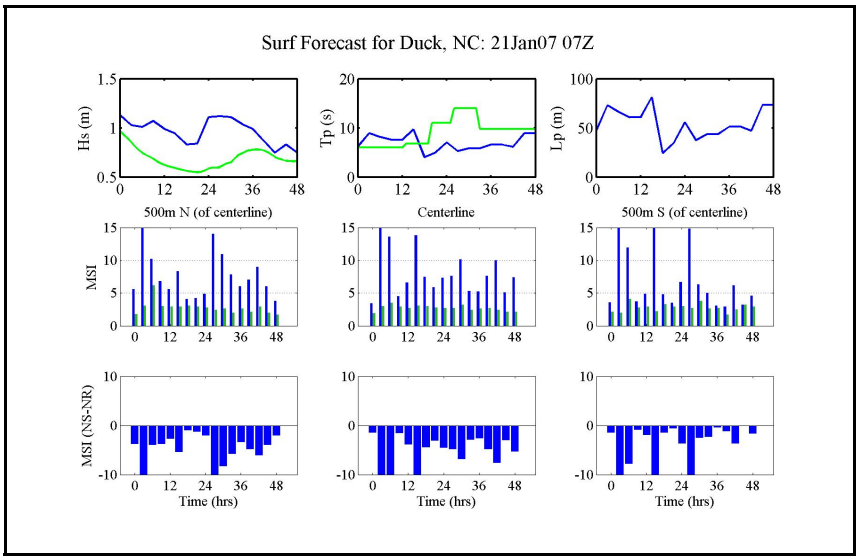

Figure 5.2.4-5. Nature Run vs. No Sensing Run, 21Jan07 07Z.

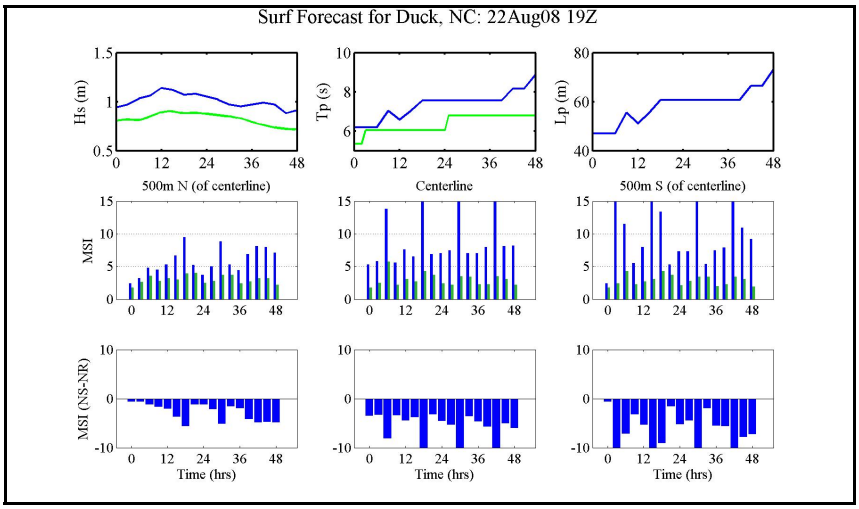

Figure 5.2.4-6. Nature Run vs. No Sensing Run, 22Aug08 19Z.

Table 5.2.4-1 provides a summary of the results of these Nature vs. No Sensing run results for the five 48-hour time periods shown above. Significant potential for warfighting effectiveness improvements is indicated in 4 of the 5 cases displayed. The fifth case (01Dec05, 13Z) is an illustration of the fact that the impact of UAS METOC data collections are affected by the wave lengths in the surveyed area; longer waves yield more accurate estimates of bathymetry.

Date and Time	Potential for UAS Sensing Improvement	Notes
25Sep04, 19Z	No Sensing model runs result in overly optimistic MSI and likely "go" decision, while the Nature model runs suggest a high likelihood of "no go" conditions.	Overly optimistic No Sensing MSI.
25Nov04, 16Z	No Sensing model runs result in overly pessimistic MSI and likely "no go" decision, while the Nature model runs suggest a moderate likelihood of "go" conditions.	Overly pessimistic No Sensing MSI.
01Dec05, 13Z	Over most of the 48-hour time period, satisfactory agreement between No Sensing and Nature MSI estimates.	Accurate No Sensing MSI. Note that the performance of the observation systems are affected by the wavelength; longer waves yield more accurate estimates of bathymetry.
21Jan07, 07Z	No Sensing model runs result in overly optimistic MSI and likely "go" decision, while the Nature model runs suggest a high likelihood of "no go" conditions.	Overly optimistic No Sensing MSI.
22Aug08, 19Z	No Sensing model runs result in overly optimistic MSI and likely "go" decision, while the Nature model runs suggest a high likelihood of "no go" conditions.	Overly optimistic No Sensing MSI.

Table 5.2.4-1. Summary Nature Run vs. No Sensing Run Comparisons.

5.2.5 Summary Conclusions

Figure 5.2.5-1 shows ground truth MSI along the x-axis vs. estimated MSI scatter plots for ScanEagle EO sensing (upper left), Fire Scout EO sensing (upper right), BAMS EO HD sensing (lower left), and Fire Scout hyperspectral sensing (lower right). Table 5.2.5-1 summarizes these results in terms of percent agreement with the Nature Run, where agreement implies MSI values within plus or minus one MSI unit of the ground truth value.

The following comments apply to these results:

1. The grid resolution of the Delft3D model is 15m x 15m. Interpolating the bathymetry derived from ScanEagle and Fire Scout (hyperspectral) results in a negligible change from "Nature Run" as far as resolution errors (due to sounding spacing) go.

2. MSI depends on a large number of interdependent quantities. Improving only one part of the problem (bathymetry) improves reliability, but not by a whole lot. If a 20% error is introduced in the significant wave height, for instance, the MSI changes by more than 1.

3. Global SWAN predictions are sometimes off by as much as 50%.

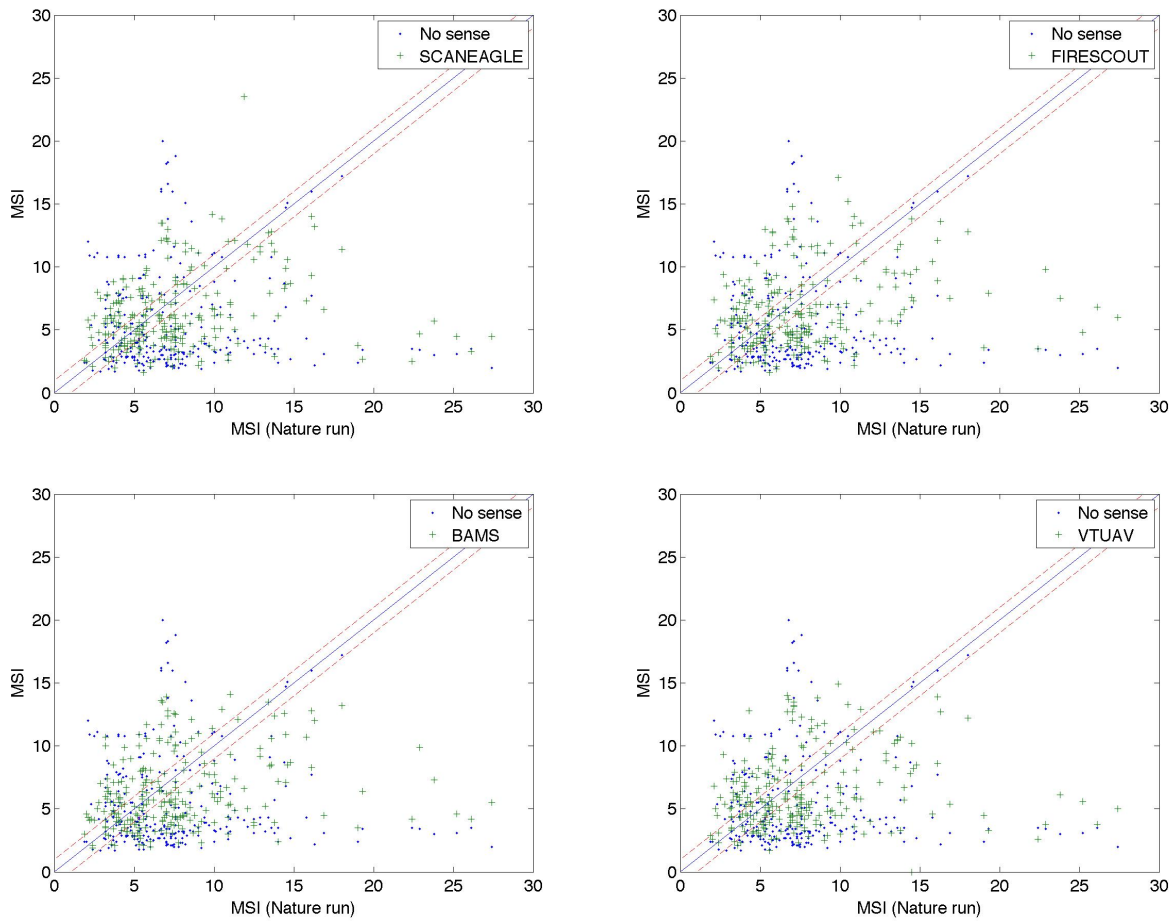

Figure 5.2.5-1. MSI Results for ScanEagle EO Sensing (Upper Left), Fire Scout EO Sensing (Upper Right), BAMS EO HD Sensing (Lower Left), and Fire Scout Hyperspectral (Lower Right).

UAS Platform	Bathymetry Error (%)	Sounding Spacing (m)	% Agreement with Nature Run
No sensing	Variable	N/A	16
BAMS EO HD	4.5	53	22
Firescout EO	5.5	35	22
ScanEagle EO	8.5	18	25
FireScout HSI	18	1	20

Table 5.2.5-1. MSI Comparison Chart for EO Options Considered

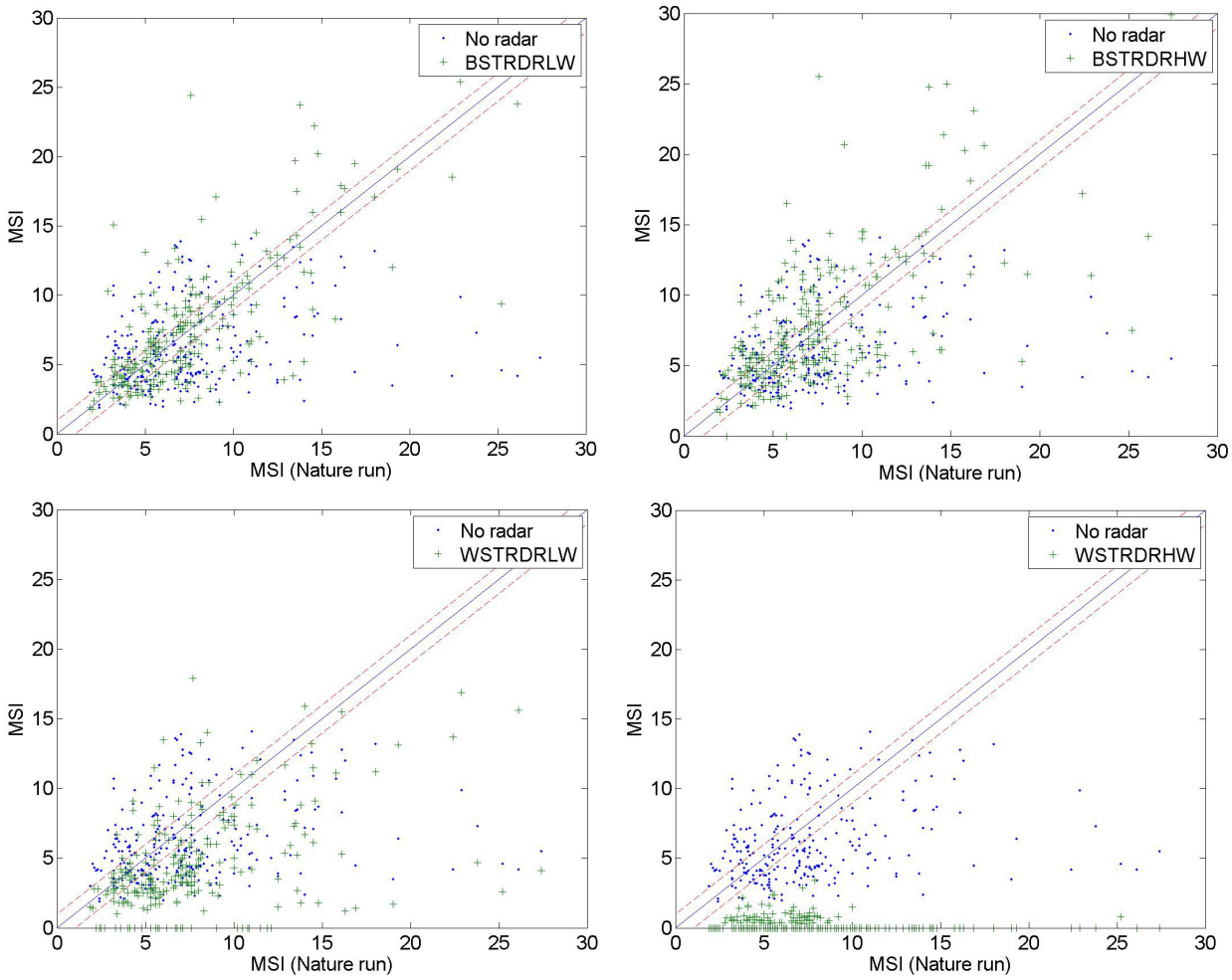

Figure 5.2.5-2. MSI Results for BAMS EO plus radar sensing best look angle, low winds (Upper Left), best look angle, high winds (Upper Right), worst look angle, low winds (Lower Left), and worst look angle, high winds (Lower Right).

Figure 5.2.5-2 shows ground truth MSI along the x-axis vs. estimated MSI scatter plots for BAMS EO plus radar sensing assuming the best radar look angle and low winds (upper left), the best radar look angle and high winds (upper right), the worst radar look angle and low winds (lower left), and the worst radar look angle and high winds (lower right). Table 5.2.5-1

summarizes these results in terms of percent agreement with the Nature Run, where agreement implies MSI values within plus or minus one MSI unit of the ground-truth value.

UAS Platform	Radar Look Angle	Assumed Winds	% Agreement with Nature Run
No Sensing	N/A	N/A	16
BAMS EO/IR	N/A	N/A	22
BAMS EO/IR + Radar	Best	Low	43
BAMS EO/IR + Radar	Best	Low	29
BAMS EO/IR + Radar	Worst	High	20
BAMS EO/IR + Radar	Worst	High	0

Table 5.2.5-2. MSI Comparison Chart for EO Plus Radar Options Considered

The following comments apply to these results:

1. The GD radar model incorporates the lost of spectral energy due to the radar resolution (not a significant factor) and due to the small-scale random ocean surface motions (a significant factor). The model does not include the re-arranging of spectral energy due to velocity bunching effects – however we do not believe this will have a significant effect on wave height statistics calculated over the spectrum.

2. The parameters in the GD radar model are radar resolution, radar look direction, R/V of the radar (R=range, V=velocity) and wind speed. For BAMS we assumed an altitude of 40,000 feet, a speed of 310 knots, a look angle of 30 degrees, and a resolution of 1 meter.

3. We also assumed that we are just using one SAR image at 1 meter resolution to estimate the spectra. This gives the worst performance in the sense that if we used a series of spotlight images over the region to estimate the spectrum, we would essentially get the actual spectrum back at the expense of increased survey times and data storage and processing requirements.

The following conclusions can be drawn from these UAS "EO only" and "EO plus radar" model results:

1. The technical feasibility of optical sensing of wave period/direction and radar sensing of wave spectra and subsequent inversion for bathymetry is well established.

2. For MSI estimation for the environment at Duck, NC, using sensors that improve only bathymetry yield marginal warfighting impact. ScanEagle EO sensing results in 25% agreement with ground truth MSI vs. 16% in the No UAS sensing case. All other sensing alternatives result in somewhat less operational impact.

3. For MSI estimation in the Duck, NC environment, bathymetry + wave spectra sensing is expected to yield a more substantial warfighting impact however. Initial model runs with radar wave spectra estimation supports this hypothesis. BAMS EO plus radar sensing yields a 43% agreement with ground truth MSI for favorable radar look angles and wind speeds and clearly suboptimal radar dwell times. It is probable that increasing radar dwell will result in substantially increased MSI estimation performance.

4. UAS employment CONOPs optimization is likely required to extract maximum benefit from UAS environmental sensing in support of MSI estimation.

5. UAS survey and the supporting data assimilation and modeling CONOPs and required C2 connectivity is apt to be complex and coordination with OCEANOPSCOM Directorates is required. We estimate that a minimum improvement of 16% in the No UAS Sensing case to 75% or greater agreement with ground truth will be required to make the investment in UAS sensing, data assimilation, and modeling a cost effective option.

5.3 Mine Hunting and Clearance TACSIT

In this TACSIT, we investigate the role of littoral area bathymetry and wavenumber sensing and estimation to providing enhanced knowledge of mine burial. Enhanced mine burial knowledge provides on-scene forces with better metrics for determining percentage of undetectable mines along potential assault routes. This knowledge affects go/no-go decisions, transit and assault line geometry, and time and tactics required by mine countermeasure (MCM) forces to clear these lanes. Mine burial also largely influences doctrinal metrics used to calculate eventual clearance time and percentage of mines cleared by MCM forces after securing the area.

The emerging technology used for prediction and determination of mine burial is the Mine Burial Expert System (MBES). Since MBES will be used by future MCM force for mine burial assessment, we use MBES to predict burial for this TACSIT. Actual maps of burial results are classified; however, in this report, we can provide background information on MBES, features of the mission area germane to MBES results, study objectives, and implementation methodology. We also discuss qualitative expectations based on the available oceanography data and other information published in the open literature.

A classified addendum to this report presents the results of the MBES analysis described above.

5.3.1 Identification of Study Team

Dr. Paul Elmore and Dr. Bill Sanders of NRL Stennis, Code 7400 are the lead analysts for the Mine Hunting and Clearance TACSIT. Eduardo Danganan of NAVAIR generated a mapping of this TACSIT area to relevant DoD planning scenarios and OPLANs.

5.3.2 Background

5.3.2.1 Mine Burial Expert System (MBES) Overview

Prior to 1998, the Navy's ability to predict mine burial was arguably poor (Ref. [23]) Since 1998, the Office of Naval Research and the Naval Research Laboratory lead efforts to rapidly advance mine burial scientific knowledge and prediction capabilities. From this program, the MBES was created and transitioned to NAVOCEANO for Fleet use.

A comprehensive technical review of MBES can be found in Rennie et al. (Ref. [24]). To summarize, MBES is a Bayesian network based prediction system, a form of artificial intelligence that allows end users to obtain the probability of a result based on probabilistic inputs (further details in Appendix G). Specifically, MBES provides probabilities for possible mine burial states for cylindrical mines due to impact and scour processes based on statistical information of the environment. As Bayesian networks require a prior training, MBES was

trained for these two processes using deterministic models and experimental data from the ONR/NRL programs.

As transitioned to NAVOCEANO, MBES was coded in MATLAB (Ref. [25]) in 2007. NRL has continuously revised this code for compatibility with subsequent Fleet exercises and this project. It is also being incorporated as C/C++ code into the MIW Environmental Post-Mission Analysis (EPMA) (Ref. [26]) for Fleet-wide use.

5.3.2.1 Scour Burial Mechanism

The TACSIT area at Duck, NC seaward of the surf zone is a characterized by a fine sand bottom with a mean grain size of 0.2 millimeters (Ref. [27]). Mine burial mechanism on this bottom is scour, the formation of pit in the bottom into which the mine sinks, caused by locally magnified velocities and turbulent eddies that arise from the physical obstruction of the local fluid flow by the mine (Refs. [28, 29]).

Trembanis et al. (Ref. [27]) and Elmore and Richardson (Ref. [30]) discuss the model used to train MBES for scour burial. Appendix I provides a review. The basis of the model is a time-stepped implementation[8] of the equation $S(t) = S_\infty(1 - \exp(t/T)^{0.6})$, where scour pit depth, $S(t)$, exponentially decays to the depth that would be achieved after an infinite amount of time, S_∞, and regulated by time constant T[9]. The key factor determining S_∞ is the frictional stress at the seabed as caused by waves action and other currents. Burial state is 100% × (maximum value of $S(t)$ over the entire time history of the mine deployment) × (1 / mine diameter). As a result, scour burial is episodic as a) S_∞ and T change temporally with the waves and currents, and b) the scour burial depth changes only when the waves and currents can cause a bigger pit than the one present at that moment.

5.3.2.3 *Doctrinal Bottom Type*

Doctrinally, the Navy uses mine burial as a factor for determining a metric called Doctrinal Bottom Type (DBT). DBT is used by algorithms in the Mine Warfare Decision Aids Library (MEDAL) for planning MCM operations, including those in support of amphibious operations – such as assault lines, hunt or sweep decisions, clearance – and providing situational awareness of mine threats to all forces present. Since DBT is a root environmental metric used for MCM tactics and planning, we need to define DBT and the environmental factors that determine it.

The DBT metric is a two-character code with letters A, B, C or D first, followed by the number 1, 2 or 3. In addition to mine burial state, sediment type and bottom roughness determine the letter portion and bottom clutter determines the number (Fig. 5.3.2.3-1). Fig. 5.3.2.3-2 reproduces unclassified figures from Naval Warfare Publication (NWP) 3-15.41 define the bottom conditions for these codes. Thus, DBT categories are a combination of Bottom Category and Cutter Category, so that possible DBT's are A1, A2, A3, B1, B2, B3, C1, C2, C3, D1, D2, and D3. The progression of Bottom Category from A to D and Clutter Category from 1 to 3 indicate progressively more difficult and time-consuming environments for mine location and neutralization.

---

[8] Quasi-static conditions are assumed over each time-step.

[9] Time constant, T, is determined by the diameter of the mine, median grain size of the sediment, and, like S_∞, frictional stress at the seabed.

For discussion on how DBT is further used for MCM operations, refer to NWP 3-15.41, *"Mine Countermeasures (MCM) Planning and Procedures"*.

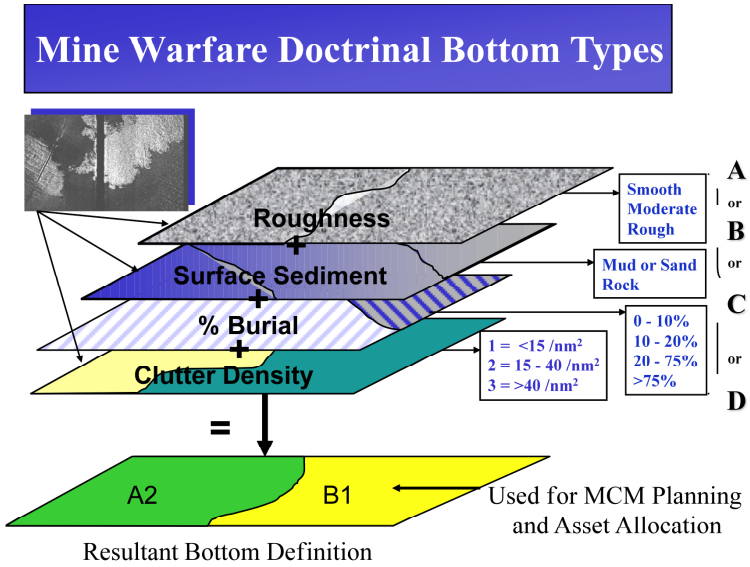

Figure 5.3.2.3-1. Four environmental parameters used to define mine warfare Doctrinal Bottom Types (DBT).

BOTTOM ROUGHNESS PERCENTAGE	SAND RIDGE HEIGHT (M/FT)	BOTTOM PROFILE GROUP
Less Than 5	Less Than 0.2/0.5	Smooth
5 To 15	0.2 to 0.3/0.5 to 1.0	Moderate
Over 15	Over 0.3/1.0	Rough

BOTTOM COMPOSITION	PREDICTED MINE CASE BURIAL %	BOTTOM PROFILE GROUP	BOTTOM CATEGORY
MUD OR SAND	0 TO 10	SMOOTH MODERATE ROUGH	A B C
	10 TO 20	SMOOTH MODERATE ROUGH	B B C
	20 TO 75	SMOOTH MODERATE ROUGH	B C C
	75 TO 100	*ALL*	D
ROCK	0	SMOOTH MODERATE ROUGH	B C C

NOMBOS/km²	NOMBOS/NM²	CLUTTER CATEGORY
<4	<15	1
≥4 and ≤12	≥15 and ≤40	2
>12	>40	3

Figure 5.3.2.3-2. Reproduction of unclassified Figs. 3-3, 3-4, and 3-7, respectively, from NWP 3-15.41 defining bottom and mine burial conditions to categories used for Doctrinal Bottom Type. NOMBOS means "Number of Mine-Like Bottom Objects" or objects that could be mistaken for a mine.

5.3.3 Mission Area (TACSIT) Overview

From Navy Tactics, Techniques, and Procedures (NTTP) 3-15.24 (Ref. [19]), *"Until the arrival of the amphibious task force (ATF), advance force operations, including mine countermeasures (MCM) activities, may last days or even weeks. The focus is to deceive the enemy, identify his vulnerability points, shape the battlespace, and identify landing beaches and sites that hold the most promise for maintaining the element of surprise. The use of deception and stealth are critical to preventing compromise of the location of the impending operation. The time required to execute necessary MCM preassault actions is a major consideration when developing the overall timeline for the amphibious operation. MCM preassault phase supporting operations, discussed in greater detail in NWP 3-15, Naval Mine Warfare, should commence early in the planning phase to ensure integration with the overall plan."*

Also from Ref. [19],*"Pre-assault operations may include:*

1. *Continued planning and coordination among ATF, landing force (LF), and MCM staff members,*
2. *Movement of MCM assets to the area of operations via means other than amphibious shipping (i.e., airlift or float-on/float-off (FLO/FLO) ships),*
3. *Use of MEDAL to search databases for environmental information, mine types and threats, previously surveyed contacts, and unmineable areas,*
4. *Conducting clandestine MCM hydrographic surveys and mine detection and reconnaissance to identify poor bottom conditions, or areas of high clutter that should be avoided by MCM forces, i.e., Naval Special Clearance Team One (NSCT 1) with marine mammal system (MMS) and unmanned underwater vehicle (UUV) platoon, Navy sea-air-land (SEAL) team members, RECON Marines, remote minehunting system (RMS), and*
5. *Determining near shore bathymetry, identifying beaches that are suitable (or not suitable) for supporting an amphibious landing, identifying minefields and obstacles for breaching or avoidance in the water and on the beach (i.e., using VTUAV COBRA), and updating MEDAL databases with new information."*

The boxes shown in Figs. 5.3.3-1 show the region where NRL generated mine burial predictions using DELFT3D and UAS derived oceanography data to drive MBES. The bounding boxes extend from the shore to the 17-meter contour. Two boxes were chosen because one set comes from historical data alone and the other from in-situ data. The historical data was extracted from the Digital Bathy Data Base – Variable Resolution (DBDB-V) maintained by the Naval Oceanographic Office. The second set is a fused data set from surveys taken at the FRF pier as discussed in Section 5.2.4.

These two sets were chosen in order to simulate predictions of mine burial for cases where only historical bathymetric data is available versus the case of having in-situ measurements as obtained by airborne sensors, unmanned underwater vehicles (UUV's), or a combination of the two. The no-sensing runs and AUV-sensing runs will use the first bathy set as we assume that no in-situ data is available for the no-sensing run and AUV will not be able to sense bathymetry depth applicable to MBES. The second set would be use nature runs as the best available data is desired for this run.

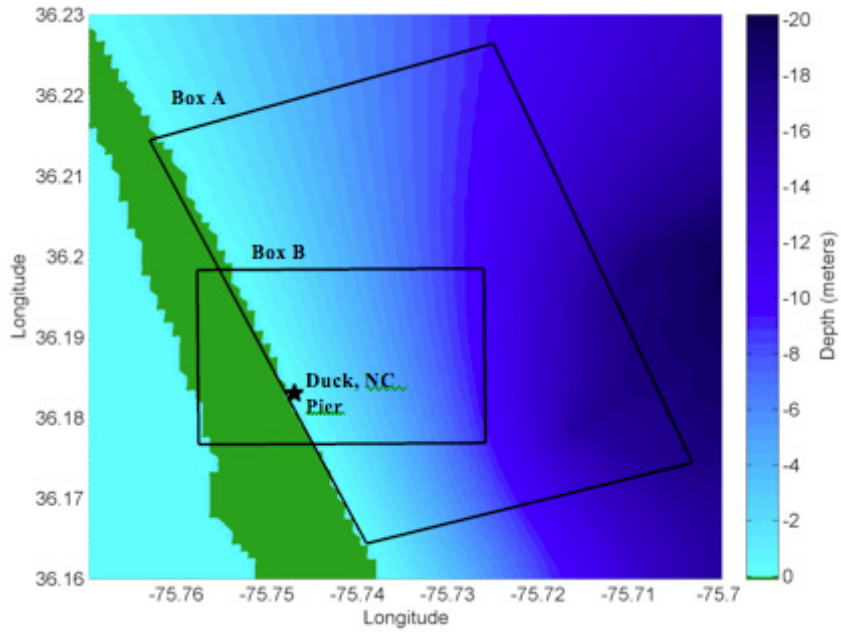

Figure 5.3.3-1. MIW TACSIT Landing and Q-Route Approach Areas.

5.3.4 Analysis Objectives and Methodology

For the MIW portion of this project, we seek quantification of how improved estimation of currents and wave spectra affect DBT and subsequent MCM metrics derived from it. While these results are in the classified addendum to this report, we can discuss the methodology for generating predictions here.

5.3.4.1. Input requirements

Figure 5.3.4.1-1 illustrates the environmental data flow through MBES for scour burial predictions with a hypothetical result. As detailed in Appendix H, the boxes represent nodes of the Bayesian network for scour burial predictions, and the arrows are the links that illustrate the causal links and the direction of forward calculations. The gray colored parent nodes show the seven required environmental inputs. The white colored child nodes show the calculated results, with "PercentBuried", the percent burial of the mine, being the result sought.

The figure shows only one value of input environmental data being specified; however, a histogram of values may be given instead for each MBES run. Table 5.3.1.1-1 shows the source of data used to fill in the input nodes and whether we use a single value or a histogram. Single value inputs represent static values at each grid point – water depth, sand grain size ("Fine"), initial burial (0%-10% from settling), and run duration (2 days). Histogram inputs are used for the oceanographic forcing – wave height, wave period, and tidal amplitude – as these quantities vary over the 2 day run period so that there are statistical distributions for these quantities.

Data Type	Units	Source	Histogram or Single Number
Significant wave height	Meters	Delft-3D	Histogram

Peak wave period	Seconds	Delft-3D	Histogram
Water depth	Meters	DBDB-V or FRF	Single number
Tidal amplitude	Meters/second	Delft-3D	Histogram
Sand grain size	Millimeters	Schwartz & Birkemeier, 2004	Single number
Duration	Days	User defined	Single number
Initial burial	Percent mine diameter	User defined	Single number

Table 5.3.4.1-1. Input data, units, source and type (histogram or single number) required for scour burial predictions by the Mine Burial Expert System.

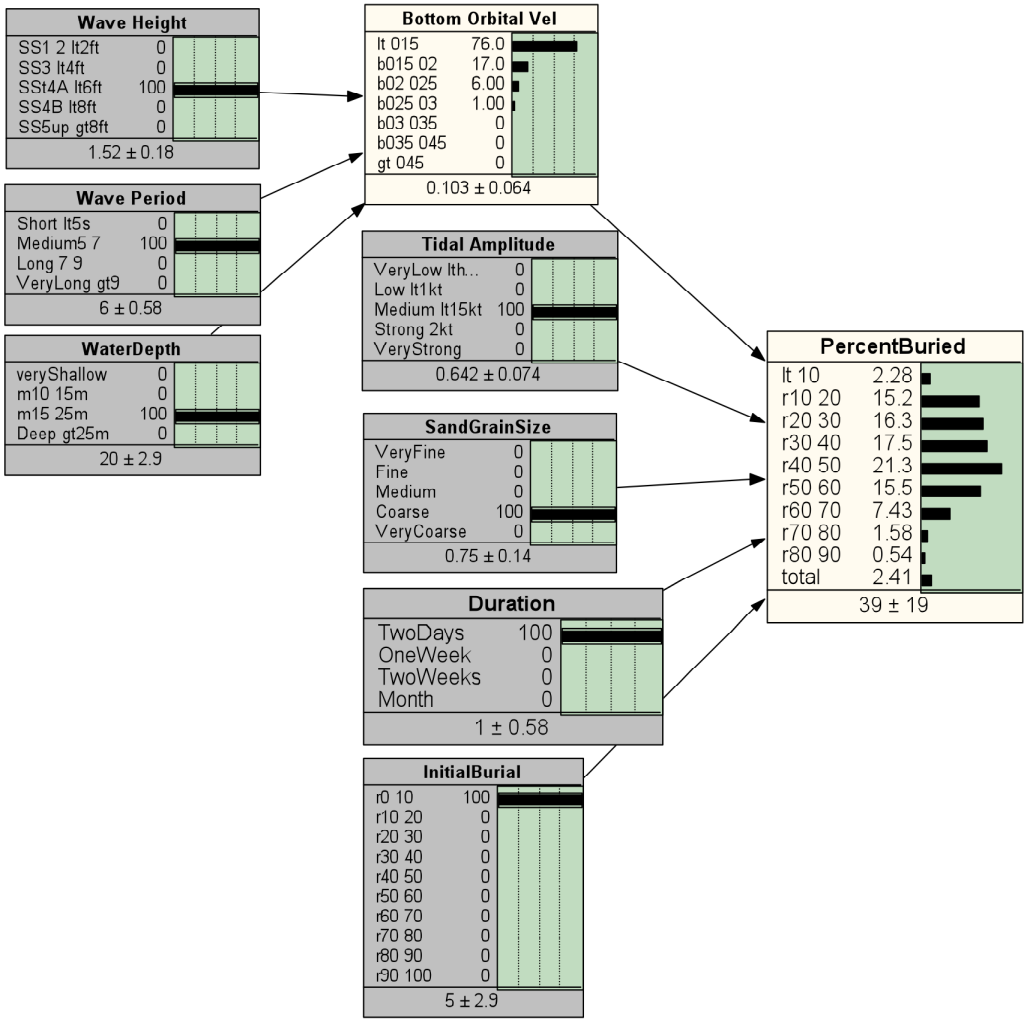

Figure 5.3.4.1-1. Bayesian network topology for the scour portion of the Mine Burial Expert System.

5.3.4.2. Preprocessing Procedures

MBES only provides burial predictions at a single location. We obtain an area result by iterating through a pre-assigned computational grid with the required environmental inputs

provided at each point. Thus, to obtain a statistical distribution of oceanography conditions at each grid point over a 2-day period, Delft-3D provided wave period, wave height and tidal amplitude in 20–minute time steps at spatial intervals of 0.0001 degrees. Histograms for the oceanographic data were then computed from 0.002 degree spatial bins of the output over the two day period. This coarser grid also serves as the output grid for the MBES computations.

These histograms were written to ASCII files for ingest into the MBES system with a file name and format specified by the MBES documentation included with the software. The static data was likewise written to ASCII files for MBES ingest. MATLAB scripts were then written so that the wrapper function for MBES was given the computational grid for the calculations and the location of the input files.

5.3.4.3. Postprocessing Procedures

The relevant output file from MBES is an ASCII file that provides histograms for percent burial at each geospatial location of the output grid. Histogram bins are in ten percent increments and given to three decimal places. MATLAB scripts were written to ingest these output files and compute a cumulative probability distribution to give burial for two cases. The first case is "likely burial", defined to be the burial state at the 50th percentile. The second case is the "percentage undetectable", defined to be the percentage of mines exceeding preset burial threshold.

5.3.5 Effectiveness Analysis Results

As discussed in Appendix I, the key mechanism of scour burial is frictional stress on the seabed caused by wave action and currents, given by Eqns. (I-3), (I-4), and (I-7) in that appendix. In an environment where the wave induced fluid velocity along the bottom – the orbital velocity (U_b) – is much greater than other currents, then burial becomes proportional to the U_b (U is effectively replaced by U_b in Eqn. (I-2)). Thus, an examination of the orbital velocities will provide an indication of the burial expected under the assumption that other currents are small.

Figures 5.3.5-1 and 5.3.5-2 provides scatter plots of orbital velocity with depth for the eight sets of nature runs, no-sensing runs, and BAMS UAV sensed runs for optical sensors (5.3.5-1) and for the optical + radar sensors (5.3.5-2). (For the latter, it is assumed that the best sensing angle is used and low winds are present, c.f. Table 5.2.5-2.) Standard deviations of the data points are ~10% of the value. Double arrows appear in the plots where hypothesis testing (the MATLAB implementation of the Wilcoxon rank-sum test with a two-sided 95% significance level was used [see Ref. 34]) showed that a) the nature run and BAMS data were both significantly different from the no-sensing run and b) the null hypothesis was acceptable between the nature run and BAMS data. The length of the double arrow shows the depth range for which these two hypothesis testing results held.

For the optical sensors (green wavelength), the December 25, 2008 runs showed that the sensing run provides predictions closer to the nature run than the no-sensing run; similar results were observed for the optical sensors on the Fire Scout and Scan Eagle UAVs. For the BAMS optical + radar sensors, significant differences are seen for two different runs: September 17, 2007 and August 22, 2008. For both sensor types, the differences become greater between the no-sensing run and the BAMS/nature runs as one get closer to shore. In the December 25 case, BAMS sensed oceanography should show lower burial than the no-sensing run. This result

means that minehunting efforts will be more successful and clearance should proceed more rapidly. For the September 17 and August 27 cases for optical + radar sensors, the no-sensing run provides a potentially over optimistic state of mine burial, so MCM should proceed more slowly or the area may need avoidance.

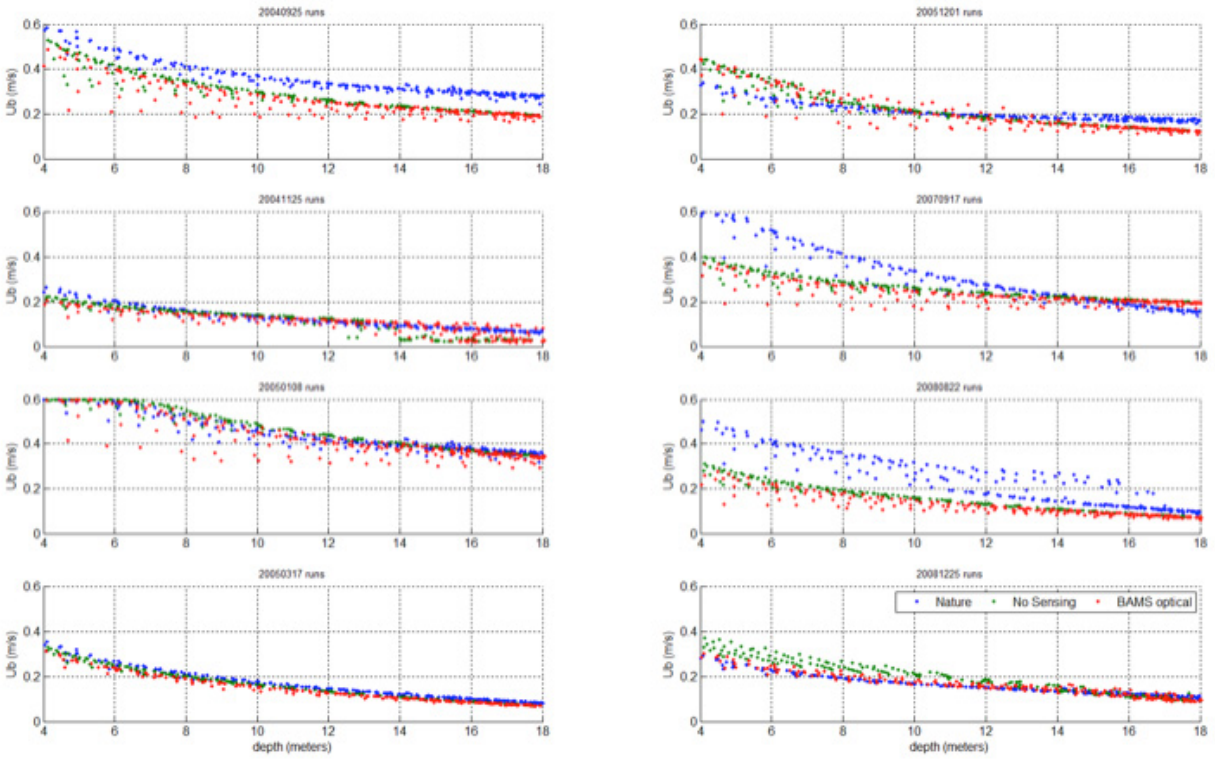

Figure 5.3.5-1. Scatter plots of orbital velocity (m/s) with depth (meters) for the eight nature (blue), no sensing (red) and BAMS optical sensing (green) runs. The double arrow in the December 25, 2008 plot shows the range in which the data passed hypothesis testing explained in Section 5.3.5. Titles give date in "yyyymmdd" format (e.g. 20040925 is Sept. 25, 2004).

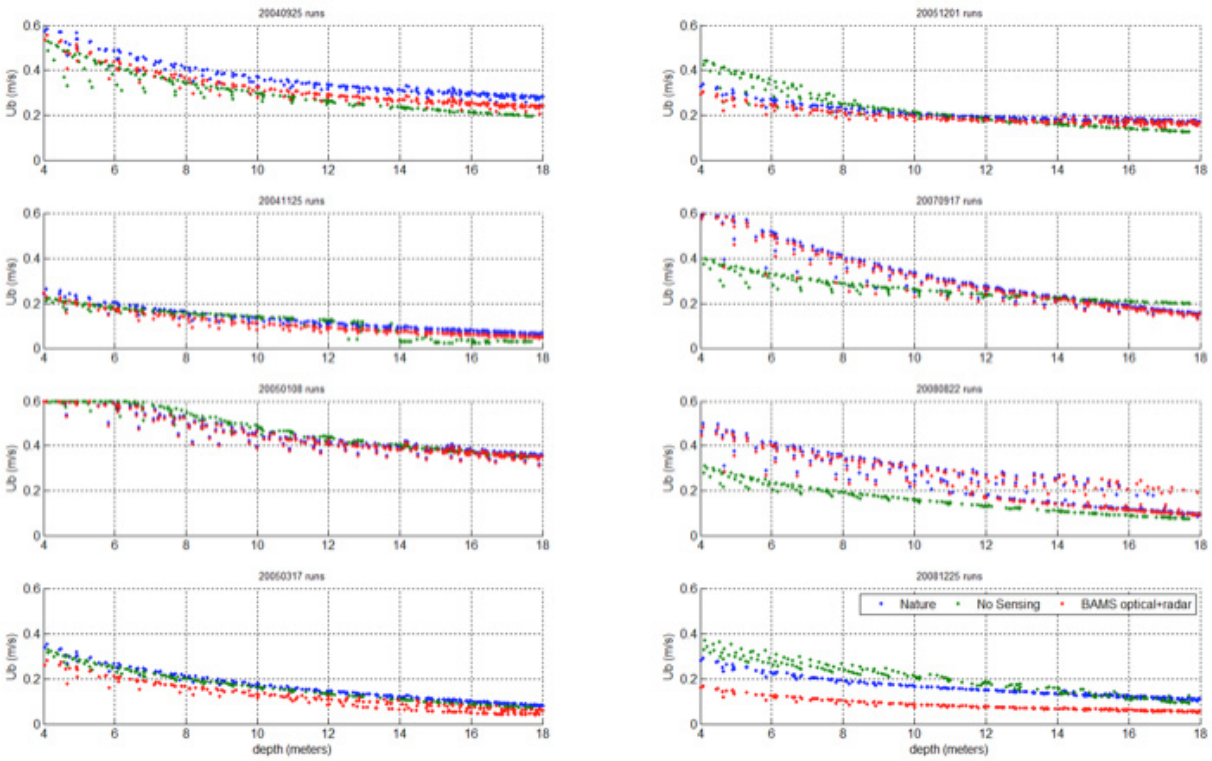

Figure 5.3.5-2. Same as Fig. 5.3.5-1 with BAMS radar used instead of the optical sensor.

5.3.6 Summary Conclusions

In this section, we have reviewed the Mine Burial Expert System (MBES), the scour burial process for which mines burial in sandy bottom environments, and the Doctrinal Bottom Type (DBT) metric used by MIW for planning MCM operations. This section also discussed the TACSIT area for which mine burial predictions will be given and the MBES methodology for generating predictions. We furthermore discussed how orbital velocity can provide qualitative expectations of burial and identified runs in which the BAMS AUV appears to provide sensed oceanography that more closely matched the nature runs.

The December 25, 2008 optical runs and the optical + radar runs of September 17, 2007 and August 22, 2008 can be analyzed further to see under what conditions this agreement occurred, if it is reproducible, and what differences there are in expected burial. It is evident that future gauging of the effectiveness of BAMS for MIW, boundary conditions for simulations should to be decoupled from the deep water SWAN model if possible. Actual in-situ BAMS data, however, should give the best assessment capability.

The following conclusions can be drawn from these Delft3D and MBES model results:

1. The technical feasibility of optical sensing of wave period/direction and radar sensing of wave spectra and subsequent inversion for bathymetry is well established.

2. For mine burial estimation in the Duck, NC environment, bathymetry estimation alone (no wave spectra estimation) yields marginal warfighting impact result.

3. For mine burial estimation in the Duck, NC environment, bathymetry + wave spectra estimation is expected to yield a more substantial warfighting impact. Initial mine burial model runs with radar wave spectra estimation supports this hypothesis. Additional model runs are needed to quantify this impact.

4. UAS employment CONOPs optimization is likely required to extract maximum benefit from UAS environmental sensing in support of mine burial estimation.

5. UAS survey and the supporting data assimilation and modeling CONOPs and required C2 connectivity is apt to be complex and coordination with OCEANOPSCOM Directorates is required. Additional connectivity with the MIW Environmental Post-Mission Analysis system also will be required. Since mine burial from wave action is largely correlated with orbital velocity at the bottom, we estimate that a minimum improvement of 16% in the No UAS Sensing case to 75% or greater agreement with ground truth will be required to make the investment in UAS sensing, data assimilation, and modeling a cost effective option.

5.4 Cruise Missile Defense, Straits Transit TACSIT

From the Committee on Environmental Information for Naval Use, of the National Research Council, see Ref. [3], the following use case illustrates the potential role of UAS METOC sensing in support of Naval fires. Similar considerations apply to the potential role of UAS METOC sensing in support of cruise missile defense and straits transit operations. *"February 2010, Somalia: An important naval gunfire support mission is called for during the early morning hours to support U.S. Marines deployed inland as part of a multinational force committed to breaking up a concentration of hostile combatants with ties to an international terrorist organization. The weather forecast predicts clear skies. The embarked METOC officer is not convinced the weather over the coastal targets will be clear enough for accurate gunfire visual spotting. He consults with his division and establishes broadband communications with the Fleet Numerical Weather Facility in Monterey and the Naval Oceanographic Office in Mississippi. An online chat session is established, and the climatological records are accessed. Forecasters, including a METOC officer with experience in Somalia, agree that an early morning temperature inversion is not unusual for that time of year. Coupled with the smoke from wood-burning fires and stoves common in developing nations, this situation can obscure visibility if winds are not present. Based on this information, the METOC officer directs that an unmanned airborne vehicle (UAV) be launched over the target area at sunrise. The optical UAV and METOC sensors, including a dropsonde, verify that visibility will be poor and visual spotting of rounds on target will be very difficult. The possibility of collateral damage will be great. The operational commander consults with senior commanders in the joint operating force and delays the operation and the gunfire support mission until 1000 hours, when the inversion layer has lifted. The mission is successfully conducted at that time."*

5.4.1 Identification of Study Team

Larry Phegley of NRL Monterey, Code 7500, Andy Pontzer of NAVAIR 5.1.2.1, and Alex Mackenzie of AOR Inc. are the lead analysts for the Anti-Ship Cruise Missile (ASCM) Defense, Straits Transit TACSIT analysis. This analysis included UAS experiments conducted at Naval Air Station (NAS) Patuxent River, Webster Field Annex. Eduardo Danganan of NAVAIR generated a mapping of this TACSIT area to relevant DoD planning scenarios and OPLANs.

5.4.2 Mission Area (TACSIT) Overview

The purpose of the Anti-Ship Cruise Missile (ASCM) Defense, Straits Transit TACSIT analysis and experimentation reported here is to explore the potential warfare value-added of conducting UAS soundings and imaging in support of numerical weather prediction (NWP). *The focus of this analysis is on near-term exploitation of the BAMS Increment 1 organic sensor suite.* There are three major near-term possibilities for leveraging the BAMS organic sensor suite in support of NWP as follows:

TAMDAR-Like Capability. The BAMS Increment 1 system has the requirement[10] to collect ambient temperature, wind speed and direction, relative humidity, and barometric pressure in near real-time (NRT). This will result in a Tropospheric Airborne Meteorological Data Reporting (TAMDAR[11]) like capability on BAMS. The resulting data will be downlinked to the BAMS mission control system, and from there could be communicated to the Fleet Numerical Meteorology and Oceanography Center (FNMOC) in Monterey, CA for assimilation into the NOGAPS and COAMPS NWP models.

In Ref. [13], the authors report that: *"An adjoint-based method is used to calculate the impact of in-situ upper-air observations from a data-austere region of high meteorological variability (Almaty, Kazakhstan) on short-range forecast error in the Navy Operational Global Atmospheric Prediction System (NOGAPS). During the May 2006 – July 2007 study period, Almaty World Meteorological Organization (WMO) Aircraft Meteorological Data Relay (AMDAR) ascent and radiosonde observations assimilated at 00 UTC have large beneficial impacts on forecast error reduction when compared to average global AMDAR ascent and radiosonde observation impacts. For Almaty, the average impact of an AMDAR ascent observation is more than twice as beneficial as that of a radiosonde observation in the reduction of forecast error in the global domain. The large beneficial impact of Almaty AMDAR ascent observations offers great promise for the beneficial utilization of weather data from unmanned aircraft systems (UAS) deployed in similar environments. Currently, the long-endurance medium-altitude Predator flown by the USAF and others is the most suitable UAS platform available for AMDAR-like surface to mid troposphere atmospheric profiling. The acquisition of both test and in-theater Predator data and the concurrent examination of how such data impacts the accuracy of short-range forecasts in data-sparse regions are ongoing at NRL."*

As a part of this study, NRL, NAVAIR, and AirDat LLC conducted a series of three UAS experiments at Naval Air Station (NAS) Patuxent River, Webster Field Annex as described below in Sections 5.4.3 and 5.4.4. The goals of these experiments included: (1) establish via experimentation that UAS temperature, pressure and humidity (TPH) and wind data collections can provide RAOB-like observations; (2) assess the value-added of UAS data collections in a data denied environment; (3) assess the tactical utility of UAS data collections for EM performance prediction accuracy and impact on ASCM or TACAIR intercept; and (4) assess the impact of winds aloft estimation on Naval Gunfire Support (NGFS). In addition, the data

---

[10] Email correspondence from Paul Eiff, paul.eiff@navy.mil, BAMS Future Capabilities, PMA 262 Support, 27 July 2009.

[11] The Tropospheric Airborne Meteorological Data Reporting (TAMDAR) system is a weather monitoring system that utilizes sensors mounted on ordinary commercial aircraft for data collection. AirDat LLC, http://www.airdat.com/ is the developer of the TAMDAR capability.

collected during these experiments will be employed in a COAMPS data denial experiment as discussed below in Section 5.4.5.

Doppler Radar Assimilation. In Ref. [23], the author reports that: *"The hourly-cycled high-resolution data retrieval and assimilation system developed at NRL for radar, satellite and surface observations for the COAMPS model will provide the Navy, through the NRL NOWCAST system, with near real-time, three-dimensional cloud and wind analyses and very short-term (0-6 hours) theater-scale weather forecasts in any region of interest to support the Navy's mission. The technology was demonstrated during Fleet Battle Experiment – Juliet with products providing up-to-date, detailed information to tactical decision makers about the three-dimensional atmospheric battlespace conditions. The high-resolution winds from both the data assimilation system and the COAMPS model forecast are also used to drive chemical/biological (CB) dispersion models, which are used for assessing contamination avoidance and decontamination strategies. While focusing on battlespace environmental applications, this work also establishes a scientific framework for utilizing radar-derived meteorological information in nowcasting and numerical weather prediction applications."* Three-dimensional wind data collections in Naval operations areas and target locations could also provide information critical for effective Naval Fires support, e.g. in support of Advanced Gun System (AGS), Long Range Land Attack Projectile (LRLAP) engagement operations.

NRL Monterey is in discussion with the BAMS Program Office concerning the potential of assimilating BAMS Multi-Function Active Sensor (MFAS) Active Electronically Steered Array (AESA) doppler radar data into COAMPS. It is believed that the BAMS Increment 1 capability will downlink the needed data to the BAMS mission control system, and from there could be communicated to Fleet Numerical Meteorological and Oceanographic Center in Monterey, CA for assimilation into the NOGAPS and COAMPS NWP models.

Dropsondes. A dropsonde is lightweight device that measures pressure, temperature, and humidity (TPH) and winds during descent from a launch platform. Dropsonde data is used widely in atmospheric research and severe weather and hurricane forecasting. For the Global Hawk UAS, a collaborative partnership has been formed between NOAA, NCAR, NASA to build, integrate, and operate an autonomous UAS dropsonde capability. This initiative is relying on NCAR Earth Observation Laboratory's long experience with dropsonde development and launching and is employing the new Miniature In-Situ Sounding Technology (MIST) sonde system. MIST is smaller and lighter than current dropsondes and has the following capability specifications:

- Mass: 175 g (~6 oz),
- Length: 30.5 cm,
- Diameter: 4.7 cm,
- Fall speed: 11 meters/second at sea surface,
- Measures pressure, temperature, humidity @ 2Hz rate,
- Measures Winds @ 4 Hz rate,
- 3-cell Lithium battery pack, and
- RF Telemetry signal in 400 MHz Meteorological band.

Figure 5.4.2-1. Miniature In-Situ Sounding Technology (MIST) Sonde System.

It is important to note that a BAMS dropsonde capability will require a wing pod. There is however no BAMS Increment 1 requirement for a wing pod and no BAMS Increment 1 platform modifications are possible at this time. On the other hand, BAMS Program Office discussions are underway concerning BAMS Increment 2 podded solutions for communications relays, SIGINT collections, and possibly other requirements/applications. Hence a BAMS dropsonde capability could be introduced as an N84 "POM 12 seam issue" for inclusion of this capability in the Increment 2 BAMS platform.

There are, however, a number of substantial issues that impact the feasibility of pod solutions, including icing, the fact that pods significantly reduce BAMS flight endurance and resulting impacts on BAMS CONOPs, BAMS power budget constraints and limits, practical pod space constraints, and competition with other BAMS missions (e.g. communications relay operations, SIGINT collections, etc.) for pod space.

5.4.3 UAS Experimentation Plan

As a part of this study, NRL, NAVAIR, and AirDat LLC have conducted a series of three UAS experiments at Naval Air Station (NAS) Patuxent River, Webster Field Annex. The goals of these experiments included: (1) establish via experimentation that UAS temperature, pressure and humidity (TPH) and wind data collections can provide RAOB-like observations; (2) assess the value-added of UAS data collections in a data denied environment; (3) assess the tactical utility of UAS data collections for EM performance prediction accuracy and impact on ASCM or TACAIR intercept; and (4) assess the impact of winds aloft estimation on Naval Gunfire Support (NGFS).

The UAS experiment plan for the 23 February through 12 March, 18-29 May, and 13-19 August experiment periods can be briefly described as follows:

- One radiosonde observation (RAOB) was taken at the start of each observing period at the Naval Air Station.

- An Aerolite small tactical UAS (similar to a ScanEagle or Raven STUAS) flew alternately at 500 feet and 1200 feet. This UAS employed a Vaisala PTU-300 sensor that can measure temperature and humidity. Wind speed and direction is measured using the aircraft navigation system.
- An Aerostar persistent UAS (similar to a Predator) flew at 14,000 and 6,000 feet. This UAS employed a Vaisala PTU-300 sensor that can measure temperature, humidity, wind speed and direction.
- A Prescott Pusher (replaced with a Pelican manned aircraft in the August experiment) flew at 20,000 feet and employed a TAMDAR sensor.
- The two UAS's and one manned aircraft flew orbits around the airfield starting at sunrise for about 4 hours. Continuous PTU-300 and TAMDAR data collections were generated. One UAS (the AeroStar) and the manned aircraft flew in the remotely piloted vehicle area across the St Mary's River from Webster Field.
- Two regularly scheduled local RAOBs (collected at the Wallops Island Flight Facility and at Dulles Airport) were also available on each experiment day.
- EM signal strength measurements was also conducted from the Webster Field control tower to the manned aircraft and from the aircraft to the tower. Signal strength was measured between the two UASs and the ground control stations being used to control them.

The experiment data collection and post analysis plan was as follows. There are three components to this plan: (1) representation of the ground truth environment; (2) comparison of RAOB and UAS data collections; and (3) assessment of the likely value-added of the UAS data collections in a data-denied environment (e.g. open ocean areas or forward areas where in situ observations are not readily available).

Representation of Ground Truth. For the purposes of these experiments, the Naval Air Station Patuxent River RAOB measured at the start of each experiment day serves as the ground truth environment. The RAOB measurements from Wallops Island and Dulles Airport provide backup ground truth measurements.

RAOB vs. UAS Measurement Comparisons. The UAS and manned aircraft ascending and descending profile data has been compared with the ground truth RAOB to confirm the accuracy of UAS TPH and wind profiling. We have also compared Advanced Refractive Effects Prediction System (AREPS) ground truth vs. measured EM range predictions. *The zeroth order experiment objective is to confirm that UAS sensors can provide RAOB like measurements.*

Model Comparisons. NRL Monterey plans to conduct COAMPS runs (2-3 day spin-up plus experiment period plus forecast period) for:

- The current operational observing system with all operational remote and in situ observations minus radiosondes and aircraft reports East of the Mississippi. This will be used to represent an Afghanistan like *data-denied environment*.
- COAMPS will also be run for the *data-denied environment* defined above with assimilation of the Webster Field UAS experiment data.

Comparisons will be made between the ground truth environment, the data-denied environment described above, and data-denied environment with assimilated UAS observations.

Impacts on local Webster Field AREPS EM range and wind speed/direction predictions will also be made. *A major experiment objective is to assess the impact of UAS sensor observations in a data-denied environment on forecast skill and EM/wind predictions as a function of UAS altitude.*

5.4.4 UAS Experiment Results

The experiment data collected during each day of each of the 23 February through 12 March, 18-29 May, and 13-19 August experiment periods includes the following:

- Summary of weather observations made at the start of each flight period.
- Temperature vs. pressure (or altitude) for the experiment RAOB, the Aerostar ascent, and the Aerostar descent.
- Relative humidity vs. pressure (or altitude) for the experiment RAOB, the Aerostar ascent, and the Aerostar descent.
- Wind speed vs. pressure (or altitude) for the experiment RAOB, the Aerostar ascent, and the Aerostar descent.

This data is provided for all flight days during the 23 February through 12 March experiment in Appendix D, for the 18-29 May flight days in Appendix E, and for the 13-19 August flight days in Appendix F.

As an illustration, the data from the 10 March 2009 experiment day is as follows:

Observed Conditions. Temperature and humidity measurements correlated with relative strength for all profiles, possibly due in part to the magnitude of the temperature and humidity fluctuations. There was an absence of a surface evaporation gradient for all profiles. A strong temperature inversion layer was at 900-820 mbar (3,250-6,000 feet). This corresponded with a strong elevated duct near the beginning of the inversion, but was too high to substantially increase detection ranges. A similar trend between ducting height and detection range is also seen with the climatology data. Trapping was noticed below 2,000 ft (942 mbar) on the UAS descent according to the refractivity profile; this seems to correspond to a modest increase in detection range at end of experiment. The middle UAS ascent profile led to the most conservative detection range, so there was no obvious trend across the day.

RAOB vs. UAS Data Collections. Figure 5.4.4-1 shows temperature vs. pressure (left graph), humidity vs. pressure (middle graph), and wind speed vs. pressure (right graph) as measured by the experiment RAOB (blue line), the Aerostar ascent (red line), and the Aerostar descent (green line). A high degree of consistency is shown between the RAOB observations and UAS ascending and descending observations.

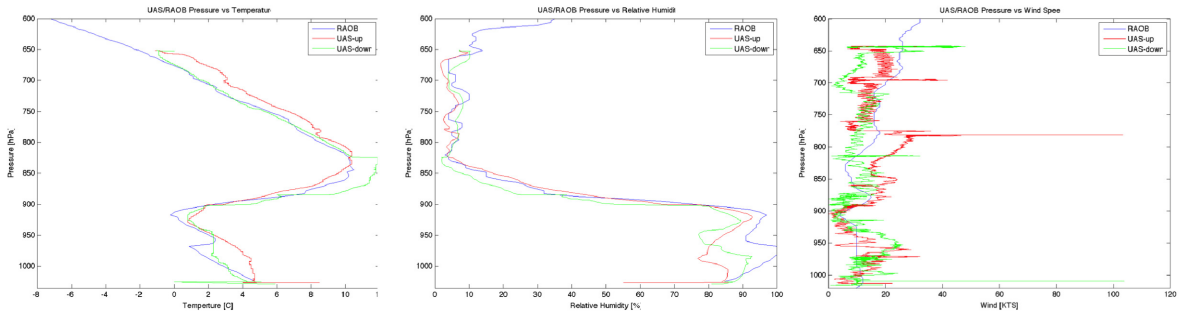

Figure 5.4.4-1. RAOB vs. UAS Data Collections.

AREPS Refractivity Plots. Figure 5.4.4-2 shows refractivity vs. height in M-units for the RAOB profile (left graph), the UAS ascending profile (middle graph), and the UAS descending profile (right graph). As expected, a high degree of consistency is shown between these RAOB and UAS ascending and descending refractivity profiles.

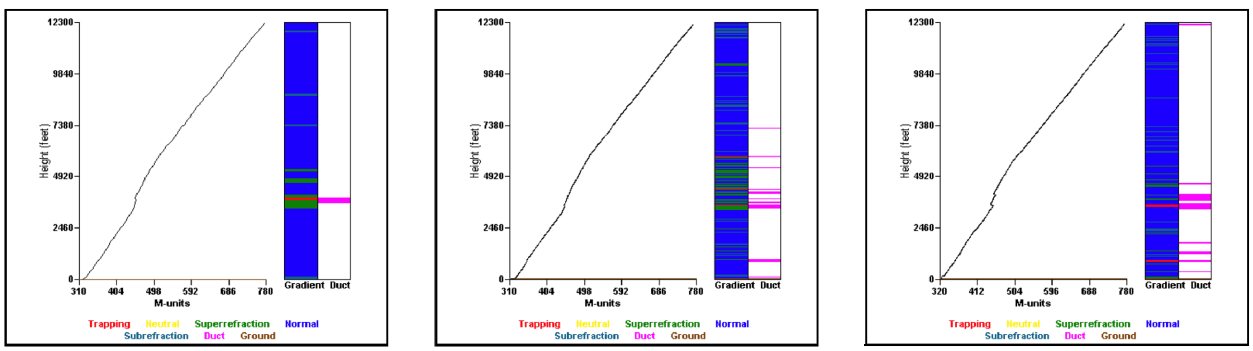

Figure 5.4.4-2. Refractivity Profiles: RAOB (Upper Left); UAS Ascending (Upper Right); UAS Descending (Lower).

5.4.5 UAS Data Denial Analysis Results

NRL Monterey plans to conduct COAMPS runs (2-3 month spin-up plus experiment period plus forecast period) for the days of the 23 February through 12 March, 18-29 May, and 13-19 August Webster Field experiment periods. Two sets of model runs will be performed as follows:

- The current operational observing system with all operational remote and in situ observations minus all CONUS in situ measurements East of the Mississippi. This will be used to represent an Afghanistan like *data-denied environment*.
- COAMPS will also be run for the *data-denied environment* defined above with assimilation of the Webster Field UAS experiment data.

Comparisons will be made between the ground truth environment, the data-denied environment described above, and data-denied environment with assimilated UAS observations. Impacts on local Webster Field AREPS EM range and wind speed/direction predictions will also be made. A major experiment objective is to assess the impact of UAS sensor observations in a date-denied environment on forecast skill and EM/wind predictions as a function of UAS altitude.

5.4.6 Potential Impact of UAS Wind Collections on Fires

U.S. Navy *Joint Surface Strike* requirements address the need for responsive long-range, sea-based precision strike capability that can effectively engage operational targets through the coordinated use of missiles and advanced gun-launched munitions. Joint surface strike targets include C2 facilities, logistics infrastructure, strategic air defense nodes and radars, airfield facilities, ballistic and tactical missile launcher/transporters and storage/assembly sites, large artillery and rocket formations, coastal defense and anti-access facilities, mechanized units and unconventional forces such as terrorist headquarters and operational cells. This includes both fixed and mobile, time sensitive targets.

Similarly, U.S. Navy *Joint Surface Fire Support* address the need to impart a broad range of desired terminal effects on missions in support of ground forces and engagement of enemy targets ashore. Joint Surface Fire Support provided from afloat units will include a collaborative and distributed planning capability. Navy assets will engage fire support targets as requested by supported units and the directing fire support coordination agency in coordination with the strike planning cell and appropriate joint of combined agencies. Joint Surface Fire Support targets include enemy indirect fire systems that threaten ground and special operations forces, air defense units that threaten aviation logistics units, C2 nodes, armor and mechanized units, dismounted infantry and unconventional forces such as terrorist units.

Long-range Naval gun fire support (NGFS) systems, e.g. the Advanced Gun System (AGS) and the Long Range Land Attack Projectile (LRLAP), are substantially impacted by upper as well as lower level winds from the afloat launch location downrange to the target area. In data-denied areas, there is hence the potential that UAS doppler radar sensing of the 3D wind field could have a substantial positive warfighting impact. One of the authors of this report (Stevens) has assessed the impact of 3D wind data collections on the LRLAP effective engagement envelope. The results of this assessment are summarized briefly below.

AGS Fire Control software currently calculates firing solutions, projectile trajectories, and engagement feasibility assuming zero winds and a standard atmosphere. For engagements well within LRLAP minimum and maximum engage range limits, under benign environmental conditions, this lack of METOC data is acceptable from an engagement accuracy point of view given that the projectile is GPS and inertial guided to the target location. On the other hand, for near minimum or maximum range engagements with substantial lower and/or upper level winds (e.g. jet stream conditions) or deviations from a standard atmosphere or other severe weather conditions, the minimum and maximum effective range of the LRLAP projectile can be substantially altered. Table 5.4.6-1 provides a summary of possible jet stream conditions and associated impacts on LRLAP minimum and maximum effective range. Under such conditions, the AGS/LRLAP engagement system as currently implemented on the DDG-1000 platform will be unable to accurately determine whether or not an acceptable (i.e. within required accuracy limits) firing solution exists for near minimum or maximum range engagements. *A METOC data inject to the AGS Fire Control System is required to address this system shortfall.*

Jet Stream Orientation Relative to LRLAP Trajectory	Impact on LRLAP Minimum Effective Range	Impact on LRLAP Maximum Effective Range

Headwind	Minimum range is reduced, *increasing* the engagement volume of AGS/LRLAP	Maximum range is reduced, *reducing* the engagement volume of AGS/LRLAP
Tailwind	Minimum range is increased, *reducing* the engagement volume of AGS/LRLAP	Maximum range is increased, *increasing* the engagement volume of AGS/LRLAP
Crosswind	Minimum range is reduced, *increasing* the engagement volume of AGS/LRLAP	Maximum range is reduced, *reducing* the engagement volume of AGS/LRLAP

Table 5.4.6-1. Impact of Jet Stream Conditions on LRLAP Engagement Volume.

In order to demonstrate the significance of the AGS/LRLAP METOC data issue described above, the following BAE Systems computer experiment was conducted using AGS fire control and LRLAP three degress of freedom (3-DOF) flyout model software[12]:

- Suppose that uniform jet stream conditions exist between the altitudes of 36,000 and 50,000 feet with parametric wind speeds of 60, 150, and 250 knots directly opposed to the LRLAP flight path.
- Assume wind speeds of 30 knots directly opposed to the LRLAP flight path at all other altitudes.
- For each jet stream velocity case, the minimum and maximum AGS/LRLAP engagement range (e.g. the minimum and maximum ranges at which engagement results consistent with applicable AGS accuracy requirements are possible) are computed.

Figure 5.4.6-2 summarizes the results of this computer experiment. Engagement range reductions of as large as 7.55 nm are predicted for strong jet stream conditions. Note that the slope of the curve displayed in Figure 1 provides one possible means to determine the accuracy with which upper air wind speed and direction need to be determined. By inspection, a 60-knot uncertainty in jet stream speed corresponds to a roughly 2 nm uncertainty in operational range. Hence for jet stream profiles of the type considered above, and for wind speed errors of up to 60 knots, the operational AGS engagement range would need to be reduced by 2 nm to avoid the possibility of collateral damage.

12 The LRLAP 3-DOF flyout model employed in this experiment has been tested and informally validated against the accredited AGS LRLAP Enhanced Flight Simulation (EFS). The results of this work have been captured in a BAE Systems internal engineering LRLAP Error Budget Report, and, to a lesser degree, in the AGS Fire Control CONOPs document.

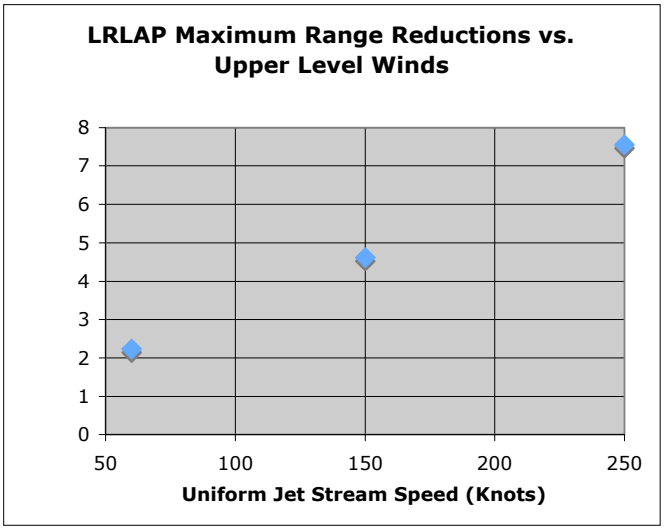

Figure 5.4.6-2. LRLAP Maximum Range Reductions.

Suppose a Naval fires platform operating in support of Joint Surface Strike or Joint Surface Fire Support operations vs. critical targets in a populated area in which collateral damage must be minimized. Assume that the battlespace geometry (e.g. location of key targets ashore) or other constraints (e.g. ship self-defense against coastal missile batteries or maritime threats) dictates near maximum range LRLAP engagements. Suppose further that the engagement area is METOC data-denied and that jet stream conditions or other severe weather effects are possible or anticipated. From the simple computer experiment cited above, it is known that the LRLAP engagement envelope may be reduced by as much as 7.55 nm in range. Engagements outside this reduced envelope will have large probabilities of collateral damage and low probabilities of successful target engagement. Furthermore, without a METOC data inject, there is no way to determine the degree to which LRLAP engagement ranges are impacted. Hence without METOC data there would no choice (assuming collateral damage must be minimized) other than to reduce the estimated maximum range of LRLAP by 7.55 nm, which might result in an incorrect decision to not engage an otherwise engageable critical target. BAMS doppler radar 3D wind collections in such a scenario could hence provide a substantial warfighting payoff in time critical Joint Surface Strike or Fire Support missions.

5.4.7 Summary Conclusions

The purpose of the Anti-Ship Cruise Missile (ASCM) Defense, Straits Transit TACSIT analysis and experimentation reported here is to explore the potential warfare value-added of conducting UAS soundings and imaging in support of numerical weather prediction (NWP). The focus of this analysis is on near-term exploitation of the BAMS Increment 1 organic sensor suite, accordingly this analysis has focused on the potential warfighting value-added of BAMS TAMDAR-like collections, MFAS Doppler radar 3D wind sensing, and dropsonde soundings. The major conclusions of this TACSIT analysis are as follows:

- Three UAS experiments conducted at Naval Air Station (NAS) Patuxent River, Webster Field Annex confirm the viability of STUAS temperature, pressure, humidity and wind speed and direction soundings consistent with RAOB observations. Note that while issues were

encountered with wind speed and direction estimation accuracies, these issues are understood and can be corrected for (see Appendix G).

- Prior analyses, e.g. see Ref. [13], have confirmed the viability of UAS temperature, pressure, humidity and wind speed and direction observations (via TAMDAR-like or future dropsonde capabilities) on NOGAPS and COAMPS forecast errors in data-denied areas. A COAMPS data denial experiment, leveraging the experiment data collected at Webster Field, is in progress.
- Prior analyses (c.f. pp. 71-72 above and Ref. [23]) have confirmed the viability of Doppler radar data assimilation as well as the potential impact of 3D wind estimation in METOC data denied areas on Joint Surface Strike and Joint Surface Fires Support scenarios.
- Most Joint and Navy UAS platforms have requirements for, at a minimum, temperature, pressure, humidity and wind speed and direction observations and METOC production center NWP data assimilation capabilities are available to leverage this data. Work is required to establish the C2 connectivity needed to deliver this data to Joint and Navy METOC production centers and to insure the timely delivery of NWP products to in-theater Naval assets.

5.5 ASW Search and Screen TACSIT

Currently, the vast majority of ocean observations are obtained by satellite sensors with coverage spread uniformly around the globe, providing reasonable horizontal coverage for planetary to synoptic scales. However, the ocean is electromagnetically shallow, and hence information obtainable by space sensors is typically limited to the upper few microns to the upper few meters of the ocean. Most space sensors also do not capture scales smaller than mesoscale, and the information is often relatively sparse in time or subject to loss due to clouds or other atmospheric conditions. Thus space observations do not resolve important processes such as sub-mesoscale vertical structures, internal waves, or the vertical extent of diurnal cycles. Under Navy's Littoral Battlespace Sensing, Fusion, and Integration (LBSF&I) Program, ocean gliders and other unmanned undersea vehicles (UUVs) are being procured and fielded in order to provide the persistent, higher spatial (in both the horizontal and vertical directions) and temporal resolution sensing capability needed to augment air, ship, buoy, and submarine conductivity temperature, and depth (CTD) probe and expendable bathythermograph (XBT) collections. The purpose of this TACSIT analysis is to explore the possibility of augmenting glider in situ sensing with UAS-based ocean in situ measurements. UAS-based ocean sensing could have potentially significant time-distance advantages over ship-launched ocean glider sensing. When coupled with remote sensing and next-generation ocean data assimilation and modeling capabilities, the potential exists for exploiting glider, other UUV and UAS observations in order to forecast tactically exploitable ocean acoustic conditions.

5.5.1 Identification of Study Team

Pete Spence, Dr. Charlie Barron and Dr. Gregg Jacobs of NRL Stennis, Code 7320 and Adrian Fontanilla of AOR, Inc. are the lead analysts for the ASW Search and Screening TACSIT. Eduardo Danganan of NAVAIR generated a mapping of this TACSIT area to relevant DoD planning scenarios and OPLANs.

5.5.2 Mission Area (TACSIT) Overview

Until very recently, Navy ASW search planning guidance was based entirely on average environmental conditions, i.e. climatology, and "range-of-the-day" system performance predictions. In this study we examine the feasibility of using ocean remote and in situ sensing, data assimilation, and numerical ocean dynamical modeling techniques to resolve and forecast the occurrence of non-climatologic ocean conditions which, if predicted with sufficient accuracy and sufficiently far in advance, could be exploited to yield an ASW tactical advantage. Recent studies, e.g. see Ref. [11], have addressed the utility of using ocean gliders to provide regional in situ ocean sensing and substantial ASW search effectiveness impacts were shown to be possible under commonly occurring ocean conditions in WESTPAC areas of interest (AOIs).

This TACSIT addresses the possibility of in the future deploying miniaturized air expendable bathythermographs (AXBTs) from UAS systems for this purpose. NAVAIR has recently released an SBIR topic relating to various UAS micro-sensors including chaff sized BT buoys that could be deployed in payloads of multiple BTs on BAMS or perhaps even on a small tactical class UAV (STUAV). NAVAIR is also investigating a UAS deployable expendable glider (X-glider) concept that could result in glider deployments from BAMS and subsequent glider deployment of mini BTs. UAS-based BT or X-glider deployments could have potentially significant time-distance advantages over ship-launched ocean glider sensing.

Hence the purpose of this ASW search and screen TACSIT analysis is to address the following questions relating to this potential future UAS METOC sensing application:

- To what extent could UAS-deployed mini AXBTs along with improvements in ocean data assimilation and modeling result in the ability to resolve and forecast tactically relevant sub-mesoscale ocean features?
- How common and how persistent are these sub-mesoscale ocean features?
- To what extent could these features be exploited tactically, given sufficiently timely and accurate predictions?
- What are the potential resulting warfighting impacts in relevant Pacific Fleet operations areas and plans?

It is important to note that a BAMS dropsonde capability will require a wing pod or equivalent dispensing mechanism. In addition, there is no BAMS Increment 1 requirement for a wing pod and no BAMS Increment 1 platform modifications are possible at this time. On the other hand, BAMS Program Office discussions are underway concerning BAMS Increment 2 wing pod solutions addressing the need for future BAMS communications relays, SIGINT collections, and possibly other requirements/applications. Hence a BAMS mini-AXBT capability could be introduced as an N84 "POM 12 seam issue" for inclusion of this capability in the Increment 2 BAMS platform.

There are, however, a number of substantial issues that impact the feasibility of pod solutions, including the likelihood that BAMS platform icing may occur at planned flight altitudes, the fact that pods significantly reduce BAMS flight endurance and the resulting impacts on BAMS CONOPs, BAMS power budget constraints and limits, practical pod space constraints, and competition with other BAMS missions (e.g. communications relay operations, SIGINT collections, etc.) for pod space.

5.5.3 Analysis Objectives and Methodology

This study was conducted as an observation system simulation experiment (OSSE), which can be subdivided into five basic steps: (1) generate a nature ocean environment; (2) compute virtual observations; (3) assimilate the virtual observations; (4) assess the impact on the resulting forecast, and (5) assess the potential tactical implications and warfighting impacts of the forecast improvement. Before describing each of these steps in the paragraphs that follow, a brief description of the region of interest and supporting observation systems is provided as a context for understanding the different OSSE components.

The region of interest is the Okinawa Trough, 17 to 34°N and 118 to 134°E, from July through October 2007. This time frame coincides with an intensive U.S. Navy observational deployment: an extensive air-deployed bathythermograph (BT) survey, a shipboard hydrographic survey, and an eight-unit Seaglider array. In addition, there exists standard satellite remote sensing and publicly available surface and publicly available in situ data from the World Meteorological Organization (WMO) Global Telecommunication System (GTS). Satellite SST observations are provided by the Polar-Orbiting Environmental Satellites (POES) Multi-Channel Sea Surface Temperature (SST). Synthetic profiles have been constructed from satellite sea surface height (SSH) observations, satellite sea surface temperature (SST) observations and historical correlations to subsurface values. The GTS observations include SST from drifters and profile temperature data provided by ships of opportunity over GTS.

<u>GDEM Run.</u> The GDEM climatology represents average conditions for each month of the year, corresponding to the 15th day of the month. Fields are linearly interpolated from these monthly averages to the day and/or hour needed for each computation. GDEM does not assimilate any observations or dynamically adjust to predicted atmospheric or ocean boundary conditions. It is a climatological average, based on historical observations only, which is always available far in advance of the actual day and shows what is available for long-range forecasts or in circumstances where local data, forcing and boundary conditions are unavailable. While real world ocean deviations from the GDEM average state can be quite large, GDEM does not currently provide bounds on these deviations. Figure 5.5.3-1 (on the left) shows the predicted sonic layer depth (SLD) in meters associated with this GDEM environment.

<u>Nature Run.</u> The nature run is the closest simulation to the real ocean that we are capable of producing with all available observation, assimilation, and modeling techniques. All of the observations discussed above are assimilated into the Navy's Relocatable Navy Coastal Ocean Model (RELO NCOM) to define the nature run. Thus the nature run combines model aspects which represent acoustically-relevant ocean dynamics such as vertical mixing, internal tides, and diurnal variability forced by wind stress and heat fluxes with a dense array of observations assimilated to guide the model into a dynamic state consistent with measured conditions. For purposes of the OSSE, the nature run is taken to define the true ocean. It is the standard truth used to assess the fidelity of alternative sampling, assimilation and prediction systems. Simulated observing systems may sample data from the nature run to be assimilated in the OSSE alternatives. Acoustic metrics are used to assess the errors between the nature run truth and predictions of the various OSSE alternatives. Figure 5.5.3-1 shows a snapshot of SLD in meters for the Nature Run on 31 October 2007 (on the right) and for the GDEM environment at the same time on the left. Table 5.5.3-1 summarizes the observation data sets that were assimilated to generate the Nature Run.

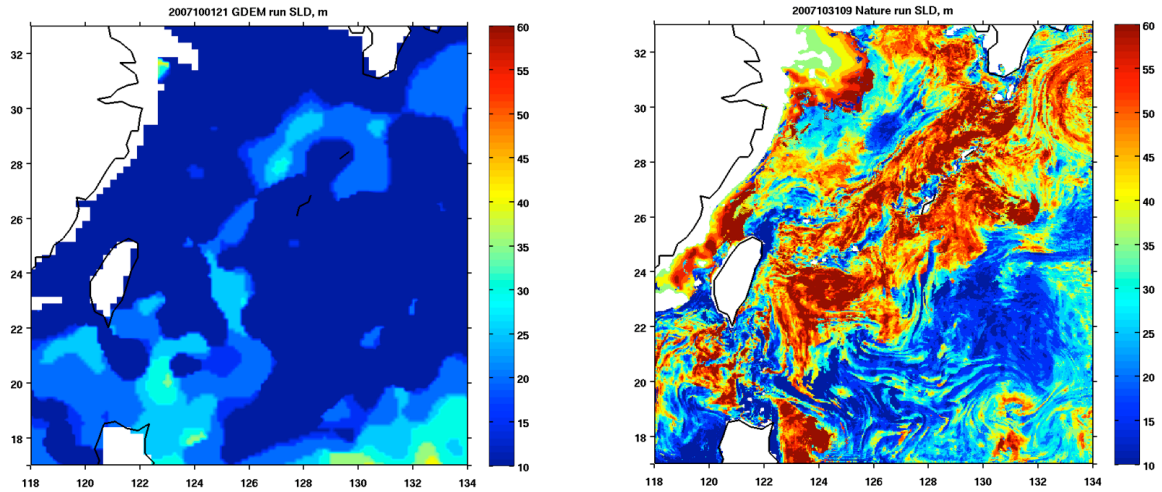

Figure 5.5.3-1. GDEM (left) and Nature Run (right) SLD in Meters for 31 October 2007.

Current Observing System Run. In the current observing system run, a RELO NCOM run is used to represent an assessment of the Navy's current ocean data assimilation and model capabilities. This run employs Navy Coupled Ocean Data Assimilation (NCODA) assimilation of real SST and SSH observations from remote sensing through synthetics. NCODA uses the RELO NCOM 24-hour forecasts as the daily analysis background rather than cycling on the prior NCODA analysis. In this way the NCODA analysis is able to respond to the predicted response to the forecast atmospheric forcing. The current observing system model outputs include forecasts every three hours out to 48 hours (Tau=00, Tau=03,…,Tau=48). This current observing system run uses the operational Navy ocean data assimilation and modeling capability. Table 5.5.3-1 summarizes the observation data sets that were assimilated to generate the Current Observing System Run.

Current Observing System Plus Regional Gliders Run. This run represents the current observing system (described above) plus a representative LBSF&I observation system composed of a large number of gliders deployed in the Okinawa Trough and surrounding region. The simulated glider data are sampled from the nature run without navigation constraints or measurement error, allowing the OSSE to focus on data assimilation rather than glider navigation errors. All simulated glider observations are processed through the Ocean Quality Control (OcnQC) pre-processing to prepare the data for assimilation. The OcnQC used in this study is the same as that used by NAVOCEANO operationally. Table 5.5.3-1 summarizes the observation data sets that were assimilated to generate the Current Observing System Plus Regional Gliders Run.

Simulated glider observations are sampled along the array pictured in Figure 5.5.3-2. This observation array consists of 90 stations sampled every 6 hours, with half of the stations sampled at 00, 06, 12, and 18 hours Zulu and the other half of the stations sampled at 03, 09, 15, and 21 hours Zulu. These station locations and sampling strategies are designed to approximate a 45-glider squadron deployment assuming that the gliders are able to travel between adjacent stations unhindered by limited mobility or opposing currents. Note that sampling effectiveness of an actual 45-glider squadron is a complex function of assumed launch and recovery platform effectiveness, glider mobility, glider reliability, accuracy of ocean current estimates, and many other factors.

OBS	GDEM	Nature	Current Observing System	Current System Plus Regional Gliders	Current System Plus Focused UAS Observations
Sat MCSST	NO	YES	YES	YES	YES
Sat SSH and SST through Synthetic Profiles	NO	YES	YES	YES	YES
GTS SST	NO	YES	YES	YES	YES
GTS profile	NO	YES	YES	YES	YES
Navy Okinawa Trough Experiment	NO	YES	NO	NO	NO
Simulated Gliders	NO	NO	NO	YES	NO
Simulated UAS	NO	NO	NO	NO	YES

Table 5.5.3-1. Types of Observations Employed in OSSE Model Runs.

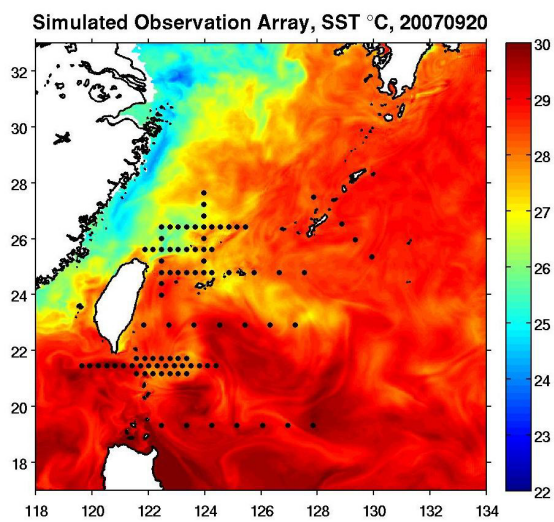

Figure 5.5.3-2. Glider Observation Array Superimposed on Nature Run SST Contours in C°.

Current Observing System Plus Focused UAS Observations Run. This run represents the current observing system (described above) plus a representative UAS observation system composed of varying numbers of UAS sorties (assuming a hypothetical mini-AXCTD capability) deployed in an approximately 200 km x 200 km search box, see Figure 5.5.3-3. UAS AXBT deployments are assumed over the 5x5 grid of measurement locations centered over the southern search box 48 and 24 hours prior to the expected barrier search time. Table 5.5.3-1 summarizes the observation data sets that were assimilated to generate the Current Observing System Plus Focused UAS Observations Run.

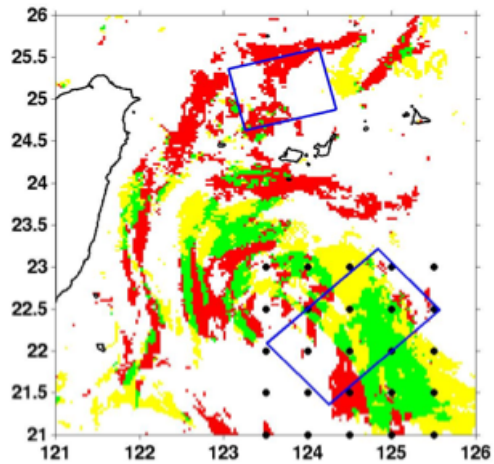

Figure 5.5.3-3. UAS Observation Array Superimposed on Mid-Frequency (MF) Active Search Box.

Tactical Analysis. In the analysis reported below, potentially exploitable sub-mesoscale ocean features were located in space and time by looking at two metrics as follows: differences between climatology based and nature environment based estimates of SLD and cutoff frequency (f_{co}). SLD is the depth at which the maximum, near surface sound velocity occurs. The cutoff frequency associated with a surface duct is the minimum search tonal frequency that will be trapped in the duct. This can be computed as follows:

$$f_{co} = 0.398 \frac{S^{3/2}}{\Delta S^{1/2} H}$$

where

S = Sound velocity at the layer depth in feet/second,

ΔS = Difference in sound velocity values measured at the layer depth and at the surface in feet/second, and

H = Layer depth in feet.

Ocean areas with large (climatology vs. nature environment) differences in SLD, and with f_{co} values in the nature environment less than acoustic frequencies of interest, were flagged as being potentially exploitable.

Given the identification of a potentially tactically exploitable ocean location and time, the following tactical analysis approach is employed to assess the potential ASW operational impact:

- An ASW search operation is postulated including search objective, search platform and sonar type, and threat type(s) and expected motion parameters.
- Five ASW search strategies are developed for each search operation, corresponding to the level of environmental knowledge assumed and Navy optimal search planning guidance: (1) no environmental knowledge (planning based on GDEM climatology); (2) perfect environmental knowledge (planning based on the Nature environment); (3) planning based on current observation, assimilation, and ocean modeling system; (4) planning based on current system plus regional glider observations; and (5) planning based on current system plus focused UAS observations.

- For the illustrative case of an ASW barrier in which searcher speed (v) is comparable with target speed (u), Navy optimal search guidance results in the recommendation of either a *linear* or *crossover* patrol (see Refs. [15] and [16]) depending on the values of u, v, total barrier length (D), and expected searcher detection range (ω). Under the assumption of uniform environmental conditions, a single searcher can, for instance, execute a crossover patrol with probability of detection P_{goal} over a subset of the barrier of length d (d < D), where

$$d = \omega \cdot \left(1 + \frac{\rho\sqrt{\rho^2 + 1}}{\rho + 1} \right) \cdot P_{goal}^{-1}$$

  and ρ=v/u. This relationship is used to define operationally feasible barrier searches; similar expressions are available for linear patrols as well as other ASW search operation types. The environment directly affects ω, and the critical decision lies in where the barrier is positioned to optimize ω.

- In order to test the five search strategy cases listed above, a discrete event simulation (DES) is employed to Monte Carlo simulate a random threat transitor vs. an optimal crossover patrol as pictured below in Figure 5.5.3-3. Each optimal linear or crossover patrol is computed as a function of u, v, d, and ω. Detection opportunities are simulated using Oceanographic and Atmospheric Master Library (OAML) acoustic prediction models (e.g. the Navy Standard Parabolic Equation - NSPE for passive and the Comprehensive Acoustic Simulation System - CASS for active), the nature environment discussed above, and underlying environmental databases (e.g. Digital Bathymetry Database Variable (DBDB-V) for bathymetry, Low Frequency Bottomloss (LFBL) for low frequency bottom loss, High Frequency Bottomloss (HFBL) for high frequency bottom loss, Lambert's Law for bottom backscatter, etc.).

- The basic tactical analysis metric computed for each ASW search location and strategy is the cumulative probability of detection, P(t), averaged over all Monte Carlo replications where searcher and target starting locations and figure of merit (FOM) values are randomly varied from replication to replication. See Ref. [11] for a description of the approach used to calculate P(t). It is also of interest to plot the collection of cumulative probability of detection curves corresponding to each Monte Carlo replication.

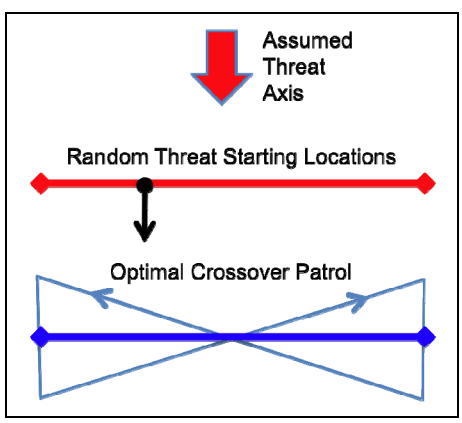

Figure 5.5.3-3. Barrier search schematic.

5.5.4 Effectiveness Analysis Results

An active acoustic ASW tactical analysis was conducted in the search box pictured in Figure 5.5.4-1. The red arrow to the SW of this box denotes the assumed threat axis. The search objective is to conduct a barrier patrol within the search box where the barrier is assumed to be oriented perpendicular to the threat axis. The exact location of the barrier within the search box, however, can be selected in order to exploit knowledge of the environment with the goal of optimizing barrier effectiveness. This search box and the associated search day and time were selected in order to exploit strongly non-climatologic conditions known to exist in the OSSE nature environment at this location and time. Figure 5.5.4-2 shows the SLD in meters for the Nature Run at the time and location of the planned search (on the left) and average predicted detection range vs. barrier location in nm from the southwestern border of the assumed search box (on the right). The optimal barrier location is shown to be approximately 60 nm from the southwest border of the search area.

Inspection of Figure 5.5.4-2 reveals a "hotspot" search area with SLD values of 60 meters or greater in the upper northeast portion of the search box. GDEM climatology represents average conditions and hence it fails to represent this exploitable hotspot area. The current NCOM observing system, as depicted below in Figure 5.5.4-3, is shown to fail to precisely locate this hotspot at the time of this search (it predicts a weakly optimal barrier location of 40 nm from the southwest border of the search area).

Hence the tactical question of interest is "*can these strongly non-climatologic features, if accurately predicted, be exploited to gain an ASW tactical advantage*?" In order to answer this question, five cases were considered as listed below in Table 5.5.4-2. The Table 5.5.4-2 GDEM row represents the "no real-time environmental information" case while the Nature row represents the "perfect environmental prediction" case. Actual search performance can be expected to lie between these two extremes. The last three rows in Table 5.5.4-2 correspond to planning based on a 45 hour forecast generated using the current operational remote and in situ observing system, the current system plus regional gliders, and the current system plus focused UAS observations respectively.

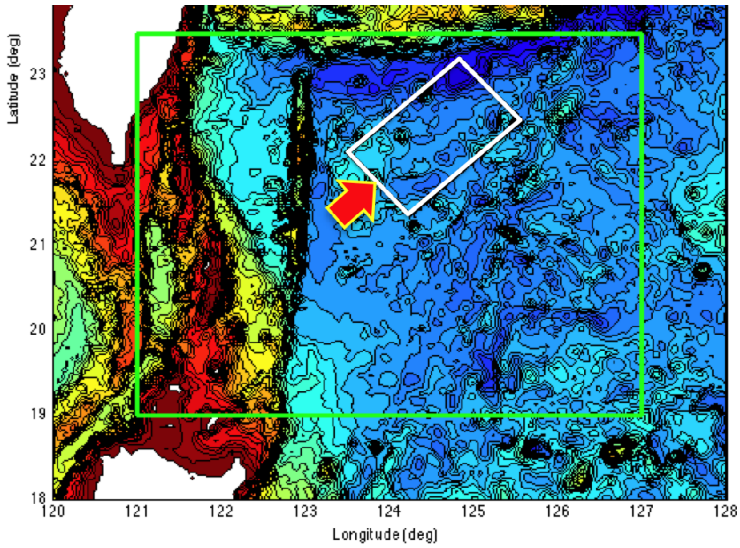

Figure 5.5.4-1. Location and orientation of the assumed ASW search area.

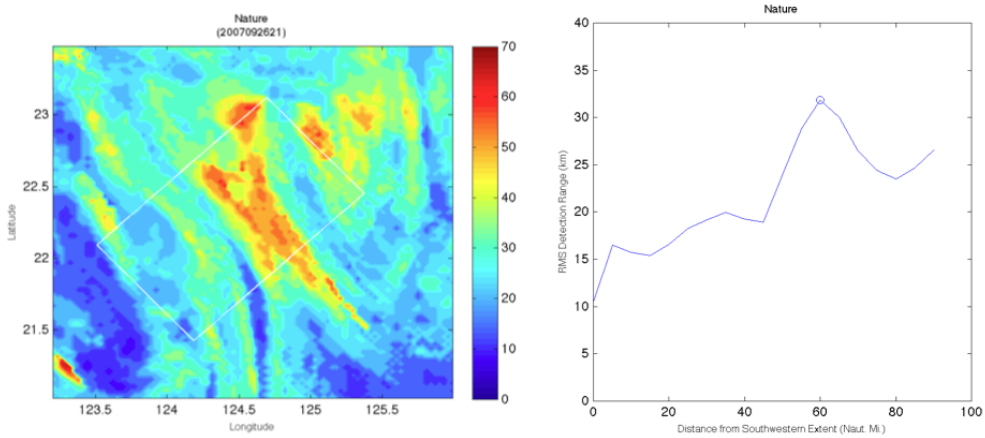

Figure 5.5.4-2. Nature SLD (left) and Detection Range vs. Barrier Location (right) Metric Plots.

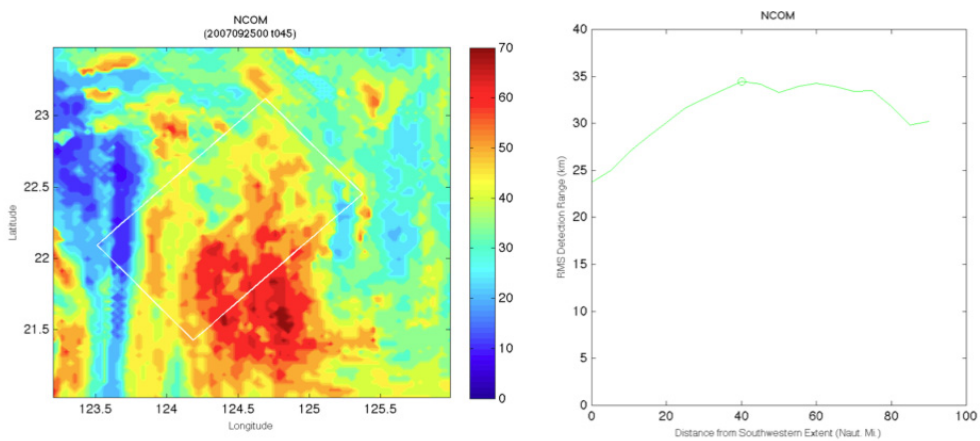

Figure 5.5.4-3. NCOM SLD (left) and Detection Range vs. Barrier Location (right) Metric Plots.

Planned Based On	Results Based On	Significance of Case
GDEM	Nature	This quantifies the potential penalty when planning without ocean predictions.
Nature	Nature	This quantifies the potential maximum benefit when planning with (perfect) ocean predictions.
45h Prior Forecast with Current Observing System	Nature	This quantifies the benefit associated with planning based on a 45h forecast with the current observing system.
45h Prior Forecast with Regional Glider Observations	Nature	This quantifies the benefit associated with planning based on a 45h forecast with the current observing system plus regional glider observations.
45h Prior Forecast with Focused UAS Observations	Nature	This quantifies the benefit associated with planning based on a 45h forecast with the current observing system plus focused UAS observations.

Table 5.5.3-2. Search Effectiveness Analysis Cases Considered.

Figure 5.5.4-4 shows the SLD in meters for the current NCOM observing system including assimilation of data generated by the regional glider observing system depicted above in Figure 5.5.3-2 at the time and location of the planned search (on the left) and average predicted detection range vs. barrier location in nm from the southwestern border of the assumed search box (on the right). With glider sensing the recommended search barrier location is approximately 85 nm from the southwestern border of the search area.

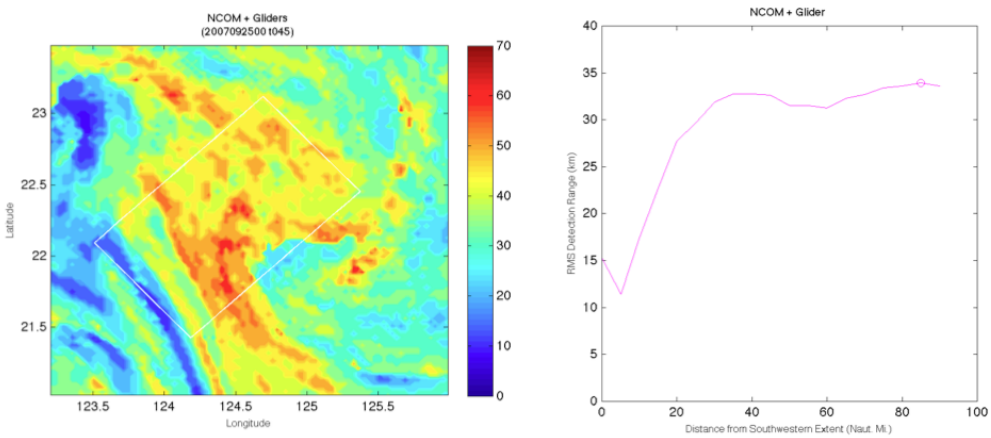

Figure 5.5.4-4. NCOM + Glider SLD (left) and Detection Range vs. Barrier Location (right) Metric Plots.

Figures 5.5.4-5 through 5.5.4-8 show the sonic layer depth (SLD) in meters for the current NCOM observing system including assimilation of data generated by the local UAS observing system depicted above in Figure 5.5.3-3 at the time and location of the planned search (on the left) and average predicted detection range vs. barrier location in nm from the southwestern border of the assumed search box (on the right). Four cases are considered as follows: one UAS sortie 24 hours prior to the search, two UAS sorties 24 and 48 hours prior to the search, two UAS sorties 24 and 12 hours prior, and four UAS sorties 48, 36, 24, and 12 hours prior. With UAS sensing the recommended search barrier locations range from approximately 40-60 nm from the southwestern border of the search area.

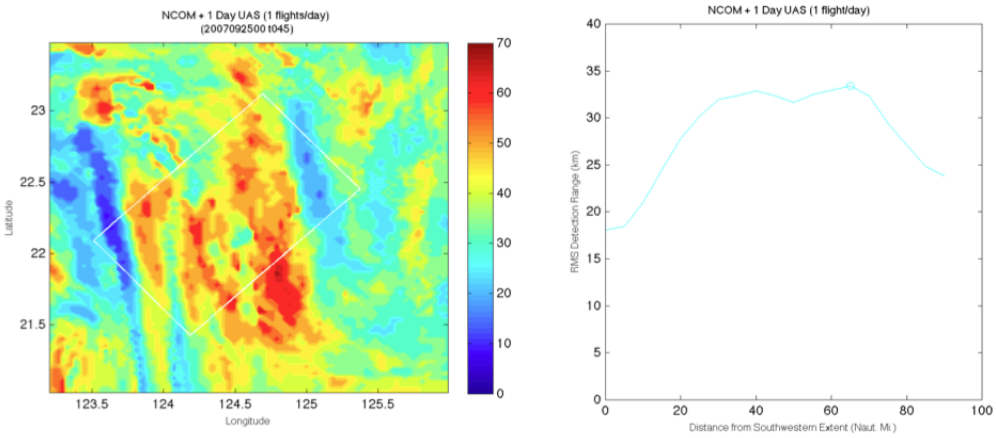

Figure 5.5.4-5. NCOM + UAS SLD (left) and Detection Range vs. Barrier Location (right) Metric Plots. UAS Sorties fly 24 Hours Prior to Search Operation.

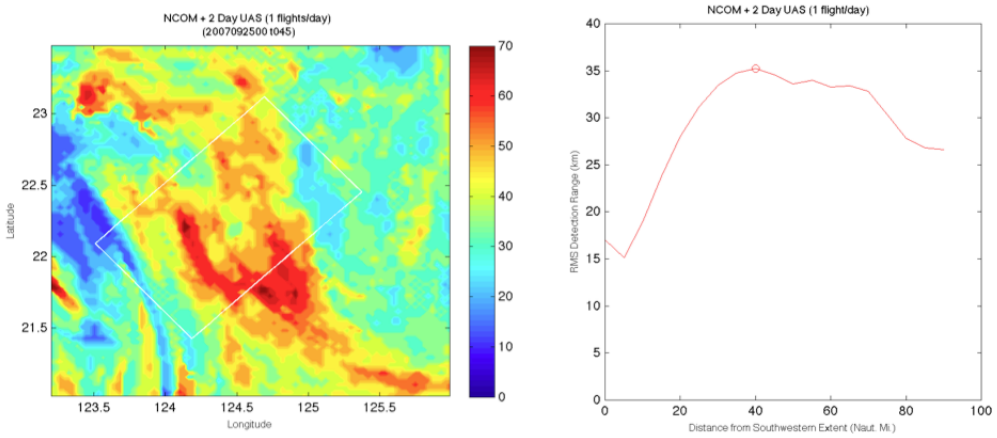

Figure 5.5.4-6. NCOM + UAS SLD (left) and Detection Range vs. Barrier Location (right) Metric Plots. UAS Sorties fly 24 and 48 Hours Prior to Search Operation.

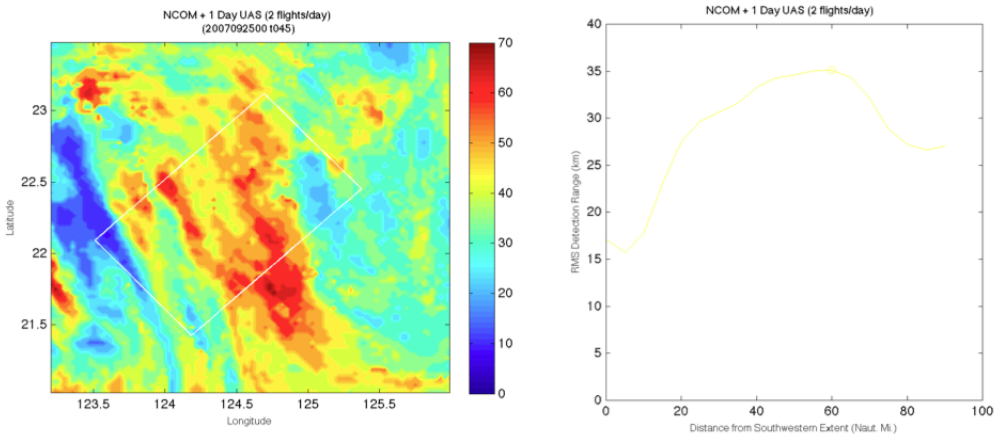

Figure 5.5.4-7. NCOM + UAS SLD (left) and Detection Range vs. Barrier Location (right) Metric Plots. UAS Sorties fly 24 and 12 Hours Prior to Search Operation.

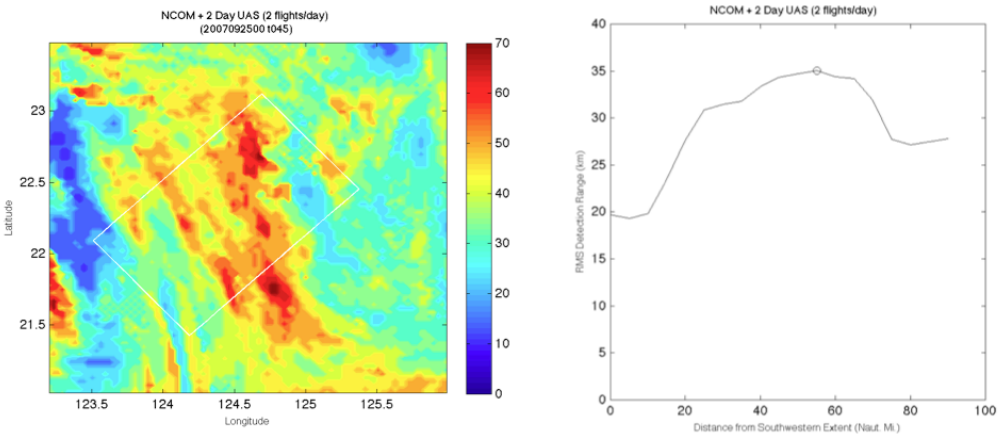

Figure 5.5.4-8. NCOM + UAS SLD (left) and Detection Range vs. Barrier Location (right) Metric Plots. UAS Sorties fly 48, 36, 24, and 12 Hours Prior to Search Operation.

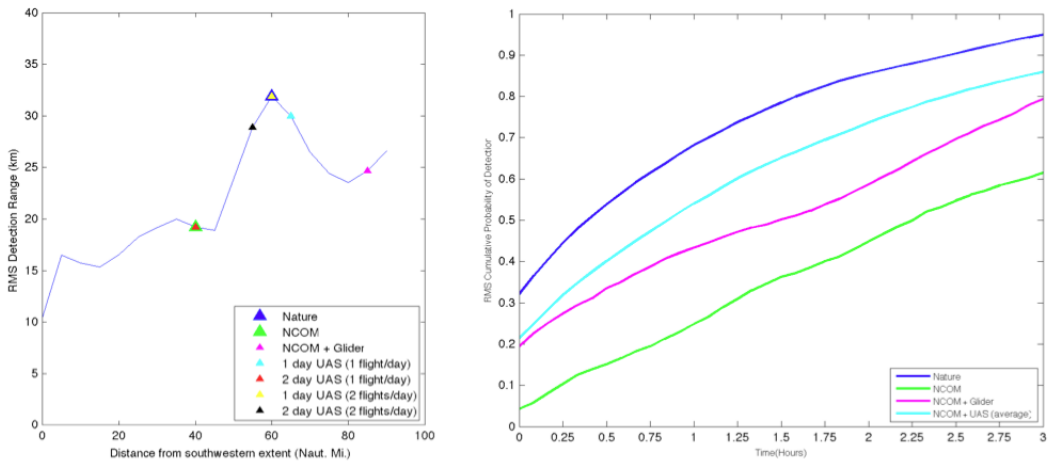

Figure 5.5.4-9. Summary Impact of Glider and UAS Sensing on Search Effectiveness.

Figure 5.5.4-9 (graphic on the left) summarizes the barrier location recommendations consistent with the Nature, NCOM, NCOM + glider observations, and NCOM + UAS observations alternatives. Recommended barrier locations are shown to range from roughly 40 nm to 85 nm from the southwestern border of the search area. Resulting cumulative probability of detection (CPD) vs. time results are shown on the graphic on the right side of Figure 5.5.4-9. The highest CPD values correspond to the barrier location assuming full knowledge of the Nature environment. The lowest CPD values correspond the barrier location based on NCOM model predictions without the benefit of glider or UAS in situ sensing. Lying between these two extremes are CPD values assuming NCOM predictions plus glider or UAS (an average of the four cases discussed above) in situ sensing. Both glider and UAS in situ sensing are shown to provide a tactically significant increase in barrier CPD.

5.5.5 Summary Conclusions

The purpose of this TACSIT analysis is to explore the possibility of augmenting glider in situ sensing with UAS-based ocean in situ measurements. UAS-based ocean sensing has the potential to provide a tactical-level, temporally and spatially focused correction to regional, wide-area ocean glider sensing. When coupled with remote sensing and next-generation ocean data assimilation and modeling capabilities, the potential exists for exploiting glider, other UUV and UAS observations in order to forecast tactically exploitable ocean acoustic conditions. The working conclusions for this TACSIT analysis are as follows:

- Prior analysis, see Ref. [11], showed the value of persistent, regional glider sensing in support of mid-frequency (MF) active ASW search effectiveness. Persistent, wide area glider sensing results in model-driven forecast improvements.
- This analysis shows the impact of spatially/temporally localized UAS sensing in the search area. Spatially and temporally localized sensing in the search area results in data-driven forecast improvements comparable and complementary to wide area, persistent glider (or other UUV/USV/manned) in situ sensing improvements. Note that while the average UAS cumulative probability of detection (CPD) improvement exceeds the mean glider CPD improvement, there is considerably more variation in the UAS result. Persistent and spatially/temporally dense glider observations tend to provide a reliable

CPD improvement. Short term, local UAS observations are more "hit or miss"; UAS CPD improvements tend to be near optimal (when observations happen to capture key local oceanographic features) or minimal (when they do not).

- A BAMS or VTUAV mini-AXBT (or X-glider) capability will require a BAMS wing pod. While there is no BAMS Increment 1 requirement for a wing pod, BAMS PO discussions are underway concerning BAMS Increment 2 wing pod solutions for communications relays, SIGINT collections, etc.
- BAMS pod solutions have drawbacks, including the likelihood of icing at flight altitudes complicating pod operations, substantially reduced BAMS flight endurance and resulting impacts on BAMS CONOPs, BAMS power budget constraints and limits, pod space constraints, and competition with other BAMS missions (e.g. communication relay operations, SIGINT collections, etc.) for pod space.
- The combined impact of persistent, regional glider observations and spatially and temporally focused UAS observations in the search area was not considered in this study.
- Impact on low frequency (LF) passive search operations is TBD.

5.6 Other TACSITs

As was discussed above in Section 5.1, and summarized in Figure 5.1-1, a number of other relevant Tactical Situations (TACSITs) were considered but not specifically addressed in this UAS METOC Sensing AoA. These included a High Altitude Helo TACSIT analysis that would have examined the utility of UAS temperature, pressure, humidity, and wind speed and direction observations in support of high altitude helo safety of flight operations. Another TACSIT was proposed which would have addressed the utility of BAMS EO/radar observations plus certain NRL UAS "synthetic dwell" algorithms to generate weather (Wx) imagery from the stratosphere. These TACSITs could be the subject of future analysis.

6.0 Year One Study Results

While still a work in progress, the following working conclusions can be cited based on the analysis performed in support of the UAS METOC Sensing Analysis of Alternatives (AoA). The UAS METOC Sensing AoA Study Team included the following organizations, researchers and technical roles:

- **NAVAIR** (Doug Backes, Paul Eiff, Andrew Pontzer and Eduardo Danganan): UAS platform and sensor programmatic representation. UAS experimentation. Mapping of TACSITs to DoD scenarios and operational plans (OPLANs).
- **NRL Code 7400** (Dr. Todd Holland and Dr. Paul Elmore): UAS sensor feasibility analysis and MIW TACSIT analysis.
- **NRL Code 7300** (Dr. Gregg Jacobs, Dr. Jay Veeramony, Dr. Charlie Barron, Pete Spence): EXW/NSW and ASW TACSIT analyses.
- **NRL Code 7500** (Larry Phegley): AW UAS experimentation and AW TACSIT analysis.
- **Applied Operations Research, Inc.** (Dr. Bill Stevens, Alex Mackenzie and Adrian Fontanilla): Study team coordination and reporting, AW UAS experimentation and TACSIT analysis support, ASW TACSIT search effectiveness analysis.

6.1 Summary Warfighting Impact Assessment

The major conclusions of the FY-09 Unmanned Aircraft System (UAS) METOC Sensing Analysis of Alternatives (AoA) can be summarized as follows:

Air Sensing Feasibility Analysis:

- Three UAS experiments conducted at Naval Air Station (NAS) Patuxent River, Webster Field Annex confirm the viability of small tactical UAS (STUAS) temperature, pressure, humidity, and wind speed and direction soundings consistent with radiosonde observations (RAOBs). Note that while issues were encountered with wind speed and direction estimation accuracies, these issues are understood and can be corrected for (see Appendix G).
- Prior analysis, e.g. Ref. [13], has confirmed the viability of UAS temperature, pressure, humidity and wind speed and direction observations (via onboard sensors or future dropsonde capabilities) on Navy Operational Global Atmospheric Prediction System (NOGAPS) and Coupled Ocean/Atmosphere Mesoscale Prediction System (COAMPS) forecast errors in data-denied areas. A COAMPS data denial experiment, leveraging the experiment data collected at Webster Field, is planned.
- Most Joint and Navy UAS platforms have requirements for, at a minimum, temperature, pressure, humidity and wind speed and direction observations and METOC production center NWP data assimilation capabilities are available to leverage this data. Work is required to establish the C2 connectivity needed to deliver this data to Joint and Navy METOC production centers and to insure the timely delivery of NWP products to in-theater Naval assets.

Ocean Sensing Feasibility Analysis:

- The technical feasibility of optical sensing of wave period/direction and radar sensing of wave spectra and subsequent inversion for bathymetry is well established.
- UAS employment CONOPs optimization is likely required to extract maximum benefit from UAS environmental sensing in support of Modified Surf Index (MSI) and percent mine burial estimation.
- Coupled full wave spectra estimation (wave direction, period, and height) plus bathymetry estimation is required to substantially impact MSI and percent mine burial estimation. Wave direction and period can be estimate passively (e.g. via video), while wave height requires active sensing (e.g. using radar, possibly LIDAR, or an in situ wave buoy).

Expeditionary Warfare, Naval Special Warfare TACSIT Analysis:

- For MSI estimation for the environment at Duck, NC, using sensors that improve only bathymetry yield marginal warfighting impact. ScanEagle EO bathymetry sensing results in 25% agreement with ground truth MSI vs. 16% in the No UAS sensing case. All other sensing alternatives result in somewhat less operational impact.
- For MSI estimation in the Duck, NC environment, bathymetry + wave spectra sensing is expected to yield a more substantial warfighting impact however. Initial model runs with radar wave spectra estimation supports this hypothesis. BAMS EO plus radar sensing yields a 43% agreement with ground truth MSI for favorable radar look angles and wind speeds and clearly suboptimal radar dwell times. It is probable that increasing radar dwell will result in substantially increased MSI estimation performance.
- UAS surveys and the supporting data assimilation and modeling CONOPs and required C2 connectivity is likely to be complex and coordination with OCEANOPSCOM Directorates is required to establish an operationally feasible CONOPs and data connectivity plan. We estimate that a minimum MSI improvement from the estimated 16% accurate in the No UAS Sensing case to 75% or greater accurate in the UAS Sensing case will be required to make the investment in UAS sensing, data assimilation, and modeling a cost effective option.

Mine Warfare TACSIT Analysis:

- For mine burial estimation in the Duck, NC FRF, bathymetry estimation yields marginal warfighting impact result.
- For mine burial estimation in the Duck, NC FRF, bathymetry plus wave spectra estimation is expected to yield a more substantial warfighting impact. Initial mine burial model runs with radar wave spectra estimation supports this hypothesis. Additional model runs are needed to quantify this impact.
- UAS surveys and the supporting data assimilation and modeling CONOPs and required C2 connectivity is likely to be complex and coordination with OCEANOPSCOM Directorates is required to establish an operationally feasible CONOPs and data connectivity plan. Additional connectivity with the MIW Environmental Post-Mission Analysis system also will be required. Since mine burial from wave action is largely correlated with orbital velocity at the bottom, we estimate that a minimum orbital velocity improvement from the estimated 16% accurate in the No UAS Sensing case to 75% or greater accurate in the UAS

Sensing case will be required to make the investment in UAS sensing, data assimilation, and modeling a cost effective option.

Air Warfare (AW) TACSIT Analysis:

- Prior analyses (c.f. pp. 71-72 above and Ref. [23]) have confirmed the viability of Doppler radar data assimilation as well as the potential impact of 3D wind estimation in METOC data denied areas on Joint Surface Strike and Joint Surface Fires Support scenarios.

Anti-Submarine Warfare TACSIT Analysis:

- Prior analysis, see Ref. [11], showed the value of persistent, regional glider sensing in support of mid-frequency (MF) active ASW search effectiveness. Persistent, wide area sensing results in tactically exploitable model-driven forecast improvements.
- This analysis shows the impact of spatially/temporally localized UAS sensing in the search area. Spatially and temporally localized sensing in the search area results in data-driven forecast improvements complementary to wide area, persistent glider (or other UUV/USV/manned) in situ sensing improvements. Note that while the average UAS cumulative probability of detection (CPD) improvement exceeds the mean glider CPD improvement, there is considerably more variation in the UAS result. Persistent and spatially/temporally dense glider observations tend to provide a reliable CPD improvement. Short term, local UAS observations are more "hit or miss"; UAS CPD improvements tend to be near optimal (when observations happen to capture key local oceanographic features) or minimal (when they do not).
- A BAMS or VTUAV mini-AXBT (or X-glider) capability will require a BAMS wing pod or similar VTUAV delivery mechanism. While there is no BAMS Increment 1 requirement for a wing pod, BAMS PO discussions are underway concerning BAMS Increment 2 wing pod solutions for communications relays, SIGINT collections, etc.
- BAMS pod solutions have drawbacks, including the likelihood of icing at high altitudes, substantially reduced BAMS flight endurance and resulting impacts on BAMS CONOPs, BAMS power budget constraints and limits, pod space constraints, and competition with other BAMS missions (e.g. communication relay operations, SIGINT collections, etc.) for pod space.
- The combined impact of persistent, regional glider observations and spatially and temporally focused UAS observations in the search area was not considered in this study.
- Impact on low frequency (LF) passive search operations is TBD.

6.2 Ranking of Likely Mission Impacts

Table 6.2-1 provides a summary of likely UAS METOC sensing operational impacts. These are broken into "Easy" and "Possible" METOC win categories. As one might expect, "easy" METOC wins are possible by solving the data distribution issues needed to leverage pervasive UAS atmospheric sounding data collections in data denied areas. Prior studies have shown that solving these data distribution issues would result in improved NWP forecast skill improvements and associated improvements in EM and wind speed and direction estimation.

Technically possible, but less straightforward, METOC wins are associated with wave spectra estimation (leveraging video, radar, LIDAR, MSI/HIS, or expendable wave buoys), inversion of the wave spectra to estimate bathymetry, and the use of expendables (mini-dropsondes, mini-AXBTs, X-gliders, and wave buoys). Wave spectra and bathymetry estimation, while founded on well-established science, implies the need for complex collection and data distribution strategies and supporting data assimilation and modeling ashore. The use of expendables implies the need for sensor miniaturization, wing pod or other dispensing mechanisms, and impacts on host tactical UAS platforms and associated employment CONOPs. Hence while the UAS METOC sensing benefits in these categories have the potential to yield a significant warfighting impact, significant technical, programmatic, and operational hurdles must be addressed.

Mission Domain	METOC "Easy" Wins	METOC "Possible" Wins
AW	• Leverage UAS organic TPH/ wind measurements. • Assimilate UAS Doppler radar for 3D wind estimation.	• Exploit possible future UAS mini-dropsonde capability. • Exploit possible future UAS MW sounder or MSI/HSI capabilities.
EXW/NSW Landing		• Exploit well-established video, radar, wave buoy wave spectra measurements and bathy inversions for MSI estimation.
MIW		• Exploit well-established video, radar, wave buoy wave spectra measurements and bathy inversions for mine burial estimation.
ASW Search		• Exploit possible future UAS mini-AXBT or X-glider capability iso ASW search ops.

Table 6.2-1. Bottomline Warfighting Impact Assessment.

6.3 Key UAS Technologies and Readiness Levels

Department of Defense technology readiness levels are defined below in table 6.3-1. All technologies evaluated in the UAS METOC sensing AoA are at TRL level 7 or higher.

Technology Readiness Level	Description
1. Basic principles observed and reported	Lowest level of technology readiness. Scientific research begins to be translated into applied research and development. Example might include paper studies of a technology's basic properties.
2. Technology concept and/or application formulated	Invention begins. Once basic principles are observed, practical applications can be invented. The application is speculative and there is no proof or detailed analysis to support the assumption. Examples are still limited to paper studies.
3. Analytical and experimental critical function and/or characteristic proof of concept	Active research and development is initiated. This includes analytical studies and laboratory studies to physically validate analytical predictions of separate elements of the technology. Examples include components that are not yet integrated or representative.
4. Component and/or breadboard validation in laboratory environment	Basic technological components are integrated to establish that the pieces will work together. This is "low fidelity" compared to the eventual system. Examples include integration of 'ad hoc' hardware in a laboratory.
5. Component and/or breadboard validation in relevant environment	Fidelity of breadboard technology increases significantly. The basic technological components are integrated with reasonably realistic supporting elements so that the technology can be tested in a simulated environment. Examples include 'high fidelity' laboratory integration of components.
6. System/subsystem model or prototype demonstration in a relevant environment	Representative model or prototype system, which is well beyond the breadboard tested for TRL 5, is tested in a relevant environment. Represents a major step up in a technology's demonstrated readiness. Examples include testing a prototype in a high fidelity laboratory environment or in simulated operational environment.
7. System prototype demonstration in an operational environment	Prototype near or at planned operational system. Represents a major step up from TRL 6, requiring the demonstration of an actual system prototype in an operational environment, such as in an aircraft, vehicle or space. Examples include testing the prototype in a test bed aircraft.
8. Actual system completed and 'flight qualified' through test and demonstration	Technology has been proven to work in its final form and under expected conditions. In almost all cases, this TRL represents the end of true system development. Examples include developmental test and evaluation of the system in its intended weapon system to determine if it meets design specifications.
9. Actual system 'flight proven' through successful mission operations	Actual application of the technology in its final form and under mission conditions, such as those encountered in operational test and evaluation. In almost all cases, this is the end of the last "bug fixing" aspects of true system development. Examples include using the system under operational mission conditions.

Table 6.3-1. Department of Defense Technology Readiness Levels (TRLs).

6.4 Initial C2 Data Flow and CONOPs Specifications

Missing from the analysis conducted to date is work to be conducted in partnership with cognizant OCEANOPSCOM Directorates develop initial CONOPS for exploitation of Dual Use organic sensor data streams as well as high payoff METOC specific and expendable sensor data streams. There is also a requirement to develop the cost factors needed to determine the inventory requirements to support the proposed UAS sensing CONOPs; e.g. as needed to support a Program Life Cycle Cost Estimate (PLCCE).

7.0 Future Study Plans and Objectives

Future support may be required as needed to provide a quantitative basis for CNO N84 participation in future budget cycles relating to Navy UAS METOC sensing.

7.1 Formulate Initial Navy UAS METOC Sensing Strategy

The goal of the future UAS METOC Sensing AoA work is to transform FY-09 field tests and studies into a recommended initial Navy UAS METOC sensing strategy. This must include the identification, field evaluation, and life cycle cost estimation for the identified UAS platform/sensor/C2/processing technologies.

7.2 Conduct Key Technology Demonstrations

Selected field tests may be required to confirm the conclusions of FY-09 simulation results, e.g. field tests may be needed to conduct a proof-of-concept test of end-to-end wave spectra estimation, bathymetry inversions, MSI estimation, and mine burial probability estimation.

7.3 Conduct Inventory Analysis and Life Cycle Cost Estimation

Formal cost factors analysis must be conducted in support of a Navy UAS METOC sensing Program Life Cycle Cost Estimate (PLCCE).

7.4 Refine Initial C2 Data Flow and CONOPs Specifications

Definition of relevant UAS survey and supporting data assimilation and modeling CONOPs and required C2 and data connectivity is required in coordination with OCEANOPSCOM Directorates.

Appendix A – References

[1] *DoD Unmanned Aircraft Systems Roadmap 2005 – 2030*, Office of the Secretary of Defense, 4 August 2005. http://www.fas.org/irp/program/collect/uav_roadmap2005.pdf

[2] *DoD Unmanned Systems Roadmap 2007 – 2032*, Office of the Secretary of Defense, 10 December 2007. http://www.fas.org/irp/program/collect/usroadmap2007.pdf

[3] *Environmental Information of Naval Warfare*, Committee on Environmental Information for Naval Use, National Academy of Engineering, Ocean Studies Board, The National Academies Press, Washington, D.C., www.nap.edu, 2003. http://www.nap.edu/openbook.php?record_id=10626

[4] Holland KT, "Application of the linear dispersion relation with respect to depth inversion and remotely sensed imagery", *IEEE Transactions on Geoscience and Remote Sensing*, Vol. 39, pp. 2060-2072, 2001.

[5] Piotrowski CC and Dugan JP, "Accuracy of bathymetry and current retrievals from airborne optical time series imaging of shoaling waves", *IEEE Transactions on Geoscience and Remote Sensing*, Vol. 40, pp. 2606 – 2618, 2002.

[6] Dalrymple RA, Kennedy AB, Kirby JT, Chen Q, "Determining depth from remotely-sensed images", *Coastal Engineering 1998: Proceedings of the 26th Intl. Conf., vol. 2, ASCE*, Copenhagen, Denmark, 22-26 June 1998, pp. 2395-2408. http://cedb.asce.org/cgi/WWWdisplay.cgi?9900897

[7] Irish JL and Lillycrop WL, "Scanning laser mapping of the coastal zone: The SHOALS system," *ISPRS Journal of Photogrammetry and Remote Sensing*, vol. 54, pp. 123–129, 1999.

[8] Sandidge JC and Holyer RJ, "Coastal bathymetry from hyperspectral observations of water radiance," *Remote Sensing of the Environment*, Vol. 65, pp. 341–352, 1998.

[9] Plant NG, Holland TK, and Haller MC, "Ocean wavenumber estimation from wave-resolving time series imagery", *IEEE Transactions on Geoscience and Remote Sensing*, Vol. 46, Sept 2008.

[10] Hwang PA, "Measurement of directional wave spectra using aircraft laser altimeters", *Journal of Atmospheric and Oceanic Technology*, Vol. 22, pp. 869-885, 2005.

[11] Coelho EF, Farbe, JP, Rowley CD, Jacobs GA, Bishop CH, Cummings JA, and Hong X. "Targeting observations to reduce acoustic prediction uncertainty", *U.S. Navy Journal of Underwater Acoustics*, Vol 60, pp. 125-152, 2010 (Unclassified: Distribution authorized to DoD and U.S. DoD contractors only).

[12] *Environmental Requirements for Through the Sensors Support of Mine Warfare*, Avera W and Harris M, NRL/MR/7440-00-8236, Naval Research Laboratory, 13 March 2000 (Unclassified: Distribution authorized to DoD and U.S. DoD contractors only).

[13] Vogel G, Langland R, Phegley L, Pauley P and Love G, *Sensitivity of NOGAPS Forecasts to UAS like Observations*, NRL/MR/7540-10-9158, Naval Research Laboratory, 26 March 2010.

[14] Zhao AQ, *Improved Doppler Radar/Satellite Data Assimilation*, Marine Meteorological Division, Naval Research Laboratory, Award Number: N0001407WX20639, 2008.

http://www.onr.navy.mil/reports/FY09/mmzhao.pdf

[15] Koopman BO, *Search and Screening: General Principles with Historical Applications*, Military Operations Research Society (MORS) Heritage Series, 1999. http://www.amazon.com/Screening-General-Principles-Historical-Applications/dp/0080231357/ref=sr_1_1?ie=UTF8&s=books&qid=1282244450&sr=8-1

[16] Wagner DH, Mylander WC, Sanders TJ, *Naval Operations Analysis, Third Edition*, Naval Institute Press, 1999, pp. 218-223. http://www.amazon.com/Naval-Operations-Analysis-Daniel-Wagner/dp/1591149509/ref=sr_1_fkmr0_1?ie=UTF8&qid=1282244492&sr=8-1-fkmr0

[17] *Oceanography and Mine Warfare*, Ocean Studies Board, National Research Council, National Academy Press, Washington, D.C., 2000. http://www.amazon.com/Oceanography-Warfare-Ocean-Studies-Board/dp/0309067987/ref=sr_1_1?ie=UTF8&s=books&qid=1282244523&sr=8-1

[18] *Oceanography and Naval Special Warfare*, Ocean Studies Board, National Research Council, National Academy Press, Washington, D.C., 1997. http://www.amazon.com/Oceanography-Naval-Special-Warfare-Opportunities/dp/0309059305/ref=sr_1_1?ie=UTF8&s=books&qid=1282244545&sr=8-1

[19] *Mine Countermeasures in Support of Amphibious Operations (NTTP 3-15.24),* Department of the Navy, Chief of Naval Operations, January 2008.

[20] Hwang PA, Stetten MA, , and Toporkov, JV. A note on Doppler processing of coherent radar backscatter from the water surface: With application to ocean surface wave measurements. *Journal of Geophysical Research – Oceans*, 115: art. C03026.

http://www.agu.org/journals/jc/jc1003/2009JC005870/

[21] Wozencraft JM and Lillycrop WJ, "SHOALS airborne coastal mapping: past, present, and future", Journal of Coastal Research, Number 38, pp 207-215, 2003

[22] Patterson MCL and Brescia A, "Integrated sensor systems for UAS", *23rd Bristol UAV Systems Conference,* April 2008.

http://www.acrtucson.com/Presentations_n_Publications/pdf/23rd_Bristol_Sensors_Conf_07.pdf

[23] Wilkens, RH and Richardson, MD, "Mine burial prediction: A short history and introduction", *IEEE Journal of Oceanic Engineering*, 32: pp. 3-9, 2007.

[24] Rennie, SE, Brandt, A. and Plant, N., "A probabilistic expert system approach for sea mine burial prediction", *IEEE Journal of Oceanic Engineering*, 32: pp. 260-272, 2007.

[25] *MATLAB, Version 7.8*. The Mathworks Inc., Natick, MA, 2009.

http://www.mathworks.com

[26] Lin BY, Myrick SA, Avera WE, and Harris MM, "The Environmental Post-Mission Analysis System: Through-The-Sensor to the Warfighter", *NRL Review*, pp. 208-209, 2009.

[27] Schwartz, R. and Birkemeier, W., "Sedimentology and morphodynamics of a barrier island shoreface related to engineering concerns, Outer Banks, NC, USA", *Marine Geology*, 211: pp. 215-225, 2004.

[28] Soulsby, R., *Dynamics of Marine Sands: A Manual for Practical Applications*, Thomas Telford: London, 1997.

[29] Trembanis, AC, Friedrichs, CT, Richardson, MD, Traykovski, P, Howd, PA, Elmore, PA and Wever, TF, "Predicting seabed burial of cylinders by wave-induced scour: Application to the sandy inner shelf off Florida and Massachusetts", *IEEE Journal of Oceanic Engineering*, 32: pp. 167-183, 2007.

[30] Elmore, PA and Richardson, MD, "Assessing scour model performance with experimental data", *MTS:IEEE Oceans 2003*, September 22-26, 2003, San Diego, CA, pp. 2350-2354.

[31] Whitehouse, R, *Scour at Marine Structures : A Manual for Practical Applications*, Thomas Telford: London, 1998.

[32] Russell, SJ and Norvig, P, *Artificial Intelligence: A Modern Approach*, 2nd, Prentice Hall/Pearson Education: Upper Saddle River, N.J., 2003.

Appendix B – Acronym List

AGS	Advanced Gun System
AMDAR	Aircraft Meteorological Data Relay
AoA	Analysis of Alternatives
AOI	Area of Interest
AREPS	Advanced Refractive Effects Prediction System
ASCM	Anti-Ship Cruise Missile
ASW	Anti-Submarine Warfare
ATF	Amphibious Task Force
AW	Air Warfare
AXBT	Air-Deployed Expendable Bathythermograph
BA	Battlespace Awareness
BAMS	Broad Area Maritime Surveillance UA
BN	Bayesian Network
BonD	Battlespace on Demand[13]
BT	Bathythermograph
C2	Command and Control
C4ISR	Command, Control, Communications, and Computers for Intelligence, Surveillance, and Reconnaissance
CASS	Comprehensive Acoustic Simulation System
CNMOC	Commander, Naval Meteorology and Oceanography Command
COAMPS	Coupled Ocean/Atmosphere Mesoscale Prediction System
COBRA	Coastal Battlefield Reconnaissance and Analysis
COF	Cutoff Frequency
CONOPs	Concept of Operations
CONUS	Continental US
CoT	Cursor on Target
COTS	Commercial Off the Shelf
CPD	Cumulative Probability of Detection
CPF	Commander, Pacific Fleet
CPT	Conditional Probability Table
CRAB	Coastal Research Amphibious Buggy
CSG	Carrier Strike Group
CTD	Conductivity, Temperature, and Depth
dB	Decibel
DBDB-V	Digital Bathymetry Database Variable Resolution
DBT	Doctrinal Bottom Type

[13] BonD is composed of the Tier I Environmental Layer, the Tier II System Performance Layer, and the Tier III Decision Layer.

EA	Effectiveness Analysis
EM	Electromagnetic
EMD	Engineering and Manufacturing Development
EO	Electro-Optic
ESG	Expeditionary Strike Group
EXW	Expeditionary Warfare
FCS	Future Combat System
FNMOC	Fleet Numerical Meteorology and Oceanography Center
FRF	Field Research Facility
GCS	Ground Control System
GDEM	Generalized Digital Environmental Model
GIG	Global Information Grid
GIG/ES	GIG Enterprise Services
GOTS	Government Off the Shelf
GPS	Global Positioning System
GTS	Global Telecommunication System
HD	High Definition
Hz	Hertz = Cycles Per Second
HFBL	High Frequency Bottom Loss Database
HSI	Hyperspectral Imaging
INTEL	Intelligence
IPE	Intelligence Preparation of the Environment
IR	Infrared
IRTSS	IR Target Scene Simulation
ISAR	Inverse SAR
ISR	Intelligence, Surveillance, and Reconnaissance
ISR-T	Intelligence, Surveillance, Reconnaissance, and Targeting
JMMES	Joint Multi-Mission Electro-optical System
kHz	Kilohertz = 10^3 Cycles Per Second
LADAR	Laser Detection and Ranging
LARC-V	Lighter Amphibious Resupply Cargo
LCCE	Life Cycle Cost Estimate
LCS	Littoral Combat Ship
LF	Landing Force
LF	Low Frequency
LFBL	Low Frequency Bottom Loss Database
LIDAR	Light Detection and Ranging
LRLAP	Long Range Land Attack Projectile

MASINT	Measurements and Signatures Intelligence
MBES	Mine Burial Expert System
MCO	Major Combat Operation
MCM	Mine Countermeasures
MEDAL	Mine Warfare Environmental Decision Aid Library
MEF	Marine Expeditionary Force
METOC	Meteorology and Oceanography
MF	Mid Frequency
MFAS	Multi-Function Active Sensor
MIST	Miniature In-situ Sounding Technology
MIW	Mine Warfare
MMA	Multi-Mission Maritime Aircraft
MSI	Modified Surf Index
MSL	MSI Limit
MW	Microwave
NAS	Naval Air Station
NASA	National Aeronautics and Space Administration
NAVO	Naval Oceanographic Office
NCAR	National Center for Atmospheric Research
NCODA	Navy Coupled Ocean Data Assimilation
NCOM	Navy Coastal Ocean Model
NGFS	Naval Gunfire Support
NMAWC	Naval Mine and Anti-Submarine Warfare Command
NOAA	National Oceanographic and Atmospheric Administration
NOGAPS	Navy Operational Global Atmospheric Prediction System
NOOC	Naval Oceanography Operations Command
NOMBOS	Number of Mine-Like Bottom Objects
NRL	Naval Research Laboratory
NRT	Near Real-Time
NSPE	Navy Standard Parabolic Equation Model
NSW	Naval Special Warfare
NTTP	Navy Tactics, Techniques, and Procedures
NWP	Numerical Weather Prediction
OAML	Oceanographic and Atmospheric Master Library
OcnQC	Ocean Quality Control
OPLAN	Operations Plan
OR	Operations Research
OSE	Observing System Experiment
OSSE	Observing System Simulation Experiment
PLCCE	Program LCCE
POES	Polar-Orbiting Environmental Satellites
POR	Program of Record

QC	Quality Control
RAOB	Radiosonde Observation
RELO NCOM	Relocatable NCOM
ROE	Rules of Engagement
ROI	Return on Investment
SA	Situation Awareness
SAR	Synthetic Aperture Radar
SEAD	Suppression of Enemy Air Defenses
SIGINT	Signals Intelligence
SLD	Sonic Layer Depth
SPG	Strategic Planning Guidance
SSH	Sea Surface Height
SST	Sea Surface Temperature
STUAS	Small Tactical UAS
TACAIR	Tactical Aircraft
TACSIT	Tactical Situation
TCDL	Tactical Common Data Link
TDA	Tactical Decision Aid
TTS	Through the Sensor
UA	Unmanned Aircraft
UAS	Unmanned Aircraft System
UAV	Unmanned Air Vehicle
UGS	Unmanned Ground Systems
UMS	Unmanned Maritime Systems
USMC	US Marine Corps
USN	US Navy
USV	Unmanned (Ocean) Surface Vehicle
USW	Undersea Warfare
UUV	Unmanned Undersea Vehicle
V&V	Verification and Validation
VTOL	Vertical Takeoff and Landing
VTUAV	VTOL Tactical UAV
WESTPAC	Western Pacific
WITTW	What it Takes to Win
WMD	Weapons of Mass Destruction
WMO	World Meteorological Organization
Wx	Weather
XBT	Expendable Bathythermograph

Appendix C – U.S. Army Corps of Engineers Field Research Facility

The U.S. Army Corps of Engineers (USACE) Field Research Facility (FRF) in Dick, NC is one of the few places in the world that provides a dependable means of obtaining comprehensive measurements even during severe storms when significant coastal change occurs. Located in Duck, NC, the FRF was established by the USACE in 1977 to support its coastal engineering research requirements. Since its creation, the facility has maintained a comprehensive, long-term monitoring program of the coastal ocean including waves, tides, currents, local meteorology, and the resultant beach response. A small, highly skilled field staff and several unique vehicles support the monitoring program. Because the site is representative of many U.S. coastal locations, FRF data are used worldwide to help meet the need for field data to calibrate and verify analytical, numerical, and physical model predictions. In addition, the availability and high quality of FRF data make it ideal for use in ground-truthing a wide range of new oceanographic in situ and remote sensing sensors and techniques.

Figure C-1. The U.S. Army Corps of Engineers (USACE) Field Research Facility (FRF), Duck NC.

The FRF is located on 712,000 square meters (176 acres) which includes 1,000 m (3,300 ft) of frontage along the Atlantic Ocean and along the shallow, brackish Currituck Sound. The facility consists of a 560-m- (1,840-ft-) long research pier, a main office building, two field support buildings, and an observation tower. The research pier is a reinforced concrete structure supported on steel pilings. The pier deck is 6.1 m (20 ft) wide and extends to a nominal depth of 6 m (20 ft) at a height of 7.6 m (25 ft) above the National Geodetic Vertical Datum (NGVD) of 1929. Located on the pier is the crane-like Sensor Insertion System (SIS), which can be moved to any location on the pier. It is equipped with wave gauges, current meters, and sediment-transport sensors, can be operated in 5 m (16 ft) waves, and is able to reach 15 to 24 m (50 to 75 ft) out from the pier to minimize the local influence of the pier on the measurements. The SIS is ideal for deploying or testing oceanographic sensors. The 40 m (130 ft) tall observation tower is

climbable and designed to support video remote sensing observations and to hold radio antennas. FRF vehicles include the 10.70 m (35 ft) tall Coastal Research Amphibious Buggy (CRAB), See Figure C-2, used primarily for surveying and other tasks in the nearshore such as instrument deployments and maintenance, sand sampling and vibracoring, cable laying, towing instrumented sleds, and functioning as a mobile platform for diving operations. In addition, two 10.7 m (35 ft) tall Lighter Amphibious Resupply Cargo (LARC-V) vehicles, see Figure C-3, support operations in deeper water or remote from the FRF. These vehicles support diving operations, conduct hydrographic surveys, tow sidescan and sub-bottom seismic instruments, lay and retrieve cables, and deploy and maintain buoys and instruments.

Figure C-2. Coastal Research Amphibious Buggy (CRAB).

Figure C-2. Lighter Amphibious Resupply Cargo (LARC-V).

Appendix D – Webster Field UAS Experiment (23 Feb - 12 Mar 2009)

D.1 Experiment Results – Observed Conditions

Observed Conditions, 24-Feb-09. No strong inversion layer present (except for a "blip" around 920 mbar), modest changes in temperature and humidity profiles for duration of experiment. There was an absence of an evaporation gradient or surface ducts for all profiles; no strong difference in detection ranges.

Observed Conditions, 25-Feb-09. A temperature inversion between 850 and 800 mbar (4,800-6,400 ft) was observed in the AM with lowering of layer by 50 mbar during afternoon UAS descent. There seemed to be a general trend of lifting of the lower duct elevations that corresponded to a reduction in detection range. A surface "evaporation" duct at time of RAOB measurement was responsible for the extended detection range during that measurement.

Observed Conditions, 26-Feb-09. Salient temperature inversion layer starting at 1000 mbar (364 ft) and lifting through 960 mbar to 910 mbar (3,240 ft) at end of experiment; inversion weakened in magnitude. The lifting of the inversion layer corresponded to a lifting of the duct/trapping conditions as observed in refractivity profiles. Detection ranges reduced modestly with this lifting.

Observed Conditions, 10-Mar-09. Temperature and humidity measurements correlated with relative strength for all profiles, possibly due in part to the magnitude of the temperature and humidity fluctuations. There was an absence of a surface evaporation gradient for all profiles. A strong temperature inversion layer was at 900-820 mbar (3,250-6,000 feet). This corresponded with a strong elevated duct near the beginning of the inversion, but was too high to substantially increase detection ranges. A similar trend between ducting height and detection range is also seen with the climatology data. Trapping was noticed below 2,000 ft (942 mbar) on the UAS descent according to the refractivity profile; this seems to correspond to a modest increase increase in detection range at end of experiment. The middle UAS ascent profile led to the most conservative detection range, so there was no obvious trend across the day.

Observed Conditions, 12-Mar-09. There was a temperature inversion layer at 875 to 825 mbar (around 4,000-6,000 ft) that coincided with an increased wind speed within this feature. It was observed that the inversion layer was lowered by 25 mbar by end of experiment. This corresponded with a strengthening and lowering of an elevated duct that was all the while too high to extend detection range. No surface ducting conditions were observed. The radiosonde refractivity profile showed no ducting for all elevations and had the most conservative detection range.

D.2 RAOB vs. UAS Data Collections

RAOB vs. UAS data collections were conducted for all experiment days. This data, which is available but is not shown here in the interest of brevity, shows temperature vs. pressure, humidity vs. pressure, and wind speed vs. pressure respectively for the experiment RAOB (blue line), the AeroStar ascent (red line), and the AeroStar descent (green line). A high degree of

consistency has been observed across all cases between the RAOB observations and the UAS ascending and descending observations.

D.3 AREPS Reflectivity Plots

Advanced Refractive Effects Prediction System (AREPS) refractivity plots were also generated for all experiment days. This data, which is available but is not shown here in the interest of brevity, shows refractivity vs. height in M-units for the RAOB profile, the UAS ascending profile, and the UAS descending profile respectively. As expected, a high degree of consistency is shown between theses RAOB and UAS ascending and descending refractivity profiles.

Appendix E – Webster Field UAS Experiment (18-29 May 2009)

E.1 Experiment Results – Observed Conditions

Observed Conditions, 18-May-09. A temperature inversion was observed at 820 mbar (5,750 ft). A sharp surface humidity ceiling was observed at 820 mbar and dropped to 860 mbar (4,750 ft) between the UAS soundings. This corresponded with a drop in the trapping layer as observed in the refractivity profile.

Note that the RAOB did not record data below 6,100 ft (817 mbar). It was too windy for Aerolight to fly. Sky was overcast with ceiling at 10,000ft at 6:00 but was clear by 7:30AM. Visibility was 10 NM. The UAS takeoff occurred at 07:40AM and UAS landing at 12:22PM.

Observed Conditions, 19-May-09. There was a modest temperature inversion at 825 mbar (5,500 ft) in AM UAS ascent, dropping to 875 mbar (4,000 ft) in afternoon. The upper level humidity remained steady throughout the day however, a dramatic humidity decrease at the bottom of the profile is apparent in afternoon UAS descent. This decrease coincided with a modest increase in surface temperatures. Both the lowering and sharpening of an elevated humidity gradient (4,000 ft) correlated with the lowering and strengthening of an elevated ducting condition in the refractivity profile of the UAS descent. While the elevated ducting tended to strengthen throughout the afternoon, the surface duct weakened. There was a dissipation of a miniature surface temperature inversion feature which coincided with this weakening. The morning UAS ascent aligned closest with surface ducting detection range climatology and the afternoon descent aligned closest with the typical/elevated duct climatology. An increase in wind speed was also associated with the elevated temperature inversion layer.

Note that the Prescott Pusher did not collect data this day due do a nose gear collapse. The skies were clear during experiment, and the visibility was 10 NM. Surface winds were calm at 5:50 AM, but picked up to 6 knots by noon. AeroStar UAS takeoff was at 07:08AM and landing at 12:25PM. The Aerolight UAS takeoff was at 07:40 and landing at 08:55.

Observed Conditions, 20-May-09. A temperature inversion layer was observed at 900 mbar (3,240 ft). Surface air temps warmed noticeably throughout day as seen in UAS descent with the upper air column remaining stable. Moist layers below 925 mbar (2,250 ft) and between 775 mbar (7,000 ft) and 725 mbar (9,000 ft) were observed. The upper level temperature and humidity layer was strongest with the RAOB profile and this sharpness was carried over to the refractivity profile as well. A general and expected trend of surface temperature increase with humidity decrease was observed. Modest change between profiles was observed. Detection ranges aligned closer to surface duct climatology for all profiles.

Note that surface winds were calm at 6:00AM, visibility was 10NM, and the skies were clear. AeroStar UAS takeoff was at 07:07AM and landing was at 12:32PM. Aerolight UAS takeoff was at 07:32AM and landing was at 08:44PM.

Observed Conditions, 10-Jun-09. A temperature inversion was observed at 975 mbar to 950 mbar (1000-1770 ft) coincided with both a dry layer and ducting conditions. The prominence of this feature changed very little throughout the experiment as did the ducting at the level.

E.2 RAOB vs. UAS Data Collections

RAOB vs. UAS data collections were conducted for all experiment days. This data, which is available but is not shown here in the interest of brevity, shows temperature vs. pressure, humidity vs. pressure, and wind speed vs. pressure respectively for the experiment RAOB (blue line), the AeroStar ascent (red line), and the AeroStar descent (green line). A high degree of consistency has been observed across all cases between the RAOB observations and the UAS ascending and descending observations.

E.3 AREPS Reflectivity Plots

Advanced Refractive Effects Prediction System (AREPS) refractivity plots were also generated for all experiment days. This data, which is available but is not shown here in the interest of brevity, shows refractivity vs. height in M-units for the RAOB profile, the UAS ascending profile, and the UAS descending profile respectively. As expected, a high degree of consistency is shown between theses RAOB and UAS ascending and descending refractivity profiles.

Appendix F – Webster Field UAS Experiment (13-19 August 2009)

Data from the Webster Field UAS Experiment that took place on 13-19 August 2009 is still being processed. This Appendix will be updated when this data is available.

F.1 Experiment Results – Observed Conditions

Observed Conditions, 13 August 2009. Clear skies were observed the morning of the launch with a visibility of 9 NM. Morning ground temperatures were measured to be 23 C and a dew point of 22 C. Surface winds were 3 KTS coming from 60 degrees. Atmospheric pressure was 29.97 inHg. There was a general absence of temperature inversions in all three soundings, with the lowest temperature gradient from 950 to 800mb (1,773-6,394 ft). The UAS only flew to 850mb (4,781 ft), but the RAOB measured a slightly faster, smoother and very linear decline in temperature above 800mb (6,394 ft) similar to the 950mb (1,770 ft) level and below. The humidity levels were fairly volatile for all three measurements, with a very sharp dry layer sandwiched between two humid layers at 875mb (4,000ft). This layer lowered very slightly through the day. Capturing the upper profile, the morning RAOB sounding showed a saturated humidity layer at 825 mb (5,500 ft) and sharp and extremely dry layer at 625mb (13,000 ft). As the temperature was generally decreasing smoothly with height, the rapid humidity fluctuations suggest stratified moisture layers rather than an atmosphere of homogenous water vapor content.

Observed Conditions, 18 August 2009. Skies were clear with a visibility of 9 NM. Atmospheric pressure increased over the weekend to 30.11 inHg. Morning temperatures were 23C with a dew point of 21C. Surface winds were 5 KTS coming from 200 degrees. The morning began with a slight temperature inversion 975 mb (1,000 ft), however this abated as the lower atmosphere warmed slightly during the day at and below the top of this inversion level. Temperatures above this elevation were fairly stable temporally, and can be described as decreasing with a more rapid and smooth decline above 900mb (3,243 ft). There was a humid layer at 975 mb (1,000 ft), which abated by the 925mb (2,500 ft) level. The atmosphere was wet above this level initially, but dried by the afternoon. The morning UAS sounding did not transmit weather data until it was above 917mb (3,000 ft).

Observed Conditions, 19 August 2009. Light rain was observed in a portion of the sky, yet the general visibility was 10 NM. Atmospheric pressure fell from the previous morning to 29.98 inHg. Morning temperatures were 28C with a dew point of 22C. Surface winds were 5 KTS coming from 250 degrees. Air temperatures decreased very smoothly and continuously from the ground to 600mb (13,801 ft). The humidity increased from the ground level to near saturation at 675 mb (11,000 ft), from where it began to decline. There were dry layers at 960 mb (1,500 ft) and 810 mb (6,000 ft). The monotony of the temperature profile suggests the dry layers are due to actual low vapor levels rather than a greater ability for the air to retain a homogenous vapor level by means of a temperature spike.

F.2 RAOB vs. UAS Data Collections

RAOB vs. UAS data collections were conducted for all experiment days. This data, which is available but is not shown here in the interest of brevity, shows temperature vs. pressure, humidity vs. pressure, and wind speed vs. pressure respectively for the experiment RAOB (blue line), the AeroStar ascent (red line), and the AeroStar descent (green line). A high degree of consistency has been observed across all cases between the RAOB observations and the UAS ascending and descending observations.

F.3 AREPS Reflectivity Plots

Advanced Refractive Effects Prediction System (AREPS) refractivity plots were also generated for all experiment days. This data, which is available but is not shown here in the interest of brevity, shows refractivity vs. height in M-units for the RAOB profile, the UAS ascending profile, and the UAS descending profile respectively. As expected, a high degree of consistency is shown between theses RAOB and UAS ascending and descending refractivity profiles.

Appendix G – UAS Wind Estimation Errors

Unanticipated UAS magnetic compass heading errors have so far limited the usefulness of UAS wind collections in the Webster Field UAS Experiments described above in Appendices D-F. This heading dependence in the UAS wind data remains uncorrected. A more accurate version might be available at a later time. NRL, NPS and AOR are currently working on this issue. It now appears that soft and/or hard iron in the UAS platform/payload may be augmenting the earth's magnetic field, yielding a heading dependent error in the measured heading. Because this error propagates to introduce error into the winds, but should be mitigated with proper compass calibration, the uncorrected wind plots vs. altitude do not yet fully represent the potential accuracy of UAS wind data collections. See Figure G.1 below.

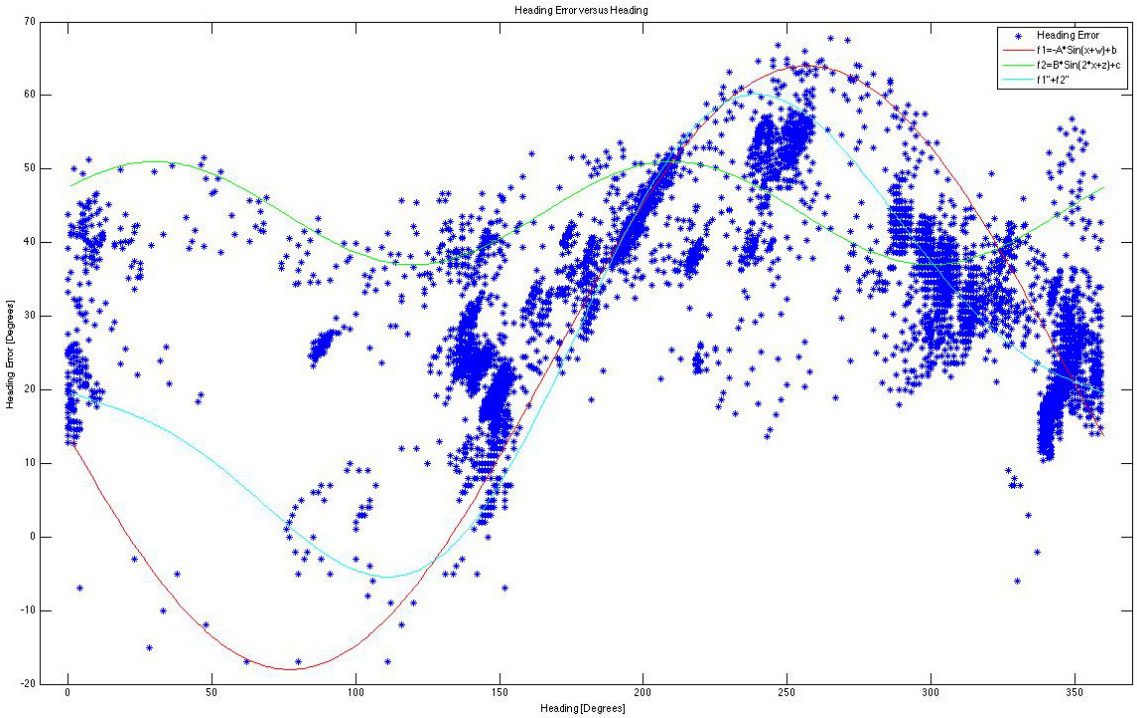

Figure G.1. Heading Error in Degrees vs. Heading: the magnetic properties of the UAS platform + payload can result in substantial heading dependent heading errors (with 20 degrees or more of spread at some headings) as shown here.

Ref: *Applications of Magnetic Sensors for Low Cost Compass Systems*, by Michael J. Caruso, Honeywell Microelectronics & Precision Sensors.

Appendix H – MBES Key Bayesian Network Implementation

Textbooks such as Russell and Norvig (Ref. [32]) provide good introductions to Bayesian networks (BN). To summarize the relevant details as applicable to MBES, BN's are a form of artificial intelligence that allows end users to obtain the probability of a result based on probabilistic inputs. The network can be small in design, such that there are immediate relations between inputs and result, or more complicated, so that there may be intermediate results computed before the final result. The front-end of MBES translates environmental inputs into histograms for the BN's within the system. The histograms are weighted by the probability for one of the inputs to be the correct one or by the distribution of multiple inputs present all at once. The output is a histogram of possible burial states.

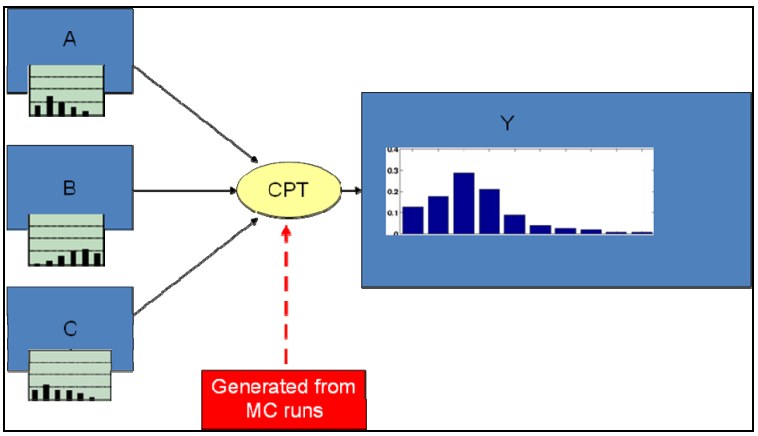

Figure H-1. Concept of Bayesian Network. Nodes *A*, *B*, and *C* are parents of node *Y*, meaning that *A*, *B* and *C* collectively cause effect *Y*. In this particular case, the figure indicates that the CPT table was created (i.e., the BN was "trained") from Monte Carlo (MC) simulations.

Topologically, a BN is an acyclic directed graph – i.e., there is a one-way forward direction for performing calculations. Figure A1 shows an example. Histogram information, either in the input, intermediate results, or final results, is stored in "nodes" of the network. Causal relationships between nodes are called "links"; links, illustrated by arrows in BN diagrams, show forward computational direction. The relationships between linked nodes are specified by the conditional probabilities of the result in the subsequent node, or "child" node, given the distribution in the predecessor nodes, or "parent" nodes. Thus, if node X is the only parent node of Y, the conditional probability relating the two is $P(Y \mid Parent(Y)) = P(Y \mid X)$. More generally, if nodes A, B, C, etc. are parent nodes of Y, then $P(Y \mid Parents(Y)) = P(Y \mid A, B, C, \ldots)$. Nodes that have no causal relationship are conditionally independent.

The set of conditional probabilities that specify the links between parent nodes A, B, C, etc. and child node Y are stored in conditional probability tables (CPT's). The columns of the CPT are the set of variables (i.e., possible outcomes) for the child node. The rows of the CPT are the set of all possible combinations of parent node variables so that each row specifies the histogram of Y's variables given one combination of parent variables or $P(Y \mid A=a, B=b, C=c, \ldots)$. Thus, the CPT provides the joint probability in a decomposed form. Methods for populating the CPT's include beliefs of subject matter experts, experimental data, computational results, or some

combination thereof.

When the state of the parent nodes are themselves represented by a histogram of their variables, as is more generally the case for MBES, the state of *Y*, the value for each of *Y*'s variables, is a weighted sum of the conditional probabilities. The weight for each term is the product of the marginal probabilities for the applicable value from each parent. For example, if parent nodes *A*, *B* and *C* each had a distribution of variables (a_1, a_2, … , a_j), (b_1, b_2, … , b_k), and (c_1, c_2, … , c_l), respectively, then the probability for the value for the ith variable in *Y*, y_i, is:

$$P\left(Y = y_i\right) = \sum_j \sum_k \sum_l P\left(Y = y_i \mid A = a_j, B = b_k, C = c_l\right) P\left(A = a_j\right) P\left(B = b_k\right) P\left(C = c_l\right) \qquad \text{(H-1)}$$

This rule is also called the "marginalization principle" (Ref. [24]).

Note that (H-1) is a forward calculation for obtaining result *Y* from causes *A*, *B*, *C*, etc. One can use Bayes theorem to perform reverse calculations with the network to obtain the probability that *Y* was caused by a certain input configuration at the parent nodes, but that application is outside the scope of the use of a BN's for MBES. The key feature of the BN for MBES is that it greatly reduces the computational and input data requirements for estimating uncertainty compared to the burial process models used for network training.

Appendix I – Scour Model Review

The scour model used to train MBES comes from a set of equations developed by HR Wallingford Ltd. (a United Kingdom civil engineering firm) and presented in books by Soulsby (Ref. [28]) and Whitehouse (Ref. [31]). It was developed to predict scour in steady state conditions, but was adapted to changing environments by assuming a quasi-steady state of root-mean-squared bottom orbital velocities and/or bottom currents over a small time period and evaluating model output in a time-stepped fashion. Trembanis et al. (Ref. [29]) validated the model. The discussion that follows is adapted from Elmore and Richardson (Ref. [30]).

The depth of the scour pit, $S(t)$, for steady state flow after an amount of time, t, has been determined empirically to be

$$S(t) = S_\infty \left(1 - \exp(-t/T)^p\right), \tag{I-1}$$

where S_∞ is the scour pit depth after an infinite amount of time, T governs the rate of scour pit growth, and p is determined by the geometry of the scouring body. For a 5:1 cylinder, $p = 0.6$. The other two variables (S_∞, T) are calculated from oceanographic conditions and physical properties of the sediment. The next two subsections describe the sequence of calculations required to obtain S_∞ and T at each time step, using the statistics of the oceanographic conditions for that time period.

A. Calculating $\boldsymbol{S_\infty}$

1) Basic Relation

Whitehouse's book gives the value of S_∞ as a relationship between the velocity at the sediment bed, U, relative to the velocity required for the sediment to become mobile, U_{cr}, (the critical velocity) in the following manner

$$S_\infty = \begin{cases} 0, & U < 0.75U_{cr} \\ 1.15D_0\left(2U - 1.5U_{cr}\right)/U_{cr}, & 0.75U_{cr} < U < 1.25U_{cr} \\ 1.15D_0, & U > 1.25U_{cr} \end{cases} \tag{I-2}$$

where D_0 is the diameter of the mine.

It is more convenient, however, to rewrite (I-2) so that the magnitude of the stress at the sediment bed, $\tau = \rho_W C_r U^2$, is compared to the critical stress, $\tau_{cr} = \rho_W C_r U_{cr}^2$, required for the sediment to become mobile. (In these relations, ρ_W is the density of water at the sediment interface and C_r is a dimensionless mechanical resistance constant related to the roughness of the seafloor and strength of the flow.) The reasons for this change are that the critical stress has been deduced from laboratory experiments, the stress at the seabed can be calculated from currents and oceanographic conditions, and the critical velocity has to be obtained from knowledge of C_r, which is difficult to assess for $U = U_{cr}$.

The stresses are evaluated in terms of the non-dimensional Shields parameter, θ,

$$\theta = \tau / \left(\left(\rho_s - \rho_w \right) g d_{50} \right), \tag{I-3}$$

where ρ_s is the average bulk density of the sediment, g is gravitational acceleration, and d_{50} is the median diameter of the sediment particles. For $\tau = \tau_{cr}$, the critical Shield's parameter is θ_{cr}. It can be seen from the above relationships between stress and velocity and stress and the Shield's parameter that $\theta^{1/2} / \theta_{cr}^{1/2} = U / U_{cr}$.

Rewriting (I-2) in terms of the Shield's parameters, one obtains

$$S_\infty = \begin{cases} 0, & \sqrt{\theta/\theta_{cr}} < 0.75 \\ 1.15 D_0 \left(2\sqrt{\theta/\theta_{cr}} - 1.5 \right) & 0.75 < \sqrt{\theta/\theta_{cr}} < 1.25 \\ 1.15 D_0, & \sqrt{\theta/\theta_{cr}} > 1.25 \end{cases}, \tag{I-4}$$

The critical Shield's parameter has been evaluated empirically to be

$$\theta_{cr} = \frac{0.3}{1 + 1.2 D_*} + 0.055 \left(1 - \exp\left(-0.02 D_* \right) \right) \tag{I-5}$$

where

$$D_* = d_{50} \left(\left(s - 1 \right) g / \nu^2 \right)^{1/3}, \tag{I-6}$$

$s = \rho_s / \rho_w$, and ν is the kinematic viscosity of seawater.

2) Obtaining θ from Oceanographic Conditions

The last remaining unknown in (I-4) is θ. Soulsby's book provides the following methodology for obtaining total stress, τ, which gives θ by (I-3). The total stress is obtained from the stresses induced by wave motion, τ_w, and by current, τ_c. The following equation relates these stresses to the total stress at the seabed,

$$\tau = \left[\left(\tau_m + \tau_w \cos\phi \right)^2 + \left(\tau_w \sin\phi \right)^2 \right]^{0.5}, \tag{I-7}$$

where ϕ is the angle between the current stress and wave stress vectors and

$$\tau_m = \tau_c \left[1 + 1.2 \left(\frac{\tau_w}{\tau_c + \tau_w} \right)^{3.2} \right]. \tag{I-8}$$

The quantity τ_m is the mean shear stress induced by waves and currents. (Equation (5) accounts for nonlinear interactions between τ_w and τ_c; τ_m is in the same vector direction as τ_c.) In (5), τ_c is calculated from the assumption

$$\tau_c = \rho_w C_D \overline{U}^2, \tag{I-9}$$

where $\overline{U}$ is the depth averaged current velocity evaluated from

$$U(z) = \begin{cases} (z/0.32h)^{1/7}\overline{U}, & 0 < z < 0.5h \\ 1.07\overline{U}, & 0.5h < z < h \end{cases} \tag{I-10}$$

and C_D is the drag coefficient given by

$$C_D = \left[\frac{0.4}{\ln(12h/d_{50})-1}\right]^2, \tag{I-11}$$

where h is water depth.

The other stress, τ_w, is assumed to have a form identical to (I-9). Depth averaged current velocity is replaced with the orbital velocity, U_b, and the drag coefficient is replaced by a wave friction factor, $0.5f_w$, so that

$$\tau_w = 0.5\rho_w f_w U_b^2, \tag{I-12}$$

where

$$f_w = \exp(5.5(U_b T_w/2\pi d_{50})^{-0.2} - 6.3), \tag{I-13a}$$

$$U_b = \pi H_s / \left(\sqrt{2}T_w \sinh(kh)\right), \tag{I-13b}$$

H_s is significant wave height, T_w is peak wave period, and k is peak wavenumber.

B. Obtaining T

Once S_∞ is evaluated for the current time step from (I-2), T is the only remaining variable in (I-1) needing to be evaluated. An empirical relation for T is given in Whitehouse's book as

$$T = T^*\left((s-1)gd_{50}^3\right)^{-1/2} D^2 \tag{I-14}$$

where

$$T^* = A\theta_\infty^B, \tag{I-15}$$

A = 0.095 and B = -2.02 for a free cylinder. The ∞ subscript on the Shield's parameter means that this quantity is evaluated for when the mine is absent. Placing θ in for θ_∞ in (I-15) and putting the result into (I-14) produces

$$T = A\theta^B\left((s-1)gd_{50}^3\right)^{-1/2} D^2. \tag{I-16}$$

C. Time stepping S(t) to calculate mine burial and re-exposure

Now that (I-1) can be evaluated, it needs to be re-expressed in a time-stepped fashion to make it applicable to quasi steady-state conditions. The procedure given in Trembanis et al. will be used for this purpose. At the jth time step, the quasi steady-state starts at $t=t_j$ and ends at $t=t_j + \Delta t = t_{j+1}$, where Δt is the size of the time step. At $t=t_j$, the values for $S(t)$, T and S_∞ are $S(t_j)$, $T(t_j)$ and $S_\infty(t_j)$. Thus, (I-1) becomes

$$S(t_{j+1}) = S_\infty(t_j)\left(1 - \exp\left(-\left(t + \Delta t\right)/T(t_j)\right)^p\right). \tag{I-17}$$

The appropriate value to use for t is the time it would take for $S(t) = S(t_j)$ under a steady state condition with zero initial scour, $T = T(t_j)$ and $S_\infty = S_\infty(t_j)$.

$$t = -T(t_j)\left(\ln\left(1 - S(t_j)/S_\infty(t_j)\right)\right)^{1/p} \tag{I-18}$$

This condition calculates the process along the appropriate portion of the $S(t)$ curve. Equation (I-18), however, assumes that $S(t_j) < S_\infty(t_j)$. ($S(t_j) \geq S_\infty(t_j)$ gives a complex time, which is physically unmeaningful.) This condition will be false when the scouring current is weakening because $S(t_j)$ was calculated at the end of the previous time step while $S_\infty(t_j)$ is applicable to the present time step. In this instance, $S(t_{j+1}) = S_\infty(t_j)$ is set. Hence, (I-18) is rewritten as follows

$$S(t_{j+1}) = \begin{cases} S_\infty(t_j)\left(1 - \exp\left(-\dfrac{(t_j + \Delta t)}{T(t_j)}\right)^p\right), & S(t_j) < S_\infty(t_j) \\ S_\infty(t_j), & S(t_j) \geq S_\infty(t_j) \end{cases} \tag{I-19}$$

To predict the amount of mine burial, B_D, it is assumed that the mine immediately settles to the bottom of the scour pit as the pit grows. Thus, $B_D(t_j)$ is the maximum value of $S(t < t_j)$.